MODELLING OF SOLAR MAGNETIC FIELD AND PROMINENCE STRUCTURES

Grant Number NAG8-085

FINAL REPORT

Period of Performance: October 1, 1986 - September 30, 1988

Prepared by:

Shi Tsan Wu
Center for Space Plasma and Aeronomic Research
and Department of Mechanical Engineering
The University of Alabama in Huntsville
Huntsville, AL 35899

For

National Aeronautics and Space Administration
George C. Marshall Space Flight Center
Marshall Space Flight Center, Alabama 35812

October 1988

TABLE OF CONTENTS

SUMMARY

In this study we have achieved the following:

(i) Theoretical Aspect

Using the plasma theory, we study the interaction between the high frequency waves and magnetohydrodynamic (MHD) in which a set of coupling equations resulted. On the basis of this formalism, we examined the modulation instabilities by an electromagnetic soliton in a current sheet and showed that there is a resistive instability, which eventually turns into an eruptive instability at the onset of the magnetic field reconnection. This mechanism could be used to explain the onset of a solar flare.

(ii) Experimental Aspect

In order to have better measurements for vector magnetic fields with high resolution on the solar surface, we have examined the possibility of increasing the present state-of-the-art optics so we may use it to improve the design and fabrication of a new space-borne solar vector magnetograph as part of SAMEX (Solar Active Measurements Experiments). The detailed study is presented in Section 3 of this report.

INTRODUCTION

The operations of satellites, space shuttle and space station for communications, tracking, and survelliance can be interrupted, degraded, or even endangered as a result of powerful explosions, that we know as solar flares, on the surface of the Sun. These spectacular eruptions release shock waves, hot plasma clouds, highly accelerated atomic nuclei, and bursts of x-rays, untraviolet and visible-band electromagnetic radiation into interplanetary space. When the path of propagation of these high-energy emissions intersects our terrestrial environment it is impacted in various ways that may produce deleterious effects on the operations of the

systems mentioned above.

Observations have shown that physical conditions in the solar atmosphere are strongly controled by the solar magnetic fields. The appearance of solar flares, seen in enhanced emissions in H-alpha and different lines in the ultraviolet and extreme-ultra-violet as well as in white light observations, provides indications of prevalent nature and importance of solar magnetic fields. Consequently, to understand the physics of active regions, the storage and release of flare energy and formtion of hot plasmas and mass ejections, it is imperative that we understand and study the evolution of the Sun's magnetic field. To achieve such as goal, we took both theoretical and experimental approaches. In the theoretical aspect, we investigate the triggering mechanism of the solar flares by studying the resistive and eruptive instability. This result is presented in Section 2 of this report. In the experimental aspect, we investigate the possibility of improving the resolution of the optics for the space-borne solar magnetograph. The results are included in Section 3.

2. THEORETICAL STUDY: Resistive and Eruptive Instability by Pondermotive Force with High-Frequency Plasma Oscillation.

We investigated the subtle interaction between the magnetohydrodynamic (MHD) and high frequency plasma waves and we derived the coupling equations for these phenomena. On the basis of this formalism, we examined the modulation instabilities by an electromagnetic soliton in a current sheet and showed that there is a resistive instability for constant-ψ approximation (i.e., uniform magnetic field configuration), which eventually turns into an eruptive instability at the onset of the magnetic field reconnection.

2.1 Introduction

It is known that the electromagnetic radiation from a plasma often is trapped by the self-induced electromagnetic field and forms a soliton (Krall and Trivepiece, 1978). It is also realized that the width of a two-dimensional soliton is inversely proportional to its own strength. Therefore, the existence of a strong electromagnetic soliton expected in the thin currrent sheets (Li, 1985). Under these circumstances,the current and solitons through the ponderomotive force, within the current sheet will be intimately coupled; these interactions will cause the instability of the magnetic field configuration in the current sheet. Therefore, the electromagnetic soliton-induced instabilty within a current sheet becomes an interesting and fundamental problem in space and laboratory plasma.

In Section 2.2 of this investigation, we present the fundamental coupling equations between magnetohydrodynamics (MHD) and high frequency plasma and also discuss the fast and slow-time scale. In Section 2.3, the electromagnetic soliton-induced resistive instability and in Section 2.4 we present the soliton-induced eruptive instability. We present a numerical example concerning solar coronal plasma in Section 2.5 and concluding remarks in Section 2.6.

2.2 Coupling Equations Between MHD and High Frequency Plasma

The following equations govern a two component magnetized plamsa in a gravitational field with two time-scale approximation.

$$\frac{\partial n_e}{\partial t} + \nabla \cdot (n_e \vec{v}_e) = 0 \ , \tag{2.1}$$

$$\frac{\partial n_e}{\partial t} + \nabla \cdot (n_i \vec{v}_i) = 0 \ , \tag{2.2}$$

$$\frac{\partial \vec{v}_e}{\partial t} + (\vec{v}_e \cdot \nabla)\vec{v}_e = \frac{e}{m_e}(\vec{E} + \frac{1}{c}\vec{v}_e \times \vec{B}) - \frac{\nabla P_e}{m_e n_e} + \nu_{ei}(\vec{v}_e - \vec{v}_i), \tag{2.3}$$

$$\frac{\partial \vec{v}_i}{\partial t} + (\vec{v}_i \cdot \nabla)\vec{v}_i = \frac{-e}{m}(\vec{E} + \frac{1}{c}\vec{v}_i \times \vec{B}) - \frac{\nabla P_i}{m_i n_i} - \vec{g} + \nu_{ei}(\vec{v}_i - \vec{v}_e) \tag{2.4}$$

$$\nabla \times \vec{E} = -\frac{1}{c}\frac{\partial \vec{B}}{\partial t}, \tag{2.5}$$

$$\nabla \times \vec{B} = \frac{1}{c}\frac{\partial \vec{E}}{\partial t} + \frac{4\pi}{c}(en_e\vec{v}_e - en_i\vec{v}_i), \tag{2.6}$$

$$\nabla \cdot \vec{B} = 0 \tag{2.7}$$

Note these symbols and their meanings: n = the number density, $\vec{v}$ = the velocity, P = the thermal pressure, $\vec{E}$ = the electric field, $\vec{B}$ = the magnetic field, $\vec{g}$ = the gravitational field, e = the electric charge, m = the mass of of particle and ν_{ei} = collisional frequency between electron and ion. The subscripts e and i indicate the electron and the ion respectively.

Based on the two time-scale approximation (Li, 1985), all the quantities could be defined by

$$A = (n_e, n_i; \vec{v}_e, \vec{v}_i; p_e, p_i; \vec{E}, \vec{B}) = A_f + A_s \tag{2.8}$$

It could be assumed that the assemble average value of fast time-scale components over the slow time-scale vanishes;

$$\langle A_f \rangle = 0. \tag{2.9}$$

Hence, in the slow time-scale region,the charge neutrality condition holds,

$$\langle n_e e - n_i e \rangle = 0 \tag{2.10}$$

Thus,

$$n_{e,s} = n_{i,s} \equiv n_s \tag{2.11}$$

where, the subscript s indicates the slow time-scale.

In the meantime, we shall employ this concept to analyze the set of governing equations (2.1) through (2.7). Beginning at the electron component of plasma, Eq. (2.1) the equation becomes,

$$\frac{\partial}{\partial t}\,(n_s + n_f^e) + \nabla \cdot \left[(n_s + n_f^e)\ (\vec{v}_s^{\,e} + \vec{v}_f^{\,e}) \right] = 0. \tag{2.12}$$

From now on, the superscript indicates the species, and the subscript indicates slow or fast time-scale. The assemble average of Eq. (2.12) over the slow time-scale becomes

$$\frac{\partial}{\partial t}\,(n_s) + \nabla \cdot \left[n_s \vec{v}_s^{\,e} + \langle n_f^{e} \vec{v}_f^{\,e} \rangle \right] = 0 \tag{2.13}$$

Eq. (2.13) subtracted from Eq. (2.12) becomes

$$\frac{\partial}{\partial t}\,(n_f^e) + \nabla \cdot (n_s \vec{v}_f^{\,e} + n_f^e \vec{v}_f^{\,e} + n_f^e \vec{v}_s^{\,e} - \langle n_f^e \vec{v}_f^{\,e} \rangle) = 0, \tag{2.14}$$

From Eq. (2.3), we obtain the lowest order component equation for the fast time-scale, as shown by

$$\frac{\partial \vec{v}_f^{\,e}}{\partial t} \simeq \frac{e}{m_e}\,\vec{E}_f \tag{2.15}$$

If we use the relationship in Eq. (2.15) to analyze the terms in, Eq. (2.14), the equation becomes

$$\left| \frac{\nabla \cdot (n_f^e \vec{v}_f^{\,e})}{\frac{\partial}{\partial t}\,(n_f^e)} \right| \sim \frac{k\, n_f^e\, v_f^e}{\omega n_f^e} \sim \frac{k}{\omega}\ \frac{|e| E_f}{m_e \omega} \sim \left(\frac{k}{k_d}\ \frac{-1/2}{\omega_f} \right) \left(\frac{\omega_{pe}}{\omega} \right)^2 \tag{2.16a}$$

and

$$\frac{\nabla \cdot (n_f^e v_s^e)}{\frac{\partial}{\partial t}(n_f^e)} \sim \left(\frac{k}{k_d}\right)\left(\frac{\omega p_e}{\omega}\right)\left(\frac{v_s^e}{v_{Te}}\right), \tag{2.16b}$$

where k and ω are the wave numbers and the frequency respectively, and k_d and ω_{pe} are the characteristic wave numbers chosen to be the width of the current sheet and the electron plasma frequency respectively. The fast time-scale component energy density is defined by

$$\bar{W}_f = \frac{E_f^2}{4\pi n_e^0 T_e} \tag{2.16c}$$

Corresponding to the slow time-scale fluid motion (i.e., collective motion),

$$|\vec{v}_s^e| \leq v_{Te} \tag{2.17}$$

with v_{Te} representing electron thermal speed.

Hence, in the case of

$$\frac{v_{Te}}{v_\phi} << 1, \quad (v_\phi \equiv \omega/k) \tag{2.18a}$$

and

$$\frac{v_{Te}}{v_\phi} << \left(\frac{\omega}{\omega_{pe}}\right) \bar{W}_f^{-1/2}, \tag{2.18b}$$

Eq. (2.14) could be simplified as,

$$\frac{\partial n_f^e}{\partial t} + \nabla \cdot (n_s \vec{v}_f^e) = 0. \tag{2.19}$$

By combining Eqs.(2.15) and (2.19), we obtain the following approximate values:

$$v_f^e \sim \frac{|e|E_f}{m_e \omega} \sim \frac{\omega_{pe}}{\omega} \bar{W}_f^{-1/2} v_{Te} , \tag{2.20}$$

$$\frac{n_f^e}{n_s} \sim \frac{k}{\omega} v_f^e \sim \left(\frac{k}{k_d}\right)\left(\frac{\omega_{pe}}{\omega}\right)^2 \bar{W}_f^{1/2} << 1, \tag{2.21}$$

Comparing Eqs. (2.17), (2.18b) (2.20) and (2.21) with the terms in Eq. (2.13) yields,

$$\left|\frac{n_f^e \vec{v}_f^e}{n_s \vec{v}_s^e}\right| \sim \left(\frac{k}{k_d}\right)\left(\frac{\omega_{pe}}{\omega}\right)^2 \bar{W}_f^{1/2} \left(\frac{\omega_{pe}}{\omega} \bar{W}_f^{1/2}\right)\left(\frac{v_{Te}}{|\vec{v}_s^e|}\right) << 1, \tag{2.22}$$

Thus, Eq. (2.13) becomes

$$\frac{\partial}{\partial t}(n_s) + \nabla \cdot (n_s \vec{v}_s^e) = 0. \tag{2.23}$$

For the ion, we may repeat our calculation by using Eqs. (2.12) through (2.22) together with the condition of Eq. (2.18b), which leads to a weak condition

$$\left(\frac{k}{k_d}\right)\left(\frac{\omega_{pe}}{\omega}\right)\left(\frac{m_e}{m_i}\right) << \left(\frac{\omega}{\omega_{pe}}\right) \bar{W}_f^{-1/2} . \tag{2.24}$$

Therefore, we obtained a similar expression of Eq. (2.19), as represented by

$$\frac{\partial}{\partial t} n_f^i + \nabla \cdot (n_s \vec{v}_f^i) = 0, \tag{2.25}$$

From Eqs. (2.20) and (2.21), it could be shown, that

$$v_f^i \sim \left(\frac{\omega_{PE}}{\omega}\right) \bar{W}_f^{1/2} v_{Te} \left(\frac{m_e}{m_i}\right) , \tag{2.26a}$$

and

$$n_f^i/n_s \sim \left(\frac{k}{k_a}\right)\left(\frac{\omega_{pe}}{\omega}\right) \bar{W}^{1/2} \left(\frac{m_e}{m_i}\right) << 1, \tag{2.26b}$$

Thus, we also found

$$\frac{\partial n_s}{\partial t} + \nabla \cdot (n_s \vec{v}_s^{\,i}) = 0. \tag{2.27}$$

By examining the electron and ion momentum equations according to Eq. (2.8) together with the principles of the order of magnitude approximation, we found the slow time-scale momentum equation for the electron as

$$\frac{\partial}{\partial t} \vec{v}_s^{\,e} + (\vec{v}_s^{\,e} \cdot \nabla)\, \vec{v}_s^{\,e} = \frac{e}{m_e}\left[\vec{E}_s + \frac{1}{c}\vec{v}_s^{\,e} \times \vec{B}_s\right] - \frac{1}{m_e n_s}\nabla p_s$$

$$- \nu_{ei}\,(\vec{v}_s^{\,e} - \vec{v}_s^{\,i}) + \vec{g} + \vec{F}_p^{\,e}\,. \tag{2.28}$$

where $\vec{F}_p$ is the pondermotive force due to the high frequency plasma and MHD interaction

$$\vec{F}_p^{\,e} = -\frac{1}{2}\nabla \langle (\vec{v}_f^{\,e})^2 \rangle + \frac{e}{m_e c} \langle \vec{v}_f^{\,e} \times \nabla \times (\vec{\phi}_e \times \vec{B}_s) \rangle.$$

and

$$\vec{v}_f^{\,e} = \frac{\partial}{\partial t}\vec{\phi}_e \tag{2.29}$$

with $\vec{\phi}_e$ being an arbitrary function.

Similarly, we obtain the slow time-scale momentum equation for ion,

$$\frac{\partial}{\partial t} \vec{v}_s^{\,i} + (\vec{v}_s^{\,i} \cdot \nabla)\, \vec{v}_s^{\,i} = \frac{-e}{m_i}\left[\vec{E}_s + \frac{1}{c}\vec{v}_s^{\,i} \times \vec{B}_s\right] - \frac{1}{m_i n_s}\nabla p_s^{\,i}$$

$$+ \nu_{ei}\,(\vec{v}_s^{\,e} - \vec{v}_s^{\,i}) + \vec{g} + \vec{F}_p^{\,i}\,, \tag{2.30}$$

where $\vec{F}_p^{\,i}$ is the pondermotive force corresponding to the ion,

$$\vec{F}_p^{\,i} = -\frac{1}{2}\nabla \langle (\vec{v}_f^{\,i})^2 \rangle - \frac{e}{m_i c} \langle \vec{v}_f^{\,i} + \nabla \times (\vec{\phi}_i \times \vec{B}_s) \rangle,$$

with

$$\vec{v}_f^{\,i} = \frac{\partial}{\partial t}\,\vec{\phi}_i . \tag{2.31}$$

From (2.6), the fast time-scale field equation can be derived as,

$$\nabla \times \vec{B}_f = \frac{1}{c}\frac{\partial \vec{E}_f}{\partial t} + \frac{4\pi e}{c}\Big[n_s \vec{v}_f^{\,e} + n_f^{e} \vec{v}_f^{\,e} + n_f^{e} \vec{v}_s^{\,e} - \langle n_f^{e} \vec{v}_f^{\,e} \rangle - n_s \vec{v}_f^{\,i} - n_f^{i} \vec{v}_s^{\,i} - n_f^{i} \vec{v}_f^{\,i} + \langle n_f^{i} \vec{v}_f^{\,i} \rangle \Big] \tag{2.32}$$

It also can be shown that

$$\left| \frac{n_f^{e} \vec{v}_s^{\,e}}{n_s \vec{v}_f^{\,e}} \right| \sim \left(\frac{\omega_{pe}}{\omega}\right)\left(\frac{k}{k_d}\right)\left(\frac{|\vec{v}_s^{\,e}|}{v_{Te}}\right) << 1$$

$$\left| \frac{n_f^{e} \vec{v}_s^{\,e}}{n_s \vec{v}_f^{\,e}} \right| \sim \frac{n_f^{e}}{n_s} << 1 ,$$

so that Eq. (2.31) becomes

$$\nabla \times \vec{B}_f \simeq \frac{1}{c}\frac{\partial \vec{E}_f}{\partial t} + \frac{4\pi e}{c}\, n_s \vec{v}_f^{\,e} . \tag{2.33}$$

Further, using the followwng expressions,

$$\frac{\partial}{\partial t}\,\vec{v}_f^{\,e} = \frac{e}{m_e}\,\vec{E}_f + \frac{e}{m_e c}\,\vec{v}_f^{\,e} \times \vec{B}_s \tag{2.34}$$

and

$$\vec{B}_f = -\frac{m_e c}{e}\,\nabla \times \frac{\partial \vec{\phi}_e}{\partial t} + \nabla \times (\vec{\phi}_e \times \vec{B}_s), \tag{2.35}$$

we derive the following equation:

$$\nabla \times \nabla \times \vec{\phi}_e + \frac{1}{c^2}\,\vec{\phi}_e + \frac{1}{c^2}\,\frac{4\pi e^2}{m_e}\, n_s \vec{\phi}_e - \frac{1}{c^2}\,\omega_{Be}\,\vec{\phi}_e \times \left(\frac{\vec{B}_s}{B_s}\right) - \frac{e}{m_e c}\,\nabla \times \nabla \times \left(\vec{\phi}_e \times \vec{B}_s\right) = 0 \tag{2.36}$$

where

$$\left.\begin{aligned} \vec{\phi}_e &= \frac{\partial \vec{\phi}_e}{\partial t} = \vec{V}_f^e \\ \omega_{Be} &= \frac{eB_s}{m_e c} \end{aligned}\right\} \tag{2.37}$$

By defining

$$\left.\begin{aligned} \rho &= n_s(m_i + m_e) \\ \vec{u} &= \frac{(m_i \vec{V}_s^i + m_e \vec{V}_s^e)}{(m_i + m_e)} \end{aligned}\right\} \tag{2.38}$$

Using Eqs (2.32) and (2.27), we obtained

$$\frac{\partial}{\partial t} \rho + \nabla \cdot (\rho u) = 0 \tag{2.39}$$

The LHS (left hand side) of Eqs (2.29) and (2.31) can be written as

$$\frac{\partial}{\partial t} (m_\alpha n_s \vec{V}_s^\alpha) + \nabla \cdot (m_\alpha n_s \vec{V}_s^\alpha \vec{V}_s^\alpha) \quad , \quad \alpha = e,i.$$

where $\vec{v}_s^\alpha \vec{v}_s^\alpha$ is the dyad of vector $\vec{v}_s^\alpha$ which is a second order tensor.

Since,

$$\rho \vec{u}\,\vec{u} = \frac{n_s}{m_i + m_e} \left[(m_e \vec{v}_s^e + m_i \vec{v}_s^i)(m_e \vec{v}_s^e + m_i \vec{v}_s^i) \right]$$

$$= \sum_a (n_s m_\alpha \vec{V}_s^\alpha \vec{V}_s^\alpha) + m_e n_s [\, \vec{v}_s^i (\vec{v}_s^e - \vec{v}_s^i) + \vec{v}_s^e (\vec{v}_s^i - \vec{v}_s^e)],$$

in which,

$$\vec{J}_s^0 = e n_s (\vec{v}_s^e - \vec{v}_s^i) \tag{2.40}$$

then,

$$\Sigma\, n_s m_\alpha \vec{v}_s^{\,a} \vec{v}_s^{\,a} = \rho \vec{u}\,\vec{u} + \frac{m_e m_s}{e^2 n_s^2}\, \vec{j}^{\,o}\, \vec{j}^{\,o}\ , \tag{2.41}$$

By introducing the pressure tensor at the center of the mass system, we obtained

$$\hat{\vec{P}} = n_s \left[m_e \left\langle (\vec{v} - \vec{u})(\vec{v} - \vec{u}) \right|_{fe} \right\rangle + m_i \left\langle (\vec{v} - \vec{u})(\vec{v} - \vec{u}) \right|_{fi} \right\rangle \tag{2.42}$$

According to Eqs.(2.38) and (2.40), we have

$$\vec{v}_s^{\,e} \sim \frac{1}{en_s}\, \vec{j}_s^{\,o} = \vec{u}\ ,$$

$$\vec{v}_s^{\,i} \sim \vec{u} - \frac{m_e}{m_i}\frac{1}{en_s}\, \vec{j}_s^{\,o}\ . \tag{2.43}$$

Incorporating these relationships into Eq. (2.42) yields

$$\hat{\vec{P}} = m_e n_s \left\langle (\vec{v} - \vec{v}_s^{\,e})(\vec{v} - \vec{v}_s^{\,e}) \right|_{fe} > + m_i n_s \left\langle (\vec{v} - \vec{v}_i)(\vec{v} - \vec{v}_i) \right|_{fi} >$$

$$+ \left(1 + \frac{m_e}{m_i}\right) \frac{m_e}{n_s e^2}\, \vec{j}_s^{\,o} \vec{j}_s^{\,o} = \hat{\vec{P}}_s^{\,e} + \hat{\vec{P}}_s^{\,i} + \frac{m_e}{n_s e^2}\, \vec{j}_s^{\,o} \vec{j}_s^{\,o} \tag{2.44}$$

Multiplying Eqs. (2.28) and (2.30) by $m_e n_s$ respectively and then adding them together results in

$$\rho\left(\frac{\partial \vec{u}}{\partial t} + (\vec{u} \cdot \nabla)\, \vec{u}\right) = \frac{1}{c}\, \vec{j}_s^{\,o} \times \vec{B}_s - \nabla p + \rho \vec{g} + \vec{F}_p . \tag{2.45}$$

In deriving the above equation, we employed the relation $\vec{F}_p^{\,i} \ll \vec{F}_p^{\,e}$, so that

$$\vec{F}_p = -\frac{1}{2}\left(\frac{m_e}{m_i}\right) \rho \nabla \left\langle (\vec{v}_f^{\,e})^2 \right\rangle + \frac{e}{m_i c}\, \rho \left\langle \vec{v}_f^{\,e} \times \nabla \times (\vec{\phi}_e \times \vec{B}_s) \right\rangle, \tag{2.46}$$

In addition, we employed the general Ohm's law similar to those given by

Krall and Trivelpiece (1973) by combining Eqs. (2.28) and (2.30) and multiplying the terms of e/m_e and $-e/m_e$ respectively In case we neglected the second order terms together with the pressure gradient, gravitational force and pondermotive force, we get

$$\eta \vec{J}_s^{\,0} = \vec{E}_s + \vec{u} \times \vec{B}_s/c \tag{2.47}$$

where

$$\eta = m_e \nu_{ei}/(n_s e^2) \tag{2.48}$$

From Eq. (2.6), the slow time-scale current becomes

$$\vec{J}_s = e n_s (\vec{v}_s^{\,e} - \vec{v}_s^{\,i}) + e \langle n_f^{e} \vec{v}_f^{\,e} - n_f^{i} \vec{v}_f^{\,i} \rangle \tag{2.49}$$

According to Eq. (2.26), the second term on the RHS (right hand side) of Eq. (2.49) can be delected, thus

$$\vec{J}_s = \vec{J}_s^{\,0} = e n_s \, (\vec{v}_s^{\,e} - \vec{v}_s^{\,i}) \tag{2.50}$$

Therefore,

$$\nabla \times \vec{B}_s = \frac{1}{c} \frac{\partial \vec{E}_s}{\partial t} + \frac{4\pi}{c} \vec{J}_s^{\,0} \simeq \frac{4\pi}{c} \vec{J}_s^{\,0} \tag{2.51}$$

We dropped the displacement current because $\nu_{ei} \ll \omega_{pe}$.

Finally, we derived a set of global coupling MHD equations with pondermotive force,

$$\frac{\partial}{\partial t} \rho + \nabla \cdot (\rho \vec{u}) = 0 \tag{2.52}$$

$$\rho \left[\frac{\partial \vec{u}}{\partial t} + (\vec{u} \cdot \nabla) \, \vec{u} \right] = \frac{1}{c} \vec{J} \times \vec{B} - \nabla p + \rho \vec{g} + \vec{F}_p \tag{2.53}$$

$$\nabla \times \nabla \times \left(\frac{\partial \vec{\phi}}{\partial t} \right) + \frac{1}{c} \frac{\partial^3 \vec{\phi}}{\partial t^3} + \frac{1}{c^2} \frac{4\pi e^2}{m_e m_i} \frac{\partial \vec{\phi}}{\partial t} - \left\{ \frac{\omega_{Be}}{c^2} \frac{\partial^2 \vec{\phi}}{\partial t^2} \times \left(\frac{\vec{B}}{B} \right) + \frac{e}{m_e c} \nabla \times \nabla \times (\vec{\phi} \times \vec{B}) \right\} = 0 \tag{2.54}$$

with

$$\vec{F}_p = \frac{e}{m_i e}\,\rho\,\langle\vec{\phi}\times\nabla\times(\vec{\phi}\times\vec{B})\rangle - \frac{1}{2}\frac{m_e}{m_i}\,\rho\,\nabla\left\langle\left(\frac{\partial\vec{\phi}}{\partial t}\right)^2\right\rangle \tag{2.55}$$

Ohm's law,

$$\eta\vec{j} = \vec{E} + \vec{u}\times\vec{B}/c \tag{2.56}$$

Maxwell equation,

$$\left.\begin{aligned}\nabla\times\vec{B} &= \frac{4\pi}{c}\vec{j}\\ \nabla\times\vec{E} &= -\frac{1}{c}\frac{\partial\vec{B}}{\partial t}\\ \nabla\cdot\vec{B} &= 0\end{aligned}\right\} \tag{2.57}$$

In the case of $\omega_{pe} >> \omega_{Be}$; $\omega >> \omega_{Be}$ and $\vec{\phi}\,||\,\vec{B}$ (i.e., the high frequency amplitude parallel to the magnetic field), the Eq. (2.54) and (2.55) are reduced to

$$\nabla\times\nabla\times\vec{v}_f + \frac{1}{c^2}\frac{\partial^2\vec{v}_f}{\partial t^2} + \frac{1}{c^2}\frac{4\pi e^2}{m_e m_i}\rho\vec{v}_f = 0 \tag{2.58}$$

$$\vec{F}_p = -\frac{1}{2}\frac{m_e}{m_i}\,\rho\,\nabla\langle(\vec{v}_f)^2\rangle \tag{2.59}$$

with energy equation, this set of equations form a closed set of governing equations for the described problem.

2.3. Resistive Instability by Soliton

It has been recognized that one way to convert magnetic energy to kinetic energy is through the resistive instabilities. Although the foundation of this study has been made by Furth, Killeen and Rosenbluth (1963 thereafter it will be referred to as FKR), Priest (1986), the analysis including the

pondermotive force is still lacking. Thus, we shall present a detailed analysis for the resistive instability by soliton for a transverse plasma wave in a slab geometry.

For convenience, we shall perform an incompressible analysis, which can be justified in the most physical region (Furth, Killeen and Rosenbluth, 1963; Shivamoggi, 1985). The motion of plasma is along the x-direction and the unperturbed field is B_{0y} in perpendicular to the x-direction, and assuming that the gravitational effect is negligible, we have the governing equation as follows:

$$\frac{\partial \rho}{\partial t} + \nabla \cdot (\rho \vec{u}) = 0 \tag{3.1}$$

$$\rho \left(\frac{\partial \vec{u}}{\partial t} + (\vec{u} \cdot \nabla)\vec{u} \right) = \frac{1}{4\pi} (\nabla \times \vec{B}) \times \vec{B} - \nabla p - \frac{1}{2} \frac{m_e}{m_i} \rho \nabla \langle \vec{v}_f^2 \rangle \tag{3.2}$$

$$\frac{\partial \vec{B}}{\partial t} = \nabla \times (\vec{u} \times \vec{B}) + \frac{\eta c^2}{4\pi} \nabla^2 \vec{B} \ . \tag{3.3}$$

$$\nabla \times \nabla \times \vec{v}_f + \frac{1}{c^2} \frac{\partial^2 \vec{v}_f}{\partial t^2} + \frac{1}{c^2} \frac{4\pi e^2}{m_e} \frac{\rho}{m_i} \vec{v}_f = 0, \tag{3.4}$$

$$\nabla \times \vec{E} = - \frac{1}{c} \frac{\partial \vec{B}}{\partial t} \ , \tag{3.5}$$

$$\nabla \times \vec{B} = \frac{4\pi}{c} \vec{j} \ , \tag{3.6}$$

$$\nabla \cdot \vec{B} = 0. \tag{3.7}$$

Let us examine the steady state of this set of governing equations (i.e., Eqs. (3.1) through (3.2)) by setting

$$\vec{u}_0 = 0 \qquad \rho_0 = \vec{\rho} + \rho_0'(x) \tag{3.8}$$

$$\vec{B}_0 = B_{0y}(x)\ \hat{y} = \bar{B} \tanh\left(\frac{x}{L_s}\right)\ \hat{y}. \tag{3.9}$$

Within the current sheet (i.e., $|\bar{x}| = |x/L_s| << 1$), the magnetic field can be approximated by

$$\vec{B}_0 = \bar{B}\ \frac{x}{L_s}\ \hat{y} \tag{3.10}$$

where L_s represents the characteristic length of the current sheet.

Incorporating Eq. (3.8) into Eq. (3.2), we obtain

$$\frac{1}{4\pi\bar{\rho}}\ (\nabla \times \vec{B}_0) \times \vec{B}_0 - \frac{c_s^2}{\bar{\rho}}\ \nabla\rho' - \frac{1}{2}\ \frac{m_e}{m_i}\ \nabla\ \langle \vec{v}_{f0}^{\,2} \rangle = 0, \tag{3.11}$$

where c_s is the lowest order sound speed,

$$c_s^2 = \left(\frac{\partial p}{\partial \rho}\right)_0 \tag{3.12}$$

Using Eqs. (3.10) and (3.11), we obtain

$$\rho_0'(x) = -\ \frac{1}{c_s^2}\ \left(\frac{\bar{\rho}}{2}\ \frac{m_e}{m_i}\ \langle \vec{v}_{f0}^{\,2} \rangle + \frac{\vec{B}^2}{8\pi}\ \left(\frac{x}{L_s}\right)^2\right) \tag{3.13}$$

In the case of,

$$\frac{1}{8\pi}\ \vec{B}^2\ \left(\frac{x}{L_s}\right)^2 << \frac{1}{2}\ \bar{\rho}\ \frac{m_e}{m_i}\ \langle \vec{v}_{f0}^{\,2} \rangle \tag{3.14}$$

we have,

$$\rho' \simeq -\ \frac{1}{c_s^2}\ \frac{\bar{\rho}}{2}\ \frac{m_e}{m_i}\ \langle \vec{v}_{f0}^{\,2} \rangle. \tag{3.15}$$

As usual, the lowest order of fast oscillation speed of the electron can be expressed by

$$\vec{v}_{f0} = \frac{1}{2}\left[\vec{v}_0(r,t)\ e^{i\omega t} + \ldots\right] \tag{3.16}$$

With ω_0 being the lowest order fast oscillation frequency. From Eq. (3.16), it can be shown that

$$\langle \vec{v}_{f0}^{\,2} \rangle = \frac{1}{2} |\vec{v}_0|^2 , \tag{3.17}$$

$$\left| \frac{1}{\omega_0} \frac{\partial}{\delta t} \ln v_0 \right| << 1 \tag{3.18}$$

and by neglecting the second order time derivatives, Eq. (3.4) becomes

$$2i\omega_0 \frac{\partial \vec{v}_0}{\partial t} - c^2 \nabla^2 \vec{v}_0 - \left(\omega_0^2 - \frac{4\pi e^2}{m_e} \frac{\rho_0}{m_i} \right) \vec{v}_0 = 0. \tag{3.19}$$

For the transverse plasma wave,

$$\omega_0^2 \sim \omega_{pe}^2 \equiv \frac{4\pi e^2}{m_e} \frac{\bar{\rho}}{m_i} \tag{3.20}$$

Employing Eqs. (3.15) and (3.17), Eq. (3.19) becomes

$$i \frac{\partial \vec{v}_0}{\partial t} + \frac{c^2}{2\omega_{pe}} \nabla^2 \vec{v}_0 + \frac{\omega_{pe}}{8c_s^2} \frac{m_e}{m_i} |\vec{v}_0|^2 \vec{v}_0 = 0 , \tag{3.21}$$

For convenience, let us take the complex conjugate of the Eq. (3.19) which leads to a standard nonlinear Schrodinger equation.

$$i \frac{\partial v_0}{\partial t} = - \frac{1}{2} \frac{\partial^2 v_0}{\partial X^2} - \beta |v_0|^2 v_0 \tag{3.22}$$

and where

$$\left.\begin{aligned} \vec{v}_0 &= v_0(x,t)\, \hat{y}, \quad X = \frac{1}{c} \sqrt{\omega_{pe}}\, x \\ \beta &= \frac{\omega_{pe}}{8c_s^2} \mu , \qquad \mu = \frac{m_e}{m_i} \end{aligned}\right\} \tag{3.23}$$

From Eq. (3.23) it is clearly indicated that these nonlinear wave

interactions can be considered as wave packets and its wave function is proportional to $\vec{v}_0$. These wave packets can produce self-generated potential, $\beta|v_0|^2$. Since β is positive, this self-generated potential has attractive and repulsive characteristics. In other words, these nonlinear wave packets can be self-centered and form a stable structure called "soliton". For the steady state, the solution for this soliton can be expressed by

$$v_0 = v_0^0 \, \text{sech} \left(\sqrt{\beta} \, v_0^0 \, X \right) e^{i\phi} \, , \tag{3.24a}$$

$$\phi = \frac{\beta}{2} t + \phi_0 \tag{3.24b}$$

By incorporating Eqs. (3.24a) and (3.17) into Eq. (3.15), we obtain

$$\rho_0(x) = - \frac{1}{c_s^2} \frac{\rho}{4} \mu (v_0^0)^2 \, \text{Sech}^2 \left(\frac{x}{\epsilon_0} \right) \, , \tag{3.25}$$

the width of the soliton being

$$\epsilon_0 = \sqrt{\frac{8}{\mu}} \left(\frac{c}{\omega_{pe}} \right) \left(\frac{c_s}{v_0^0} \right) \, . \tag{3.26}$$

Hence, the width of the current sheet can be estimated from Eq. (3.14), such as,

$$\Delta x = \epsilon << \sqrt{\mu} \left(\frac{v_0^0}{v_A} \right) L_s \tag{3.27}$$

with v_A being the Alfven speed.

Now, let us turn our attention to the perturbed state. By using Eqs. (3.1) through (3.3), we obtained,

$$\rho_0 \frac{\partial \vec{u}}{\partial t} = - \nabla p + \frac{1}{4\pi} (\nabla \times \vec{B}) \times \vec{B}_0 + \frac{1}{4\pi} (\nabla \times \vec{B}_0) \times \vec{B}$$

$$- \frac{1}{2} \mu \rho \nabla |v_0|^2 \tag{3.28}$$

$$\frac{\partial \vec{B}}{\partial t} = \nabla \times (\vec{u} \times \vec{B}_0) - \frac{1}{4\pi} \eta c^2 \nabla \times (\nabla \times \vec{B}) \tag{3.29}$$

$$\frac{\partial \rho}{\partial t} = - (\vec{u} \cdot \nabla) \rho_0 \tag{3.30}$$

$$\nabla \cdot \vec{u} = 0 , \quad \nabla \cdot \vec{B} = 0 \tag{3.31}$$

By taking all the perturbed quantities, such as

$$A(x,y,t) = A(x) e^{\gamma t} e^{iky} \tag{3.32}$$

and substituting these perturbed quantities Eq. (3.32) and Eqs. (3.28) through (3.30) together with Eq. (3.31) to eliminate B_y, and u_y, we obtained a set of differential equations,

$$\frac{d}{dx} \left(\gamma^2 \rho_0 \frac{du_x}{dx} \right) - k^2 \left(\gamma^2 \rho_0 - \frac{1}{4} \mu \frac{dP_0}{dx} \frac{d|v_0|^2}{dx} + \frac{\gamma}{\eta c^2} B_{0y}^2(x) \right) u_x$$

$$= \frac{ik}{4\pi} B_{0y(x)} \gamma \left[\frac{4\pi}{\eta c^2} \gamma - \frac{1}{B_{0y}} \frac{d^2 B_{0y}}{dx^2} \right] B_x , \tag{3.33}$$

$$\gamma B_x = ikB_{0y}(x) u_x + \frac{\eta c^2}{4\pi} \left(\frac{d^2}{dx^2} - k^2 \right) B_x , \tag{3.34}$$

Introducing the following dimensionless quantities,

$$B_{0y}(x) = \bar{B} \bar{F}(x) , \quad \psi = \frac{B_x}{\bar{B}} , \quad \rho_0 = \bar{\rho} \theta_0(x) , \tag{3.35a}$$

$$G_0 = \left(- \frac{1}{4} \mu \frac{d}{dx} |v_0|^2 \right) \frac{1}{\bar{\rho}} \rho_0' \tau_H^2 \tag{3.35b}$$

$$x = L_s \bar{x} , \quad \alpha = kL_s , \quad s = \frac{\tau_R}{\tau_h} \tag{3.35c}$$

$$\tau_R = \frac{4\pi L_s^2}{\eta c^2} \quad , \quad \tau_H = 4\pi L_s \frac{\sqrt{\rho}}{\bar{B}} \quad , \tag{3.35d}$$

and incorporating them into Eqs. (3.33) and (3.34) yields,

$$\frac{d^2\psi}{d\bar{x}^2} = \alpha^2\psi \left(1 + \frac{\gamma\tau_R}{\alpha^2}\right) - i\, k\, \tau_R\, F\, u_x \quad , \tag{3.36}$$

$$\frac{d}{d\bar{x}}\left(\theta_0 \frac{du_x}{d\bar{x}}\right) = \alpha^2 u_x\left[\theta_0 + \frac{s^2}{\gamma^2\tau_R^2} G_0 + \frac{s^2}{\gamma\tau_R} F^2\right]$$

$$+ \left(\frac{i}{k\tau_R}\right) \psi\, \alpha^2 s^2 \left(F - \frac{1}{\gamma\tau_R}\frac{d^2F}{d\bar{x}^2}\right) \tag{3.37}$$

In order to seek solutions for this set of governing equations, we shall divide them into two regions; the region outside the current sheet and the region inside the current sheet.

i) Region outside current sheet.

In the case outside the current sheet, the $\eta \to 0$ in this region; thus, $s^2 \to \infty$, under this circumstance, Eq. (3.37) becomes

$$\left(\frac{1}{\gamma^2\tau_R^2} G_0 + \frac{1}{\gamma\tau_R} F^2\right) u_x \simeq \frac{-i}{k\tau_R} \psi \left(F - \frac{1}{\gamma\tau_R}\frac{d^2F}{d\bar{x}^2}\right) \quad ,$$

Combining this experssion with Eq. (3.36), we get,

$$\frac{ik\tau_R u_x}{F} \frac{G_0}{\gamma\tau_R} = \frac{d^2\psi}{d\bar{x}^2} - \psi\left(\alpha^2 + \frac{1}{F}\frac{d^2F}{d\bar{x}^2}\right) \tag{3.38}$$

On the other hand, Eq. (3.36) can be rewritten as

$$\frac{1}{\gamma\tau_R}\left(\frac{d^2\psi}{d\bar{x}^2} - \alpha^2\psi\right) = \psi - ik\frac{F}{\gamma} u_x \tag{3.39}$$

It is also true that $\gamma\tau_R \to \infty$ outside the current sheet, thus Eq. (3.39) reduces to

$$\psi \simeq ik \frac{1}{\gamma} F u_x \tag{3.40}$$

Combining Eqs. (3.39) and (3.40), we obtained

$$\frac{d^2\psi}{d\bar{x}^2} - \psi\left(\alpha^2 + \frac{1}{F}\frac{d^2F}{d\bar{x}^2} + \frac{G}{F^2}\right) = 0 , \tag{3.41}$$

Concerning the transverse plasma wave, G_0 is negligible outside the current sheet because the incompressible characteristics are held outside the current sheet; therefore Eq. (3.41) becomes

$$\frac{d^2\psi}{d\bar{x}^2} - \psi\left(\alpha^2 + \frac{1}{F}\frac{d^2F}{d\bar{x}^2}\right) = 0, \tag{3.42}$$

The solution for this equation is

$$\psi_{\pm} = \begin{cases} e^{-\alpha\bar{x}}\left(1 + \dfrac{\tanh\bar{x}}{\alpha}\right), & \bar{x} > 0 \\ e^{\alpha\bar{x}}\left(1 - \dfrac{\tanh\bar{x}}{\alpha}\right), & \bar{x} < 0 \end{cases}$$

The jump condition across the current sheet is

$$\Delta'_e = \frac{1}{\psi(0)}\left(\frac{d\psi}{d\bar{x}}\bigg|_{+0} - \frac{d\psi}{d\bar{x}}\bigg|_{-0}\right) = 2\left(\frac{1}{\alpha} - \alpha\right) \tag{3.43}$$

ii) Region inside the current sheet

Since, $\dfrac{d^2u_x}{d\bar{x}^2} >> \dfrac{d\theta_0}{d\bar{x}}$ inside the current sheet, then Eq. (3.37) becomes

$$\frac{\theta_0}{\alpha^2 s^2}\gamma\tau_r\left(\frac{d^2u}{d\bar{x}^2} - \alpha^2 u\right) = \left(\frac{1}{\gamma\tau_R}\frac{G_0}{\bar{F}} + F\right)\left(\frac{d^2\psi}{d\bar{x}^2} - \alpha^2\psi\right) - \frac{G_0}{\bar{F}}\psi - \psi\frac{d^2F}{d\bar{x}^2} , \tag{3.44}$$

and Eq. (3.36) can be rewritten as

$$\frac{1}{\gamma \tau_R}\left(\frac{d^2\psi}{d\bar{x}^2} - \alpha^2\psi\right) = \psi + \frac{F}{\gamma \tau_R} u \ , \tag{3.45}$$

where

$$u = - i k \tau_r u_x \tag{3.46}$$

Using Eqs. (3.8), (3.10), (3.25) and (3.35), we find,

$$F \simeq \bar{x} \ , \ \frac{d^2F}{d\bar{x}^2} = 0 \tag{3.47a}$$

and

$$G_0 = - \frac{1}{4} \mu \frac{d}{dx}\left[\left(v_0^0\right)^2 \operatorname{sech}^2 \frac{x}{\epsilon_0}\right] \frac{1}{\rho}\left[-\frac{\bar{\rho}}{c_s^2}\frac{\mu}{4}\left(v_0^0\right)\frac{d}{dx}\operatorname{sech}^2\frac{x}{\epsilon_0}\right]\tau_H^2$$

$$\simeq \frac{\mu^2}{16}\left(\frac{v_0^0}{c_s}\right)^2\left(v_0^0\right)^2\tau_H^2\left[\frac{d}{dx}\left(1 - \left(\frac{x}{\epsilon_0}\right)\right)^2\right]^2$$

$$= \pi \mu^2 \left(\frac{v_0^0}{c_s}\right)^2\left(\frac{v_0^0}{\bar{V}_A}\right)^2\left(\frac{L_s}{\epsilon_0}\right)^4 \bar{x}^2 \tag{3.47b}$$

By noticing the form of Eqs. (3.8) and (3.25), we may choose $\theta_0 \simeq 1$; thus Eqs. (3.44) and (3.45) become

$$\frac{1}{\alpha_2 s_2}\gamma \tau_R \left(\frac{d^2u}{d\bar{x}_2} - \alpha^2 u\right) = (1 + \xi)\ \bar{x}\left(\frac{d^2\psi}{d\bar{x}^2} - \alpha^2\psi\right) - \xi\psi(\alpha\tau_R)\ \bar{x}, \tag{3.48}$$

$$\frac{1}{\gamma \tau_R}\left(\frac{d^2\psi}{d\bar{x}^2} - \alpha^2\psi\right) = \psi + \frac{1}{\gamma \tau_R}\ u\ \bar{x} \ . \tag{3.49}$$

with

$$\left.\begin{aligned} \xi &= \frac{d_0^2}{\gamma \tau_R} \ , \\ d_0^2 &= \pi \mu^2 \left(\frac{v_0^0}{c_s}\right)^2\left(\frac{v_0^0}{\bar{V}_A}\right)^2\left(\frac{L_s}{\epsilon_0}\right)^4 . \end{aligned}\right\} \tag{3.50}$$

In the case of highly conducting plasma medium, then we can apply $\tau_R >> 1$ and $s >> 1$; in addition if the characteristic scale length "$\bar{x}$" is much smaller inside the current sheet in comparison with any other characteristic length, then we may apply the theory of resistive ordering suggested by Dobrott et. al., (1977), thus;

$$\gamma\tau_R \sim \delta^{-1}, \quad \bar{x} \sim \delta, \quad \psi \sim 1; \tag{3.51a}$$

From the RHS of Eq. (3.48), we note,

$$\psi \sim \delta^2 u,$$

which leads to

$$u \sim \delta^{-2} . \tag{3.51b}$$

From Eq. (3.49), we find

$$\frac{1}{\alpha^2 s^2} (\gamma\tau_R) \frac{d^2u}{d\bar{x}^2} \sim \xi\psi(\gamma\tau_R) \bar{x}$$

yielding

$$s^2 \sim \delta^{-5} . \tag{3.51c}$$

From these relationships, we observed that both functions of ψ and u are proportional to δ; thus we may expand these two functions as a series of functions respectively,

$$\left.\begin{aligned} \psi &= \psi_0 + \psi_1 + \psi_2 + \cdots \\ u &= u_0 + u_1 + u_2 + \cdots \end{aligned}\right\} \tag{3.52}$$

In Eq. (3.48),

$$\frac{1}{\gamma\tau_R}\left(\psi_0'' + \psi_1'' - \alpha^2\psi - \alpha^2\psi_1' + \cdots\right) = \left(\psi_0 + \psi_1 + \cdots\right) + \frac{1}{\gamma\tau_0} \bar{x} \left(u_0 + u_1 + \cdots\right)$$

where superscript primes represent derivatives with respect to $\bar{x}$. Using the order of approximation, we note that

$$\psi_0'' \sim \delta^{-2} \ , \ \psi_1'' \sim \delta \cdot \delta^{-2} \sim \delta^{-1} \ ,$$

$$u_0 \sim \delta^{-2}, \ u_1 \sim \delta$$

which leads to

$$\psi_0'' = 0 \tag{3.53}$$

This condition gives constant -ψ approximation,

$$\psi_0 = \text{constant} \tag{3.54}$$

Based on the expansion given in Eq. (3.52), we obtained the following successive order of approxmation governing equations: the first order equation for ψ is,

$$\frac{1}{\gamma\tau_R} \psi_1'' = \psi_0 + \frac{1}{\gamma\tau_R} u_0 \bar{x} \tag{3.55}$$

Similarly, we obtained as the first order equation for u from (3.48)

$$\frac{\gamma\tau_R}{\alpha^2 s^2} u_0'' = - \xi \psi_0 (\gamma\tau_R) \bar{x} + (1 + \xi) \bar{x} \psi_1'' \ . \tag{3.56}$$

Combining Eqs. (3.55) and (3.56), we have

$$\frac{\gamma\tau_R}{\alpha^2 s^2} u_0'' - (1 + \xi) \bar{x}^2 u_0 = (\gamma\tau_R) \bar{x}\psi_0 \ , \tag{3.57}$$

From Eq. (3.55), the jump condition within the current sheet can be computed as,

$$\Delta_i' = \frac{1}{\psi_0} \int_{-\infty}^{\infty} \psi_1'' \, d\bar{x} = \frac{1}{\psi_0} \int_{-\infty}^{\infty} (\gamma\tau_R \psi_0 + \bar{x} u_0) \, d\bar{x} \ . \tag{3.58}$$

Assume that

$$u_0(\bar{x}) = \kappa h(x): \quad \bar{x} = \Sigma x \tag{3.59}$$

where

$$\Sigma^4 = \frac{\gamma\tau_R}{\alpha^2 s^2} \text{ and } \kappa = \gamma\tau_R/\Sigma. \tag{3.60}$$

Using Eqs.(3.58) - (3.60), Eq. (3.57) becomes

$$h''(x) - (1 + \xi)\, x^2 h(x) = \psi_0 x \ ; \tag{3.61}$$

Correspondingly, Eq. (3.58) becomes

$$\Delta_i' = \frac{1}{\psi_0} (\gamma\tau_R)^{5/4} (\alpha s)^{-1/2} \int_{-\infty}^{\infty} (\psi_0 + xh(x))\, dx \ , \tag{3.62}$$

Introducing the Fourier transformation,

$$h = \int_{-\infty}^{\infty} e^{-izx}\, \hat{h}\,(z)\, dz. \tag{3.63a}$$

and its inverse transformation,

$$\hat{h}(z) = \frac{1}{2\pi} \int_{-\infty}^{\infty} e^{izx}\, h(x)\, dx. \tag{3.63b}$$

Then Eq. (3.61) becomes,

$$\hat{h}''(z) - (1 + \xi)\, \hat{h}(z)\, z^2 = \frac{1}{i} \psi_0 \delta'(z), \tag{3.64}$$

where $\delta(z)$ is the Dirac Delta function; hence Eq. (3.64) reduces to

$$\hat{h}''(z) - (1 + \xi)\, \hat{h}(z) z^2 = 0, \text{ for } z \neq 0. \tag{3.65}$$

The solution of the above equation could be represented by the MacDonald function (Krall and Trielpiece, 1973).

$$\hat{h}^+(z) = A\sqrt{z}\, K_{1/4}\left((1 + \xi)^{1/2}\, z^2/2\right) \ , \ z > 0. \tag{3.66a}$$

$$\hat{h}^-(z) = -iA\sqrt{z}\, K_{1/4}\left((1 + \xi)^{1/2}\, z^2/2\right) \ , \ z < 0. \tag{3.66b}$$

The appearance of the solution (Eq. (3.66b)) is due to the consideration of the property of an odd symmetry for the RHS of Eq.

(3.64).

For the region z = 0, Eq. (3.64) becomes

$$\hat{h}'' \simeq \frac{\psi_0}{i}\,\delta'(z)$$

By integration of both sides, we have

$$2A = \frac{\left(\frac{\psi_0}{i}\right)}{H^+(z)\Big|_{z\to 0^+}} \quad , \tag{3.67a}$$

with

$$H^+(z) = \sqrt{z}\; K_{1/4}\left((1+\xi)^{1/2}\,\frac{z^2}{2}\right). \tag{3.67b}$$

Since

$$\int_{-\infty}^{\infty}\psi_0 dx = \psi_0\int_{-\infty}^{\infty}\delta(z)dz\int_{-\infty}^{\infty}dx e^{-izx} = 2\pi\psi_0\;\delta(z)\Big|_{z=0}$$

$$\int_{-\infty}^{\infty}xh(x)dx = \int_{-\infty}^{\infty}\hat{h}(z)dz\left(\frac{\partial}{\partial z}\int_{-\infty}^{\infty}ie^{-izx}\,dx\right) = 2\pi i\int_{-\infty}^{\infty}\hat{h}(z)\;\delta'(z)dz$$

$$= -2\pi\psi_0\delta(z)\Big|_{z=0} - 2\pi i\int_{-\infty}^{\infty}\hat{h}(z)\delta(z)dz,$$

$$\int_{-\infty}^{+\infty}\hat{h}'(z)\delta(z)dz = 2\int_{0^+}^{\infty}\hat{h}'(z)\delta(z)dz.$$

We finally derived

$$\Delta_i' = -2\pi\,\frac{(\gamma\tau_R)^{5/4}}{(\alpha s)^{1/2}}\;\frac{\frac{d}{dz}H^+(z)}{H^+(z)}\Big|_{z=0^+} \tag{3.68}$$

using the characteristics of the MacDonald function,

$$\frac{d}{dz}\left(z^{1/4}\,K_{1/4}\,(z)\right) = -\,z^{3/4}\,K_{3/4}(z)$$

and the asymptotic value for $|z| \ll 1$,

$$z^{\nu}K_{\nu}(z) \simeq \frac{\pi}{2}\frac{2^{\nu}}{\sin \nu\pi}\frac{1}{\Gamma(1-\nu)}, \tag{3.69}$$

with Γ being the gama function, Eq. (3.68) becomes

$$\Delta_i' = 4\pi \frac{(\gamma\tau_R)^{5/4}}{(\alpha s)^{1/2}}\frac{\Gamma(3/4)}{\Gamma(1/4)}(1+\xi)^{1/4} \tag{3.70}$$

By equating the jump conditions inside and outside the current sheet, we find the growth rate dispersion relation from Eqs. (3.43) and (3.70),

$$4\pi \frac{(\gamma\tau_R)^{5/4}}{(\alpha s)^{1/2}}\frac{\Gamma(3/4)}{\Gamma(1/4)}(1+\xi)^{1/4} = \frac{1}{2}\left(\frac{1}{\alpha} - \alpha\right). \tag{3.71}$$

This is the key equation for determining the resistive instablility.

For the illustration, we take a coronal structure of current sheet, the typical plasma and field parameters are:

$$\left.\begin{aligned} L_s &= 10 \text{ km}, \quad \bar{B} = 100 \text{ Gauss}, \\ n_e &= 10^9/\text{cm}^3, \quad T_e = 10^6 \ ^{\circ}\text{K}. \end{aligned}\right\} \tag{3.72}$$

Based on these fundamental values, we obtained Alfven speed (v_A) to be 8.4×10^7 cm/s and the sound speed (c_s) to be 2.3×10^7 cm/s. If we take $v_0^0 \sim 3.10^7$ cm/s, from Eq. (3.50b), we find that,

$$d_0^2 = 2.2 \times 10^4. \tag{3.73}$$

Correspondingly, the resistive parameters are; $\tau_R \sim 1.3 \times 10^6$ s, $\tau_H = L_s/\bar{v}_A \sim 1.2 \times 10^{-2}$ s, $s = \tau_R/\tau_H = 10^8$. Therefore, Eq. (3.71) gives

$$\gamma \sim \eta^{1/2} \tag{3.74}$$

which says that the growth rate is proportional to the square root of resistivity, such as

$$\gamma = \frac{1}{d_0^{1/2}} \frac{\alpha^{1/2} s^{1/2}}{2\pi\left(\frac{1}{\alpha} - \alpha\right)} \frac{\Gamma(1/4)}{\Gamma(3/4)} \frac{1}{\tau_R} \sim 3 \cdot 10^{-3} \ (s^{-1}). \qquad (3.75)$$

This result is based on constant $-\psi$ solution (i.e. regular homogeneous field configuration). When the reconnection process begins, the constant $-\psi$ approximation no longer becomes valid; thus, the other kind of instability may appear. We shall examine this situation in the next section.

2.4 Eruptive Local Instability

When the constant $-\psi$ approximation becomes involved, we should re-examine the set of coupling equations (i.e. Eqs. (3.48) and (3.49)). By introducing the Fourier transformation as suggested by FKR, such as,

$$\psi = \int_{-\infty}^{\infty} \hat{\psi}(\theta) e^{-i\theta\bar{x}} \, d\theta \qquad (4.1)$$

$$u = \int_{-\infty}^{\infty} \hat{u}(\theta) e^{-i\theta\bar{x}} \, d\theta \qquad (4.2)$$

into Eqs. (3.48) and (3.49), we find that

$$\frac{\gamma\tau_R}{\alpha^2 s^2} (\theta^2 + \alpha^2) \hat{u}(\theta) = (1 + \xi) \frac{d^2\hat{u}(\theta)}{d\theta^2} + i\gamma\tau_R \frac{d\hat{\psi}(\theta)}{d\theta}, \qquad (4.3)$$

$$\frac{1}{\gamma\tau_R} (\theta^2 + \alpha^2) \hat{\psi}(\theta) = -\hat{\psi}(\theta) + i \frac{1}{\gamma\tau_R} \frac{d\hat{u}(\theta)}{d\theta}. \qquad (4.4)$$

Using Eq. (4.4) to eliminate $\frac{d\hat{\psi}}{d\theta}$ in Eq. (4.3), we obtain

$$\frac{s^2}{P}\left[\xi\frac{d^2\hat{u}(\theta)}{d\theta^2}+\frac{d}{d\theta}\left(\frac{\theta^2+\alpha^2}{\theta^2+\alpha^2+P}\right)\frac{d\hat{u}(\theta)}{d\theta}\right]-\hat{u}(\theta)\left(\frac{\theta^2}{\alpha^2}+1\right)=0 \tag{4.5}$$

with

$$P=\gamma\tau_R \tag{4.6}$$

It is worth noting that the Eq. (4.5) is identical to the Eq. (5) of FKR by setting $\xi = 0$, which implies that $\gamma\tau_R \to \infty$ or $d_0 \to 0$. Physically, this corresponds to a very thin current sheet and a high resistive region. Under the present case, we have

$$\frac{\alpha^2}{P}=\sigma << 1; \tag{4.7}$$

hence Eq.(4.5) can be written as

$$\xi\frac{d^2\hat{u}(\theta_2)}{d\theta_1^2}+\frac{d}{d\theta_1}\left(\frac{\theta_1^2+\sigma}{\theta_1^2+1}\frac{d\hat{u}(\theta_1)}{d\theta_1}\right)=A(\theta_1^2+\sigma)\hat{u}(\theta_1)\ . \tag{4.8}$$

with

$$\theta_1 = P^{-1/2}\ \theta \text{ and } A = P^3/\alpha^2 s^2 \tag{4.9}$$

Eq. (4.8) is the equation to be used to determine the solution $\hat{u}(\theta)$ and subsequently ψ will also be determined by Eq. (4.4). Finally, the growth rate for the non-constant-ψ-solution could be found.

In order to seek the solution for Eq. (4.8), we introduce the following parameters:

$$\hat{\theta}=\frac{\theta_1}{\sigma^{1/2}}=\frac{\theta}{\alpha}\ . \tag{4.10}$$

Since $\alpha = \frac{L_s}{L_y} << 1$, thus, $|\hat{\theta}| >> 1$. In this limiting case, Eq. (14.8) becomes $\bar{x} \to \pm\infty$,

$$\frac{\xi}{\sigma}\frac{d^2\hat{u}}{d\hat{\theta}^2} + \frac{d}{d\hat{\theta}}\left[(1 + \hat{\theta}^2)\frac{d\hat{u}}{d\hat{\theta}}\right] - A\sigma(\hat{\theta}^2 + 1)\,\hat{u} = 0 \qquad (4.11)$$

For $\xi > 1$, we have

$$\frac{\xi}{\sigma} >> \frac{\theta_2^1}{\sigma} \simeq \hat{\theta}^2$$

Eq. (4.11) gives

$$\frac{\xi}{\sigma}\frac{d^2\hat{u}}{d\hat{\theta}^2} + 2\hat{\theta}\frac{d\hat{u}}{d\hat{\theta}} - A\sigma(\hat{\theta}^2 + 1)\,\hat{u} = 0 \qquad (4.12)$$

The above differential equation can be simplified by the following transformation

$$\hat{u}(\hat{\theta}) = \exp\left(-\frac{\sigma}{2\xi}\hat{\theta}^2\right) w(\hat{\theta}) \,, \qquad (4.13)$$

so that, Eq. (4.12) reduces to

$$A_0\frac{d^2w}{d\hat{\theta}^2} - (B_0 + \hat{\theta}^2)\,w = 0 \qquad (4.14)$$

where

$$\left.\begin{aligned} A_0 &= \frac{\xi^2}{\sigma^2}(\xi A + 1)^{-1} \\ B_0 &= \frac{\xi(1 + A\sigma)}{\sigma(\xi A + 1)} \,. \end{aligned}\right\} \qquad (4.15)$$

Eq. (4.14) can be simplified further by introducing

$$y = \frac{\sqrt{2}}{A_0^{1/2}}\hat{\theta} \,, \qquad (4.16)$$

so that the final form of Eq. (4.14) is

$$\frac{d^2w}{dy^2} + (g + 1/2 - 1/4\ y^2)w = 0 \tag{4.17}$$

where,

$$g + \frac{1}{2} = - \frac{B_0}{2A^{1/2}}\ , \tag{4.18}$$

It is well known that Eq. (4.17) has the solution of a parabolic cylindrical function thus,

$$w = D_g(y) \tag{4.19}$$

when $g = -1$, $D_g(y)$ satisfies the following boundary condition;

$$D_g(y) \to 0, \text{ as } |y| >> 1. \tag{4.20}$$

Thus,

$$D_{-1}(y) = \sqrt{\frac{\pi}{2}}\ \exp\left(\frac{1}{4}\ y^2\right)\left(1 - \phi\ (y/\sqrt{2})\right) \tag{4.21}$$

Where $\theta(y)$ is the probability integral, its asympotic value becomes

$$1 - \phi(y/\sqrt{z}) = \frac{1}{\pi}\ e^{-y^2 z} \sum_{m=0}^{n-1} \frac{(-1)^m \Gamma(m+1/2)}{\left(\frac{1}{2}\right)^{m+1/2}\ y^{2m+1}} \qquad |y| >> 1\ , \tag{4.22}$$

Returning to Eq. (4.12) for $g = -1$ implies

$$\frac{B_0}{A_0^{1/2}} = 1\ . \tag{4.23}$$

or $$(1 + A\sigma)^2 = (1 + \xi A) \tag{4.24}$$

Using Eq. (4.24) together with Eqs. (4.7), (4.9) and (3.50), we we found the growth rate for non-constant $-\psi$ to be

$$\gamma = \frac{1}{\tau_H}\left(\frac{d_0^2}{\alpha^2} - 2\right)\ . \tag{4.25}$$

2.5 Numerical Results

In order to illustrate our theoretical results, we have chosen a coronal structure of a current sheet plasma for testing. The typical physical parameters for this kind of plasma and field are given in Eqs. (3.72) and (3.74), which leads to $\gamma = 3 \times 10^{-3}\ s^{-1}$ for the constant $-\psi$ case. As a result we use the very same values for Eq. (4.25), yielding $\gamma \simeq 1.2 \times 10^{5}\ s^{-1}$ for the non-constant $-\psi$ case. It is immediately reconized that the growth rate between these two kinds of instability has a 10^7 order of magnitude. Thus we can conclude that the constant $-\psi$ case leads to a resistive instability of slow time-scale phenomena and the non-constant $-\psi$ case leads to a much faster time-scale phenomena called "eruptive instability". Physically, we may claim that when a magnetized plasma begins its dissipation in an orderly fashion through resistive instability, the inbedded field is rather uniform. As soon as the field configuration is distorted, the energy release can be more violent because of eruptive instability.

2.6 Concluding Remarks

In this paper we have presented a theoretical result concerning the transition of resistive instability to eruptive instability with pondermotive force with high-frequency plasma ossicillations. It shows that the constant $-\psi_A$ (i.e. uniform field configuration) leads to resistive instability and that the non-constant $-\psi$ case leads to eruptive instability. The close form solutions based on plasma and field parameters are given for these two cases.

A numerical example is also given showing that the growth rate for these two cases can be different in 10^7 orders of magnitude for the solar corona structure of the current sheet.

3 ANALYSIS OF INSTRUMENTAL POLARIZATION OF IMAGING OPTICS

3.1 Introduction

The objective of the SAMEX magnetograph's optical system is to accurately measure the polarization state of sunlight in a narrow spectral bandwidth over the field of view of an active region to make an accurate determination of the magnetic fields in that region. Our design goal is to measure magnetic fields to an accuracy of one part in 10^4. To achieve this accuracy requires a polarimetric accuracy of 10^{-4} in determining the polarization components of the light as a fraction of the total intensity. This requirement means that the instrumental polarization of the optics must be reduced to levels below 10^{-5}.

All optical elements introduce some polarization change, especially when used off axis. Combinations of mirrors and antireflection-coated lenses can display a full range of polarization behavior: linear and circular polarization and linear and circular retardance. Of particular concern in the development of highly accurate polarimeters is polarization rotation which causes linearly polarized light to leak through subsequent of crossed polarizers.

Because of this instrumental polarization, the SAMEX foreoptics (the optical elements in front of the polarizer - the Cassegrain telescope and the relay lenses) must be considered as a weak polarizer in front of the polarimeter section. This instrumental polarization in the foreoptics changes the polarization state of the sunlight incident on the polarimeter

and thus introduces errors in the measurement of the solar magnetic field.

If possible, it would be preferable to place the polarimeter before the imaging optics, to locate polarizers and retarders in front of the Cassegrain telescope. Then the determination of the polarization state of light would be unaffected by the instrumental polarization of the foreoptics. This design would have the additional advantage of allowing the light to pass through the polarimeter over a smaller range of angles of incidence. However, such a design is impractical for a system with a 30 cm aperture - high quality polarizers and retarders have much smaller apertures, on the order of a few centimeters. Thus, it is necessary to use collecting optics to collect the 30 cm aperture of light and focus it through small polarizing elements in the polarimeter section. As the collected light is passed through smaller apertures, the angular spectrum of the light increases in a relationship governed by the Lagrange invariant. By reducing the beam from 30 cm to 2 cm through the tunable filter and polarimeter, the range of angles of incidence is increased by a factor of 15, from 5 min of arc to 75 min of arc, thereby increasing the angle of incidence effects in the lenses just in front of the polarimeter and in the polarimeter itself. Consequently we anticipate there will be some instrumental polarization due to the foreoptics in the light entering the polarimeter.

The goal of the analyses outlined in this section is to precisely characterize the extent of this instrumental

polarization, and to design the optics and coatings in unison to minimize this spurious polarization introduced by the foreoptics. We will show calculations of the instrumental polarization of ordinary foreoptics compared with the polarization performance of special ultra-low polarization optical coatings designed for this application.

The instrumental polarization analysis uses a program tha incorporates the theory of polarization into the standard geometrical optics and lens design codes (Chipman, 1987). By including the polarization of the optical elements in the first- and third-order design process, the effects of coatings on curved substrates can be treated. For each ray, a polarization matrix (in the Jones matrix formulation) is calculated for the ray at each optical interface. These matrices are multiplied together to calculate the polarization matrix for that ray from object space to image space. An analytic function for the rays provides the polarization behavior as a function of the exit pupil, object height, and wavelength. This technique represents a quantum jump improvement in the practical design of foreoptics in front of a polarimeter and will enable the degree of residual instrumental polarization to be reduced to $< 10^{-5}$ in the SAMEX magnetograph system.

3.2 Instrumental Polarization of Standard Cassegrain Telescopes

To establish the need for a detailed polarization analysis, we estimate the polarization effects associated with a Cassegrain telescope with aluminum thin film coatings. The

electric vector of light incident on a surface of the Cassegrain can be decomposed into two parts, the components of the vector vibrating parallel (p) and perpendicular (s) to the plane of incidence. These components have different reflections as a function of the angles of incidence. Figure 23.a shows the reflectance for s and p polarized light from an aluminum thin film coating with complex index of refraction $n = 0.7 - 7.0\,\tilde{i}$. Figure 23.b shows the phase change on reflection for the s and p components. The difference in s and p reflectance causes a weak linear polarization aligned perpendicular to the plane of incidence to be associated with reflection from all metallic interfaces. Moreover, the differences in phase change cause a weak linear retardance to be associated with reflection from mirrors.

The percent reflections from the aluminum surface for the surface parallel (s) and surface perpendicular (p) rays are approximately given by

$$R_s = 0.94 + 0.02i^2,$$

and

$$R_p = 0.94 - 0.02i^2,$$

where the reflectance rate of change per unit angle of incidence squared (i^2) is approximated from Figure 23.a. Therefore, the induced linear polarization is estimated to be

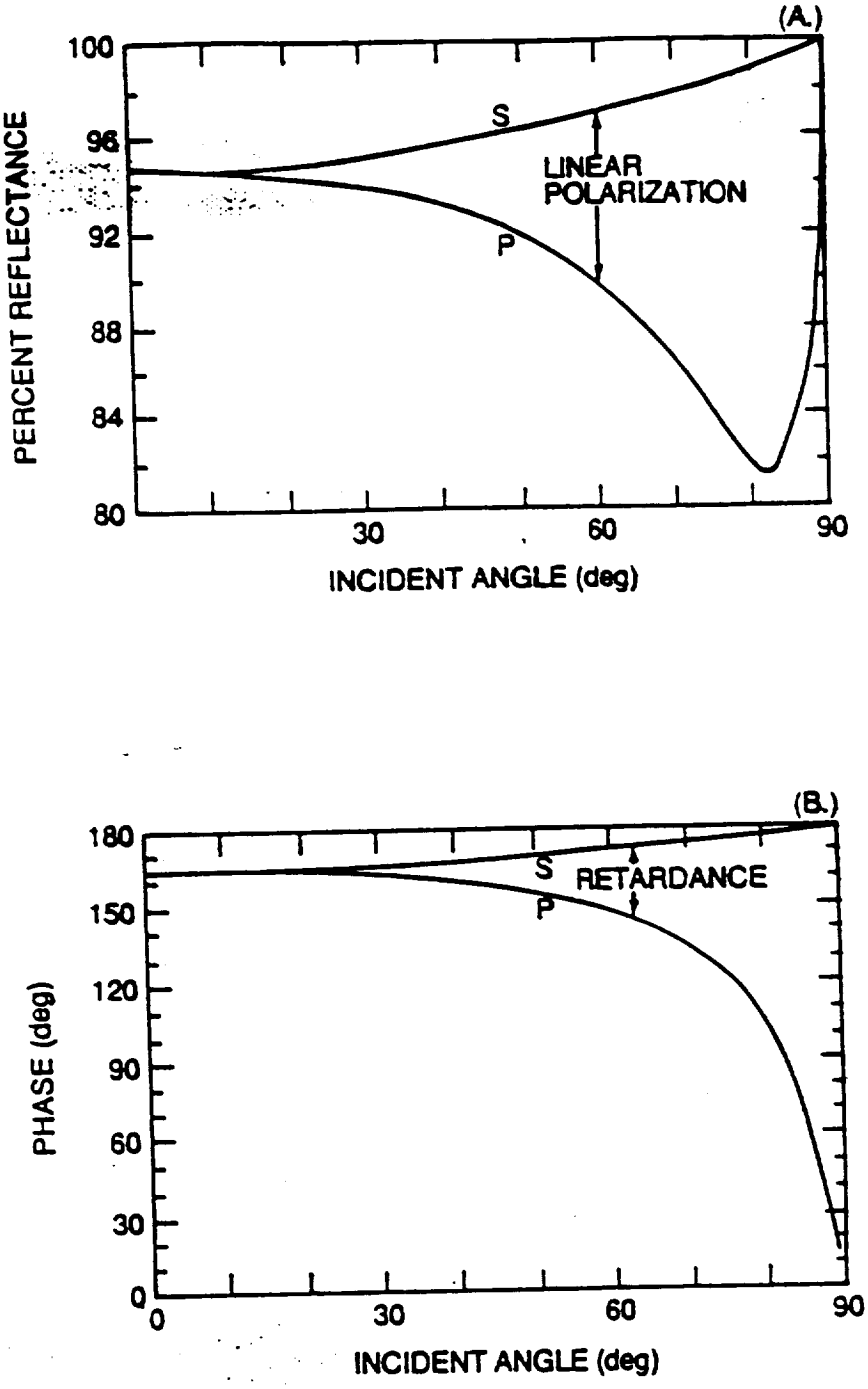

Figure 23. Linear polarization and retardance effects for a Cassegrain telescope. The percent reflectance (a) and phase change (b) on reflection from an aluminum thin-film coating is shown for both the s and p components of the incident light wave. The wavelength of the light is 5250 Å and the complex refractive index of the aluminum coating is n = 0.7 - 7.0 $\tilde{\imath}$. The differences in the s and p reflectance cause linear polarization aligned with the incident plane. The differences in the s and p phase cause a linear retardance. The differences are small for small angles of incidence, but they are not negligible for the SAMEX magnetograph design.

$$L_p = \frac{R_s - R_p}{R_s + R_p} \approx 0.02 i^2.$$

At the edge of the primary mirror of aperture D and focal length fl, a ray is reflected through a total angle of tan(D/fl) ~ D/fl = 1/f, where f is the f-ratio. Then for a Cassegrain telescope the maximum angle of incidence i_m is given approximately by one half the reciprocal of the f-ratio. For an f-ratio of 5, the angle of incidence is i_m=1/10. Hence the induced linear polarization is on the order of $\frac{0.02}{100} = 2 \times 10^{-4}$. For a linearly polarized ray this represents a rotation of its plane of polarization over a segment of the mirror, and this rotation introduces errors in the deduced polarization state. In Figure 24 the angle of incidence versus the pupil coordinate for an 'illustrative' Cassegrain telescope is shown for an on-axis and off-axis ray. The point to note is that, for the off-axis ray, the average angle of incidence is not zero, and hence there is a net polarization effect associated with the off-axis rays. Furthermore, even on-axis, we average over the square of the incident angle which gives a net polarization contribution, as shall be discussed below.

For an on-axis beam incident on either of the aluminum coated Cassegrain telescope mirrors, the magnitude and orientation of the linear polarization and linear retardance associated with the mirrors have the forms shown in Figure 25.a (polarization) and Figure 25.b (retardance) as a function of the pupil coordinates. In Figure 25.a, the linear polarization is

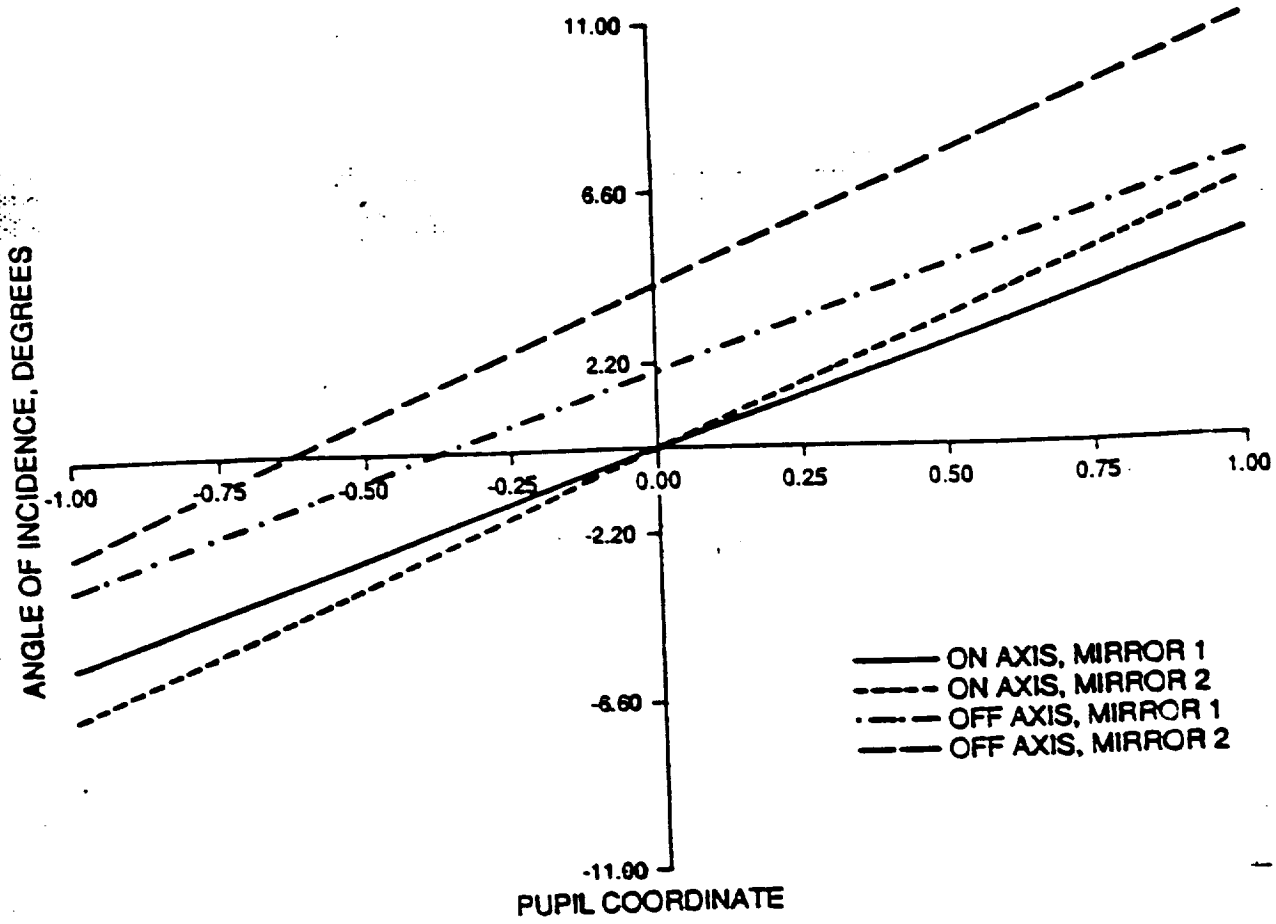

Figure 24. Illustrative example of angles of incidence at Cassegrain mirrors. These curves show the variations of the angle of incidence along the normalized pupil coordinate for on-axis and off-axis rays incident on both the primary and secondary mirrors of a Cassegrain system. The off-axis rays have a non-zero average angle of incidence at both the primary and secondary mirrors. This implies a net linear polarization associated with the telescope for off-axis rays. The example shown here is for a Cassegrain with a larger field of view than the one chosen in the SAMEX design. It was chosen to provide a vivid example of the off-axis problem.

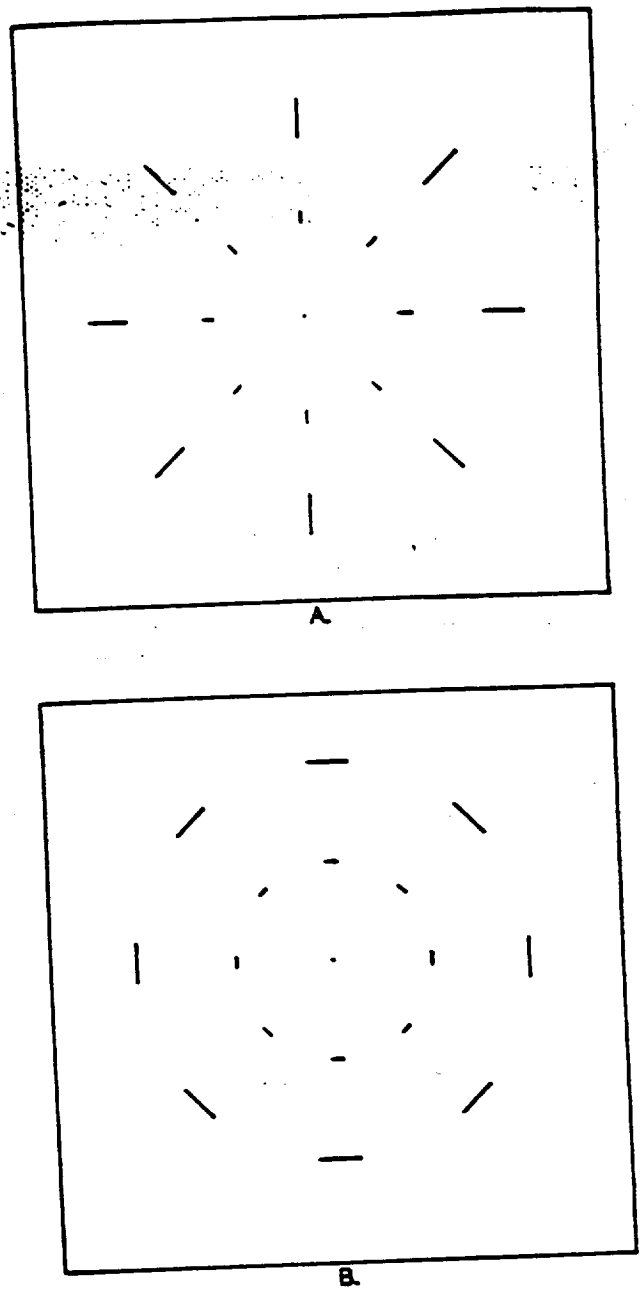

Figure 25. Patterns of linear polarization and retardance for a Cassegrain telescope. The linear polarization pattern (a) and linear retardance pattern (b) associated with an aluminum-coated Cassegrain primary mirror are shown for an on-axis beam. In (a) the magnitude and orientation of the linear polarization are given as linear segments. In (b) the linear segments represent the magnitude and fast-axis orientation of the retardance. Both patterns are quadratic functions of the pupil coordinate and are termed "polarization defocus."

zero in the center of the mirror where the beam is at normal incidence. The magnitude of the linear polarization (polarizance) increases quadratically with distance from the center of the mirror. The linear polarization is oriented tangentially. This polarization pattern (polarization aberration) is called linear polarization defocus (or quadpol). Figures 26.a and 26.b show the effect of large amounts of linear polarization defocus (about 40 times more than the conventional Cassegrain) on beams of uniform left-circularly polarized light (a) and uniform, vertical-linearly polarized light (b). The linear polarization associated with the telescope mirrors changes the polarization state of the light causing spatial variations of intensity and polarization across the beam. If the polarization state of the light is now measured with a polarimeter, a polarization state different from that incident on the mirrors is obtained. Despite the symmetry associated with the resulting transmitted polarization patterns (such as in Figure 26), the polarization variations do not cancel (due to averaging over the incident angle squared). This is best understood by considering the transmitted light as being a superposition of two polarization states: the incident state yields the correct polarization measurement; the light in the orthogonal state constitutes the error signal introduced by the instrumental polarization.

For example, in the case of Figure 26.b, the light in the orthogonal state (horizontal linear polarization) has the form across the pupil shown in Figure 27. Although the phases of this horizontal component are 180° out of phase in the four

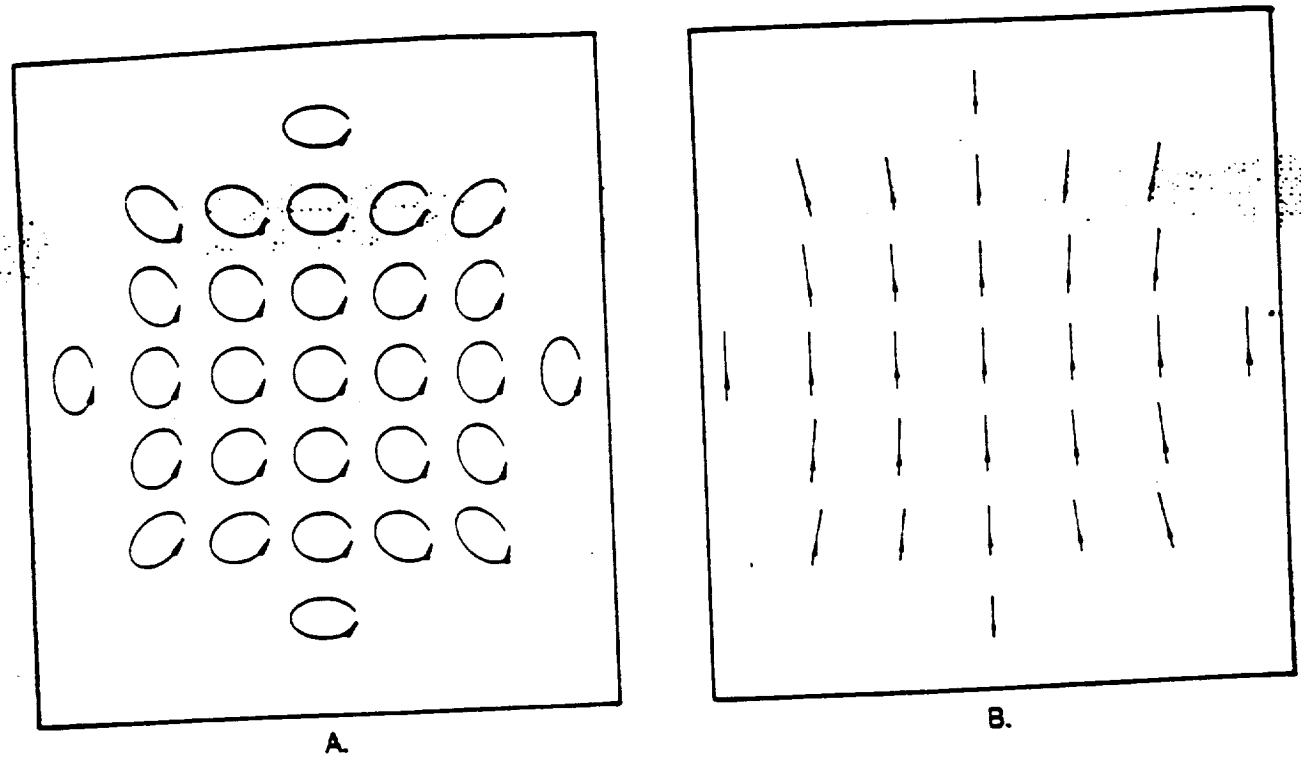

Figure 26. Linear polarization defocus effects for a Cassegrain telescope. This figure illustrates linear polarization defocus effects for a Cassegrain primary mirror for a beam of (a) uniform left circular polarization and of (b) uniform vertical linear polarization. The ellipses and arrows at the top, bottom, left, and right of the diagram represent the same relative position of the polarization ellipse of the reflected beam of a Cassegrain mirror with an exceptionally large field of view (40X the normal Cassegrain field). The location of the arrowheads represents the phase of the light where one cycle is a full wave. The defocus effect introduces the orthogonal state of polarization which represents an error signal introduced by the instrumental polarization in the measurements made with the magnetograph.

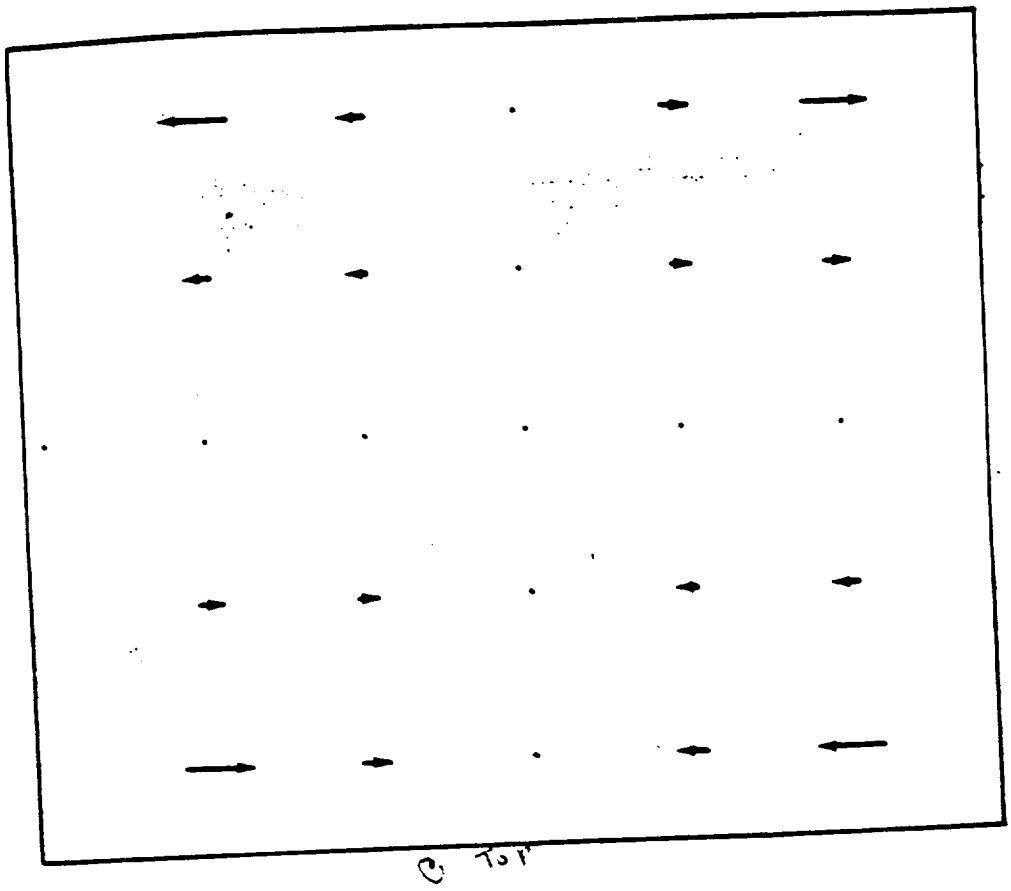

Figure 27. Polarization errors associated with a Cassegrain telescope. This figure illustrates the orthogonal state of polarization introduced by the instrumental polarization of a Cassegrain mirror for the incident linear (vertical) polarization of Figure 26 b. These horizontal components will pass through the linear polarizer of a magnetograph's polarimeter when it is in the horizontal position and thereby contribute to the error signal of the magnetograph.

quadrants (resembling astigmatism), all this light will pass through a horizontal linear polarizer and contribute to the polarization error signal. The phase differences do not cause cancellation of the polarization aberration; instead they affect the polarization accuracy and change the structure of the diffraction pattern (Kubota and Inoue, 1959).

For a metallic mirror, the effects of the linear retardance are orders of magnitude larger than the effects of the weak linear polarization. Figure 25.b shows the form of the linear retardance associated with an on-axis beam incident at a Cassegrain telescope mirror. The orientations of the lines represent the orientation of the fast axis of the retardance. The lengths of the lines signify the magnitude of linear retardance, which increases quadratically with pupil coordinate. This polarization aberration is called linear retardance defocus or quadtard. Figures 28.a and 28.b show the effect of quadtard on a uniform left-circularly polarized beam (a) and on a uniform, vertical-linearly polarized beam (b). The dominant effect of the retardance is a coupling of linear into circular polarized light and vice versa. These figures are for retardances about 40 times greater than the retardance of a conventional Cassegrain.

In general, a Cassegrain telescope displays both these polarization aberrations simultaneously, linear polarization defocus and linear retardance defocus, with the retardance being the larger term. This polarization aberration induces polarization coupling which reduces the accuracy of subsequent polarimetric measurements. The polarization coupling for a

SAMEX-type Cassegrain design but with standard aluminum coatings is 3×10^{-3}, almost two orders of magnitude greater than the radiometric accuracy of the optics. Similar amounts of polarization accuracy would be associated with relay optics utilizing standard antireflection coatings.

3.3 The SAMEX Design

It is clear from the discussion of the previous section that standard optical designs will not suffice for the SAMEX foreoptics because they produce unacceptable levels of instrumental polarization. The design of the SAMEX foreoptics resulted from the development of a new method for the analysis of instrumental polarization based on the theory of "polarization aberrations." This theory allows the description of the variations of amplitude, phase, and polarization of an optical wavefront across the exit pupil of an optical system. Because the theory naturally incorporates the polarization properties of the thin film coatings on the individual surfaces of the optical system, this method integrates the coating design with the lens design. In ordinary optical design work, these two phases of the design are normally decoupled and pursued separately.

This unified optical and coating design was performed for the SAMEX foreoptics to insure that the SAMEX magnetograph will accurately measure the polarization state of incident sunlight. To improve the SAMEX polarization accuracy over standard designs, various telescope and lens coatings were investigated. Most standard reflection-enhancing coatings for telescope mirrors were found to be substantially worse than the

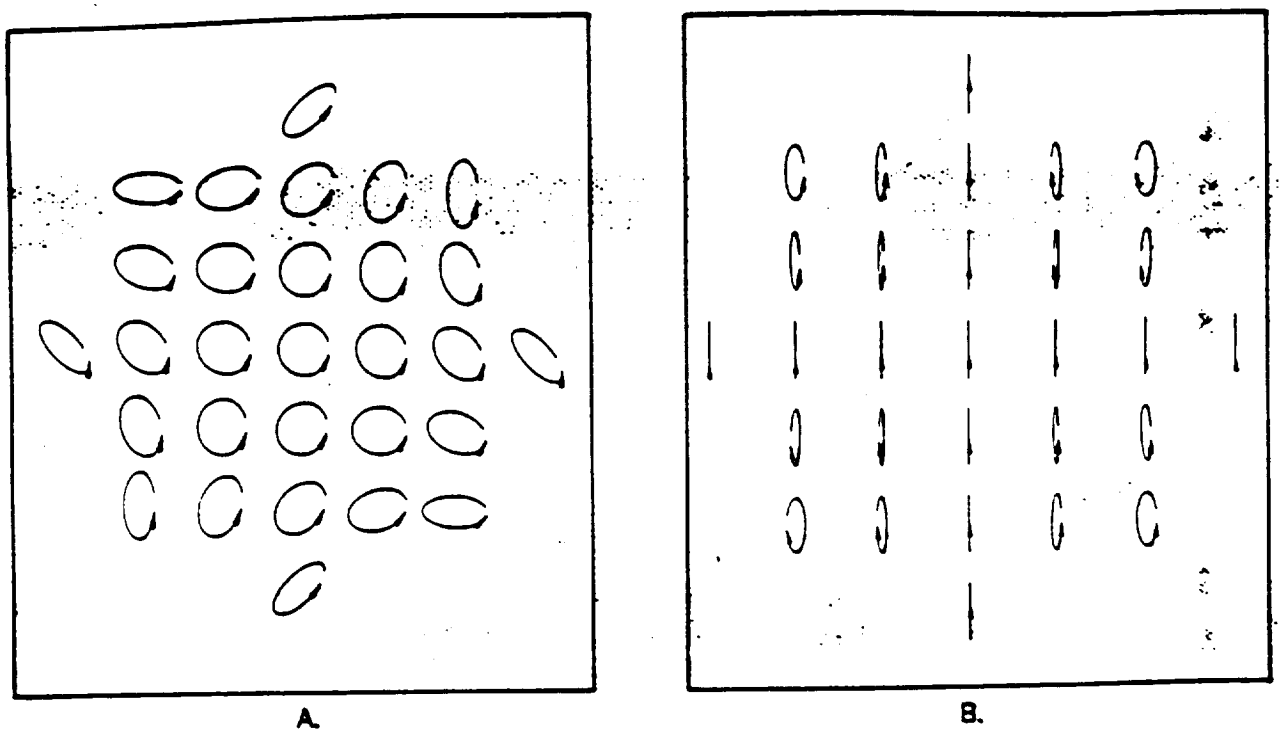

Figure 28. Linear retardance effects associated with a Cassegrain telescope. The large effect of linear retardance from a Cassegrain mirror is shown for (a) a beam of uniform left circular polarization and for (b) a beam of uniform linear (vertical) polarization. The dominant effect of linear retardance is a coupling of linear polarization into circular and vice versa.

bare aluminum. Two coatings were designed which had significantly improved polarization performance for a telescope. These coatings are described in the section on coatings (section 3.6). Figure 29 shows the linear polarization (a) and linear retardance (b) associated with a Cassegrain telescope when these coatings are utilized and when ordinary aluminum coatings are used, as a function of the height of the ray entering the telescope, from top to bottom. The amount of polarization or retardance for the three coating choices is plotted along the y-axis for (1) two aluminum coated mirrors, (2) two Q201 coated mirrors, and (3) one Q201 coated mirror and one eight-layer enhanced-reflection coating. The third design (3) balances polarization and retardance effects of opposite signs between the two mirrors to achieve a polarization performance superior to either mirror separately.

Similar design strategies have been used with the relay lenses to achieve significant improvements over conventional coatings and to balance the remaining polarization effects. As a result, the overall polarization performance for the foreoptics has been improved by a factor of ten thousand relative to conventional designs. Thus the actual attainment of the polarimetric sensitivity determined by the SAMEX requirements will presumably be limited only by whatever scattering effects are present, and not by the instrumental polarization of the optics.

The method used to achieve this dramatic result - polarization aberration theory - is outlined briefly in sections

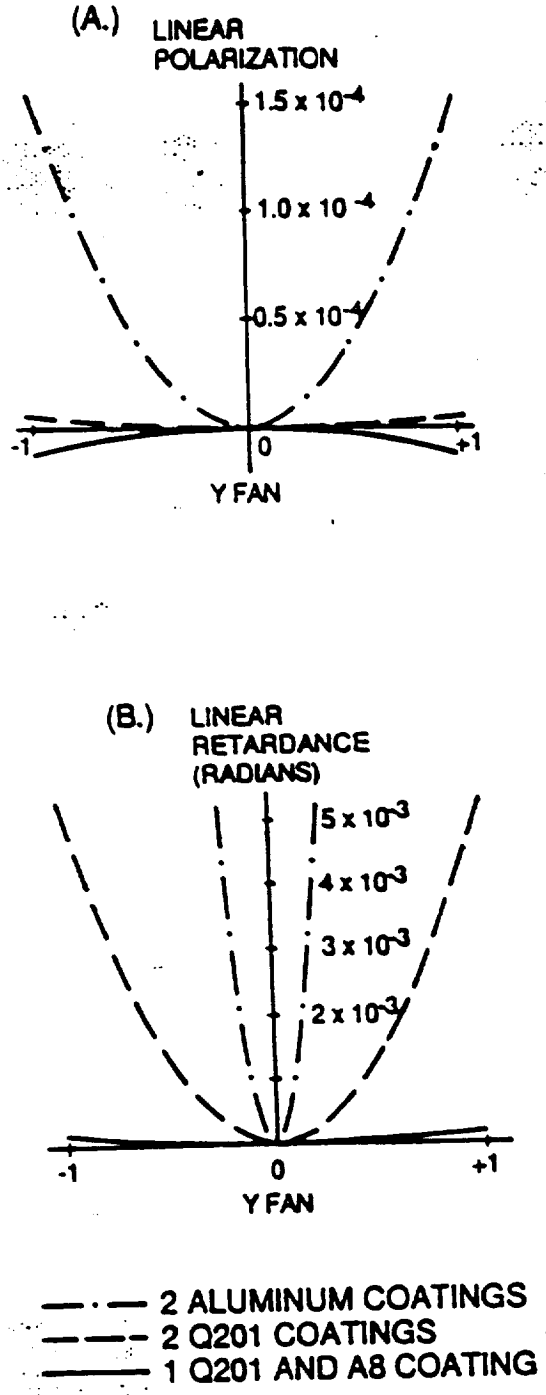

Figure 29. Instrumental polarization effects for rays through a Cassegrain telescope. Linear polarization (a) and retardance (b) as a function of pupil coordinate in a Cassegrain telescope are plotted for three different sets of reflective coatings on the primary and secondary mirrors. The three sets of coatings are: (1) two aluminum (dot-dash curve), (2) two Q201 coatings (dashed curve), and (3) one Q201 and one aluminum (solid curve). The Q201 interference coating is a 201 coating of bi-layers with high ($n = 1.52$) and low ($n = 1.45$) refractive indices.

3.4 and 3.5 and expanded upon in Appendix C. A full development of the method is given in Chipman (1987). The basic results from the method are the second-order polarization aberration coefficients which provide a quantitative measure of the polarization accuracy of any optical system. Specifically, these coefficients determine the parameter Δ_p, the polarization accuracy, defined as the maximum fraction of light which can be coupled into an orthogonal polarization state. It is given in terms of the second order polarization aberration coefficients P(1,0,2,2), P(1,1,1,1), and P(1,2,0,0):

$$\Delta_p < P(1,2,0,0)^2 + \frac{1}{2} P(1,1,1,1)^2 + \frac{1}{3} P(1,0,2,2)^2 .$$

For the SAMEX magnetograph foreoptics and coating design given herein, the value of

$$\Delta_p < 1.4 \times 10^{-7}$$

was obtained. For standard coatings of aluminum, the polarization accuracy is

$$\Delta_p = 2.7 \times 10^{-3}$$

for a Cassegrain telescope alone (no relay lenses). (The second order aberration coefficients used in these calculations are given in Table 19.) This result for Δ_p means we have achieved our design goal: the polarization state of the light from the

Sun can be determined without introducing polarizing effects from optical elements in the system. We have been able to effectively eliminate the problem of induced instrumental polarization in the SAMEX foreoptics.

3.4 Polarization Aberration Theory

The SAMEX foreoptics are intended to transmit all polarization states equally. But all optical interfaces display some polarization when used at non-normal incidence. Thus polarization is present in all systems at some level. If the system is intended to be nonpolarizing, the instrumental polarization is often termed "residual polarization" to signify its generally undesirable character. Residual polarization might be compared to wavefront aberration because both interfere with the measurement of optical fields and reduce the image forming potential of the optical system.

The principal cause of instrumental polarization in the optical systems of present solar magnetographs is the polarization due to non-normal incidence at the optical interfaces and coatings. Since each ray takes a different path through the system with its own angles of incidence and planes of incidence, each ray in general experiences a different change in its state of polarization. This residual polarization varies with wavelength, object coordinates and pupil coordinates. "Polarization aberrations" will be defined as variations of the amplitude, phase and polarization of an optical wavefront across

the exit pupil of an optical system and the dependence of these variations on wavelength and object coordinate. The polarization aberrations are extensions of the wavefront aberrations and encompass both amplitude and polarization variations, thus providing a more complete characterization of the electromagnetic fields transmitted by an optical system.

Vacuum-deposited thin films are used on most optical surfaces to control the amount of transmission and reflection. These thin films are usually less than the wavelength of light in thickness. Being so very thin, the effect of the films on ray paths are accurately modeled by treating the films as having parallel surfaces which contour the substrates on which they are deposited. Due to the closely spaced parallel surfaces, thin films have negligible influence on the ray paths through the system and are generally ignored when simulating a system by ray tracing. These coatings principally affect the amplitude and polarization of the ray and have much less effect on the optical path difference. This division, with the optical surfaces governing the ray paths and the thin film coatings governing the amplitude and transmission, allows the optical system design problem to neatly decouple into two separate problems, lens design and coating design. The wavefront performance and image quality of the system is calculated by a lens designer using a ray tracing optical design program. The amplitude and polarization calculations at individual surfaces are performed using a thin film design program.

This decoupling of optical design and coating design has usually worked well. The coatings designed to optimize the transmittance or reflectance at an interface have usually reduced the amplitude and polarization variations and thus reduced the polarization aberrations at the interface as well. For example, a quarter-wave magnesium fluoride antireflection coating on glass typically reduces reflection losses at the design wavelength by a factor of four, and reduces the instrumental polarization by a comparable factor. This fortuitous circumstance has allowed lens and coating design to remain relatively uncoupled. Thus instrumental polarization was usually ignored as a higher order effect. But it is not sufficient to design thin film coatings in isolation from the lens design for the SAMEX magnetograph - the demands on amplitude and polarization performance are too great.

For the designs of the SAMEX system special methods have been developed to calculate the instrumental polarization of the SAMEX foreoptics. These methods are described in detail in Appendix C. Calculating the instrumental polarization requires performing thin film calculations during the ray tracing process. This idea is not new, but its implementation is complex enough to have delayed this obvious integration of these two branches of optical design until specifications required it.

In this new methodology, a Jones polarization matrix is calculated for arbitrary optical paths through the optical system and includes the effects of all the specified optical coatings on the curved optical interfaces. The specific technique used for this calculation is the method of "polarization aberrations."

This is a method analogous to the aberrations of geometrical optics (spherical aberration, coma, astigmatism, etc.) except that it encompasses the polarization effects of coatings as well as the wavefront aberrations.

The analysis of the SAMEX optics proceeds in several stages and is summarized in Table 16. First, the optical system is designed using the CODE V optical design program to optimize the optical design for a spatial resolution with a minimum aperture. During this phase the angles of incidence are kept as small as possible to reduce polarization effects from coatings. Second, special thin-film, reflection-enhancing coatings are designed for the telescope mirrors and special antireflection coatings are designed for the lenses because conventional coating designs show significant polarization and retardance contributions near normal incidence. These coatings are special designs which reduce the polarization effects at small angles of incidence over the wavelength band of the magnetograph. Next, a Taylor series is calculated to represent the coating performance. Finally, the effect of these coatings in the magnetograph optical design is calculated using the polarization aberration method; this last step produces the parameter Δ_p, the polarization accuracy.

Table 16. Steps in Instrumental Polarization Simulation

1.	Design optical system using CODE V.
2.	Design low polarization, high reflectivity telescope coatings.
3.	Design low polarization, antireflective lens coatings.
4.	Determine Taylor series representation of coating performance.
5.	Calculate polarization aberration coefficients of optical system.
6.	Calculate Δ_p.
7.	Iterate 2, 3, 4, 5, 6 until satisfactory performance is achieved ($\Delta_p < 10^{-5}$).

In the following section, the method for deriving the polarization aberration coefficients and the polarization accuracy Δ_p is outlined in more detail.

3.5 Polarization Aberration Coefficients and Polarization Accuracy

The polarization states of the electromagnetic field are described by the complex two-component Jones vector, $\vec{J}$. The polarization states and hence the Jones vector are transformed when a ray passes through an optical interface which is described by the Jones matrix transformation JJ. For the SAMEX foreoptics we have homogeneous, weakly polarizing optical elements (by design) for which the transmission coefficients perpendicular, t_s, and parallel, t_p, are given in terms of a Taylor series expansion of the angles of the chief and marginal rays, i_c and

i_m, respectively. Each individual optical ray path for the rotationally symmetric system can be defined in terms of the object height, H, and the pupil coordinants, ρ and ϕ as defined in Figure 30. The cascade effect of an optical train is given by the product of the individual Jones transformation matrices for each element interface. Then the overall polarization of the foreoptics is described by the complex Jones transformation matrix which is expanded in terms of the ray coordinates (ρ, ϕ, and H) and the basis matrix set $\sigma(k)$:

$$JJ = \sum_{k=0}^{3} \sum_{u} \sum_{v} \sum_{w} P(k,u,v,w)\ H^{u}\ \rho^{v}\ \cos^{w}(\phi)\ \sigma(k)$$

where P(k,u,v,w) are the expansion coefficients. The 2 by 2 matrices, $\sigma(k)$, which define the k^{th} polarization state, are the identity matrix and the Pauli spin matrices. This expansion is in the same form as the standard wavefront aberration expansion. These polarization expansion coefficients for an expansion to second order (specified by s = 2) in the angles of incidence are a function of the total optical transmission, τ, the normalized secondard order basis set coefficients, d(k,s,q), for each individual optical element, q, and the angle of incidence of the chief and marginal rays. Hence these coefficients are dependent on the characteristics of the optical coatings and the ray tracing results. These SAMEX specifications are given in Table 19a-c.

The polarization aberration expansion for the radially symmetric system of interfaces with isotropic coatings and

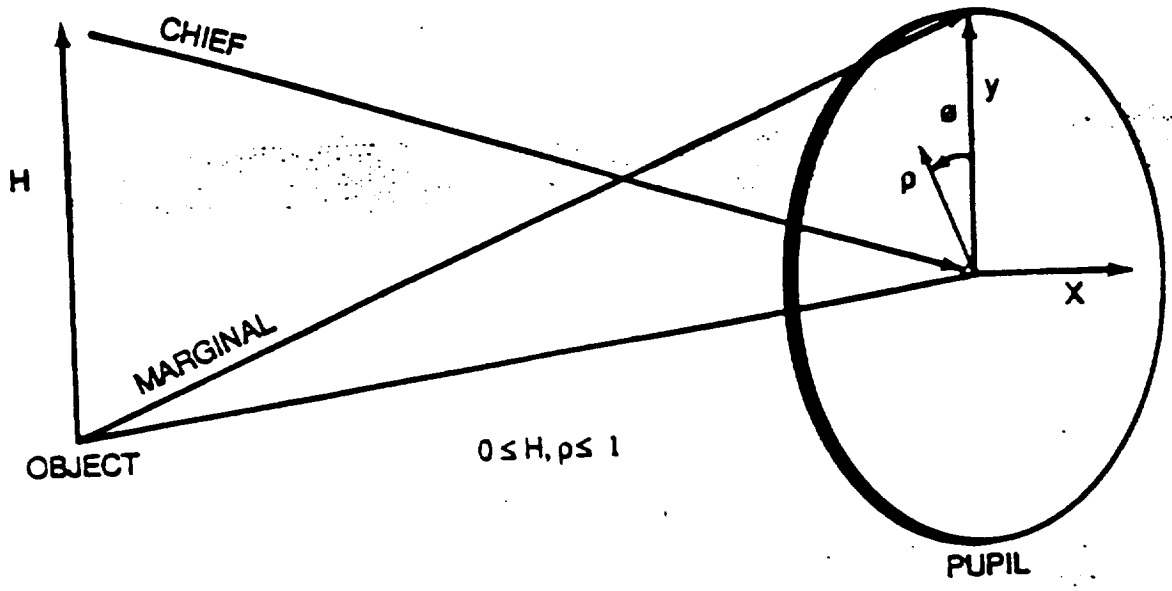

Figure 30. Paraxial coordinate system. The paraxial system is a normalized right-handed coordinate system. The z axis is the optical axis of a rotationally symmetric optical system; light initially travels in the direction of increasing z. Rays through an optical system are characterized by ray coordinates at the object and entrance pupil. H is the normalized object coordinate, ρ is the normalized pupil radius, and φ is the polar angle in the pupil measured counterclockwise from the y axis. The normalized Cartesian coordinates in the pupil are x and y. The chief and marginal rays are also shown.

nonpolarizing transparent media is given to second order in the angles of incidence by the polarization aberration expansion

$$JJ(H,\rho,\phi) = \tau[\sigma_0 + P(1,2,0,0)H^2\sigma_1 + P(1,1,1,1)H\rho(\sigma_1\cos\phi - \sigma_2\sin\phi) + P(1,0,2,2)\rho^2(\sigma_1\cos 2\phi - \sigma_2\sin 2\phi)].$$

The amplitude a_{ijkl} of the polarization aberration coefficient $P(i,j,k,l)$ describes the magnitude of the polarization aberration effects while the phase δ_{ijkl} of the coefficient describes the magnitude of the retardances. Then, given a specific incident polarization state, the polarization state of the exit beam can be calculated from this matrix. Therefore the amount of polarization in the orthogonal state can be determined. This orthogonal polarization in the exit beam then determines the accuracy Δ_p of the polarization measurement.

As an example of the coupling of the optics to an orthogonal state of polarization, i.e., polarization crosstalk, consider the following example. The on-axis linear polarization and linear retardance of the SAMEX foroptics, i.e., the term linear defocus, is described by the fourth term in the polarization aberration expansion JJ. The instrumental polarization function $J_d(H,\rho,\phi)$ for linear defocus is then

$$JJ_d(H,\rho,\phi) = \tau[\sigma_0 + P(1,0,2,2)\rho^2(\sigma_1\cos 2\phi - \sigma_2\sin 2\phi)] = \tau[\sigma_0 + (a_{1022} + \tilde{\imath}\delta_{1022}\rho^2(\sigma_1\cos 2\phi - \sigma_2\sin 2\phi)],$$

where τ is the amplitude of transmittance of the system down the optical axis. The transmittance (τ) describes the polarization independent reflection and absorption losses associated with the ray down the optical axis. P(1,0,2,2) describes the linear polarization (a_{1022}) and linear retardance (δ_{1022}) associated with the marginal ray.

At any given point in the pupil, the eigenenpolarizations are linearly polarized light, oriented radially, $\hat{J}_r$, and tangentially $\hat{J}_t$. This concept is important to the definition of polarization accuracy which is to be defined. We shall now calculate for circular and linear incident polarize light to illustrate of the effect of crosstalk.

Maximum coupling occurs when the incident light is circularly polarized, since circularly polarized light can always be decomposed into equal components of $\hat{J}_r$ and $\hat{J}_t$ everywhere in the pupil. The coupling is zero in the center of the pupil (where the polarization and retardance vanish) and increases to a maximum coupling at $\rho = 1$ of

$$I_{C,max}(H,1,\phi) = |P(1,0,2,2)|^2 = a_{1022}^2 + \delta_{1022}^2$$

at the edge of the pupil. The net fraction of incident circularly polarized light coupled into the orthogonal circularly polarized state, I_C^1, is given by the integral over the pupil,

$$I_C^1 = \frac{1}{\pi} \int_0^{2\pi} d\phi \int_0^1 \rho d\rho \left| \rho^2 P(1,0,2,2) \right|^2,$$

$$= \frac{|P(1,0,2,2)|^2}{3}.$$

If we have a Stokes vector of +V then the amount of polarization in the orthogonal state -V can be calculated. If -V is the maximum amount of crosstalk, we identify this as the polarization accuracy.

For incident linearly or elliptically polarized light, the fraction of coupled intensity is less because the light is not composed of equal fractions of eigenstates. The coupling is minimum for incident linearly polarized light, which will be in one of the eigenpolarizations along one axis in the pupil and in the orthogonal eigenpolarization along the orthogonal axis. Here the fraction of coupled energy will be calculated assuming an incident polarization state of horizontal linearly polarized light $\hat{H}$ for calculational simplicity; the same fraction is coupled for any linearly polarized incident state. The orthogonal state of vertical linearly polarized light is designated as $\hat{V}$. The polarization state transmitted by an optical system described by linear polarization defocus for $\hat{H}$ is

$$\vec{J}(H,\rho,\phi) = \tau[\hat{H} + P(1,0,2,2)\rho^2(\hat{H}\cos 2\phi - \hat{V}\sin 2\phi)].$$

The fraction of incident $\hat{H}$ light coupled into $\hat{V}$ light is equal to

$$I_c^2 = \frac{1}{\pi}\int_0^{2\pi} d\phi \int_0^1 \rho d\rho \left|\vec{J}(H,\rho,\phi)\cdot\hat{V}\right|^2$$

$$= \frac{1}{\pi}\int_0^{2\pi} d\phi \int_0^1 \rho d\rho \left|P(1,0,2,2)\rho^2 \sin 2\phi\right|^2$$

$$= \frac{|P(1,0,2,2)|}{\pi} \int_0^{2\pi} \sin^2 2\phi d\phi \int_0^{1_5} \rho \, d\rho$$

$$= \frac{|P(1,0,2,2)|^2}{6} .$$

Therefore, we defined the polarization accuracy, Δ_p, as the maximum fraction of light which can be coupled into orthogonal polarization states. The incident polarized state is given by the Jones vector, $\vec{J}$. This vector is rotated by the optical system and the rotation is given by the Jones matrix, JJ. The amount of polarization along the orthogonal state of polarization, $\vec{J}'$, of the incident polarization state is given by the projection of JJ(J) into $\vec{J}'$. i.e.

$$JJ(\vec{J}) \cdot \vec{J}' .$$

The maximum projection is used in defining the polarization accuracy. In the above example $I_c^1 > I_c^2$, and only I_c^1 is retained for the linear defocus term, P(1,0,2,2). This value is given by the square of the second order Jones matrix and is given in terms of the polarization aberration coefficients. Then the polarization accuracy is given in terms of the second order polarization abberation coefficients P(1,0,2,2), P(1,1,1,1), and P(1,2,0,0):

$$\Delta_p = \frac{1}{\pi} \int |JJ_2(1,\rho,\phi)|^2 \rho d\rho d\phi$$

or

$$\Delta_p \leq |P(1,2,0,0)|^2 + \frac{1}{2}|P(1,1,1,1)|^2 + \frac{1}{3}|P(1,0,2,2)|^2,$$

where the integrations have been carried out for the squared terms and estimated for the crossed terms as being less than or equal to the direct product terms. For the SAMEX magnetograph design, the value for the polarization accuracy,

$$\Delta_p < 1.4 \times 10^{-7}$$

is obtained for specially selected optical coatings. These second order aberration coefficients are given in Table 19. The second order coefficients are sufficient since the next order that contributes is the fourth order and their polarization effects would be on the order of $(\Delta_p)^2$. In the following section we discuss the process used to design these special optical coatings.

Table 19-a. Table of Total Second Order Polarization Aberration Coefficients for the SAMEX Magnetograph Given the Individual Surface Components of Table 19-b

---

Vector Quadratic Piston:

$$P(1,2,0,0) = \sum_q d(1,2,q)\ i_c^2(q)$$
$$= -7.72\times10^{-5} - \tilde{\imath}\ 1.50\times10^{-4} \text{ radians}^2$$

Vector Tilt:

$$P(1,1,1,1) = 2 \sum_q d(1,2,q)\ i_c(q)\ i_m(q)$$
$$= -1.42\times10^{-5} - \tilde{\imath}\ 2.70\times10^{-5} \text{ radians}^2$$

Vector Defocus:

$$P(1,0,2,2) = \sum_q d(1,2,q)\ i_m^2(q)$$
$$= -1.91\times10^{-5} + \tilde{\imath}\ 1.80\times10^{-4} \text{ radians}^2$$

Table 19-b. Surface by Surface Polarization Aberration Contributions Given Surfaces as Defined in Table 19-c

z	Vector Quadratic Piston $d(1,2)\ i_c^2(q)$ Re	Vector Quadratic Piston $d(1,2)\ i_c^2(q)$ Im	Tilt Vector $2\ d(1,2)\ i_c(q) i_m(q)$ Re	Tilt Vector $2\ d(1,2)\ i_c(q) i_m(q)$ Im	Vector Defocus $d(1,2)\ i_m^2(q)$ Re	Vector Defocus $d(1,2)\ i_m^2(q)$ Im
1	8.3e-10	8.4e-7	-3.9e-8	-3.9e-5	1.8e-6	1.8e-3
2	-1.1e-8	-1.3e-6	3.9e-7	4.6e-5	-1.4e-5	-1.7e-3
3	-4.7e-7	-1.1e-6	4.4e-7	5.8e-7	-1.3e-7	-3.0e-7
4	1.1e-5	-2.6e-5	-3.1e-6	-7.5e-6	-9.1e-7	-2.2e-6
5	-4.9e-6	-1.2e-5	3.6e-7	8.5e-7	-2.6e-8	-6.1e-8
6	-1.3e-6	0	-2.3e-6	0	-3.8e-7	0
7	-5.1e-6	-1.2e-5	-1.4e-6	-3.4e-6	-4.1e-7	-9.8e-7
8	-2.8e-5	-6.6e-5	-2.3e-6	-5.5e-6	-1.9e-7	-4.6e-7
9	-1.3e-5	-3.1e-5	-1.5e-6	-3.6e-6	-1.7e-7	-4.2e-7
10	-1.1e-8	1.1e-6	5.1e-8	-4.9e-6	-2.3e-7	-2.2e-5
11	-5.7e-7	0	1.2e-6	0	-2.7e-6	0
12	-1.1e-6	-2.7e-6	1.3e-6	3.1e-6	-1.5e-6	-3.6e-6

Note: The surface numbers S(i) are related to the surface numbers q by S(i) = q + 2, i.e. q=1 is the primary mirror and the prefilter is not considered. The notation 8.3e-10 means 8.3×10^{-10}.

Table 19-c. The Surface Definitions for the Polarization Aberration Coefficient Calculations

Surface q	Optical Coating	Paraxial Angle $i_c(q)$	Paraxial Angle $i_m(q)$	Second Order Polarization** Re	Second Order Polarization** Im	Magnitude of 2nd Order Polarization
1	ref1201	0.00134	-0.06250	2.82e-7*	2.84e-4	2.8e-4
2	layers8onAl	0.00236	-0.08519	-1.20e-6	-1.39e-4	1.4e-4
3	v10c5256	0.03862	-0.02031	-1.90e-7	-4.53e-7	4.9e-7
4	"	0.18664	0.05388	"	"	"
5	"	0.12576	-0.00908	"	"	"
6	kf9fk5	-0.30317	-0.05091	-8.91e-8	0.0	8.9e-8
7	v10c5256	-0.12743	-0.03622	-1.90e-7	-4.53e-7	4.9e-7
8	"	-0.29808	-0.02495	"	"	"
9	"	-0.20326	-0.2363	"	"	"
10	v10c525	-0.00703	0.03169	-1.38e-7	1.33e-5	1.3e-5
11	kf9fk5	-0.06243	0.13588	-8.91e-8	0.0	8.9e-8
12	vc10c5256	-0.5980	0.06974	-1.90e-7	-4.53e-7	4.9e-7

*(2.82e-7 = 2.82×10^{-7})

**The rate of linear polarization (Re) and retardance (Im) per angle of incidence squared (deg^{-2}) for the specified optical coating.

3.6 Coating Designs

A design study was performed to find coatings especially suitable for use in the SAMEX magnetograph. First, many conventional coatings were examined and found to have polarization and retardance properties that make them unacceptable for use in the SAMEX magnetograph. Alternative coating designs were devised with improved polarization performance and the best of these were specified for the instrumental polarization simulation. Coatings were designed, optimized and analyzed using two thin film coating programs: FTG Software's Filmstar and Prof. A. Macleod's (University of Arizona) FILMS.

The requirements for the SAMEX magnetograph coatings are the following:

1) They must have extremely low polarization properties near normal incidence so that they introduce a minimum of polarization or retardation into the optical system. Specifically, the differences between the s and p amplitude coefficients for reflection or transmission for less than 10° angle of incidence should be 0.01% and the phase difference should be less than 0.05°.

2) The system's transmission must not be compromised by the coatings: reflective coatings should reflect > 99.9% and transmission coatings transmit > 99.7%.

3) They must be manufacturable and not be excessively costly.

4) The amount of scattered light should be small.

5) They should have reasonable tolerances for fabrication.

Several common reflecting coatings for telescopes and antireflecting coatings for lenses were analyzed and found to be inadequate for the SAMEX magnetograph. For example, telescopes are frequently coated with bare aluminum coatings (Al) or quarter-wave stacks on top of aluminum. These coatings have very little linear polarization near normal incidence but substantial amounts of linear retardance. The common antireflection coatings for lenses (quarter-wave MgF_2 and broadband antireflective coatings) have very little retardance near normal incidence but substantial linear polarization.

Three coatings (see Table 20) have been selected from our coating design study for inclusion in the SAMEX magnetograph design. The polarization effect of these coatings has been used in the instrumental polarization simulation. These coatings demonstrate that coatings with the necessary low polarization performance can be designed. The present coatings are somewhat sensitive to fabrication errors and are very wavelength sensitive. The designs would benefit from further work to understand why they work, knowledge which should lead to fully optimized designs with improved manufacturing tolerances.

Table 20 contains the description of the three coatings specified. In addition, the optical system contains two cemented interfaces, between kf9 glass and fk5 glass, specified kf9fk5. The polarization of this interface, although negligible, was included in the instrumental polarization calculation.

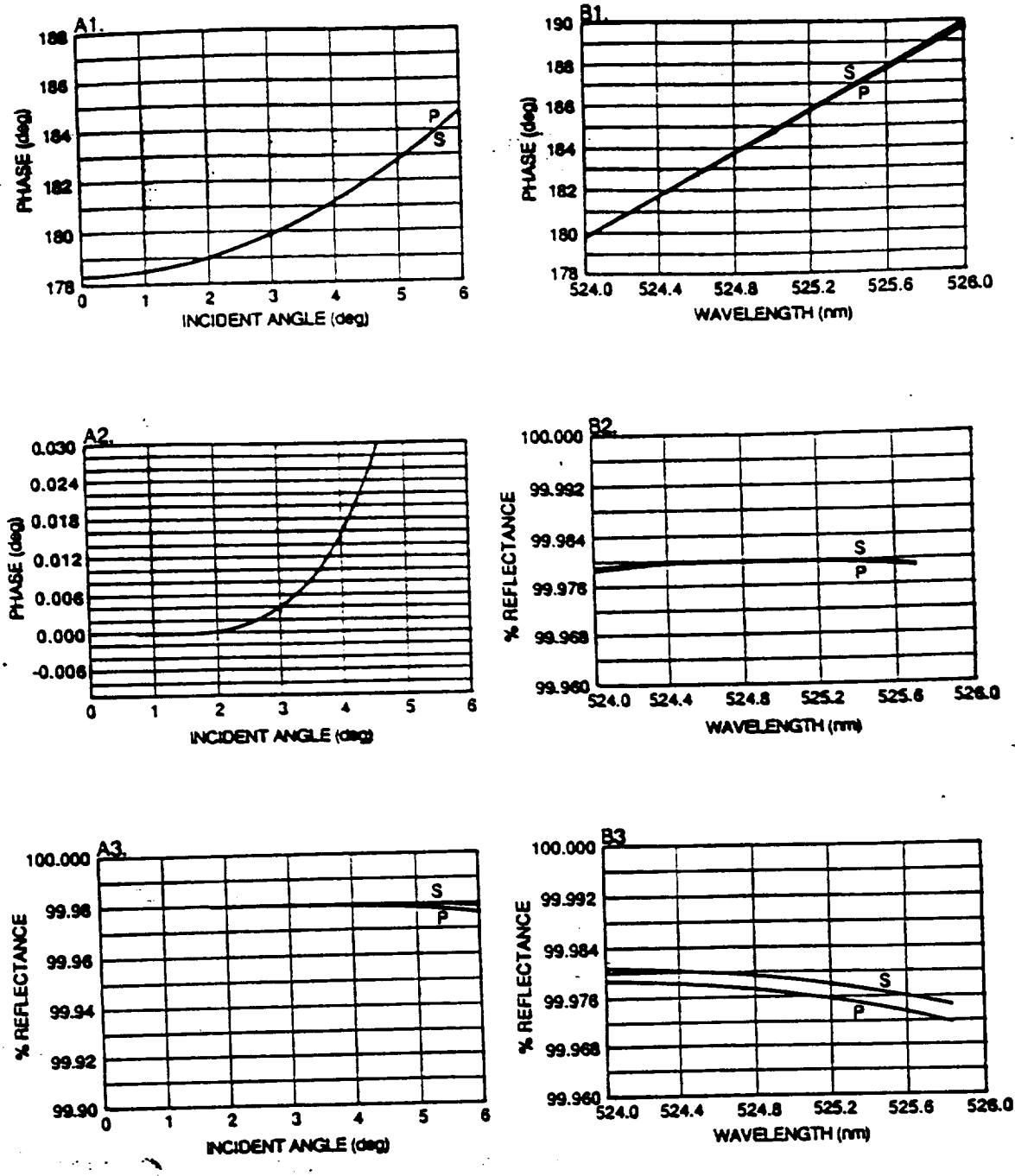

Figure 31. Optical properties of the interference coating Q201. The phase and reflectance properties of the interference coating Q201 designed for the SAMEX telescope mirrors are shown as functions of the angle of incidence (A, on the left) and wavelength (B, on the right). (A1) The phase of a reflected beam is shown as a function of the angle of incidence. The s and p components of an incident wave of wavelength 5250 Å are shown as one curve. (A2) The difference in phase of the s and p components shown in (A1) is plotted as a function of the angle of incidence. (A3) The % reflectance of a 5250 Å reflected wave is shown as a function of the angle of incidence. (B1) The phase of the reflected wave is plotted as a function of wavelength. (B2) The percent reflectance of a wave incident at an angle of 2° is shown as a function of wavelength. (B3) The percent reflectance of a wave incident at an angle of 6° is shown as a function of wavelength.

The coating Q201 is a 201-layer, quarter-wave enhanced reflection coating specified for the primary mirror. The philosophy behind this design is that the polarization effects arise because of large refractive index differences between layers. This coating uses two materials with a small index difference, fused silica at n=1.45 and evaporated glass at n=1.52. To achieve the desired reflection performance with smaller index differences requires more layers, 201 in this case. The materials chosen are both amorphous and thus quite suitable for coatings with large numbers of layers, since they don't display the microcrystalline growth patterns which lead to the unacceptable scattering and inhomgeneity associated with crystalline materials. Figure 31 shows performance curves for Q201 both as a function of angle of incidence and wavelength. Figure 31.a-1 shows the absolute phase change on reflection for the s and p components. The quadratic portion of these curves is the defocus introduced by the coating. The parameter of greatest interest is the retardance, the difference between the s and p phase changes; it is plotted separately in 31.a-2. This retardance is below 0.1° over the angles of incidence of importance. Figure 31.a-3 shows the s and p intensity reflectance as a function of angle of incidence. The difference between the s and p reflectance is the linear polarization, here less than 0.01%.

The coating specified for the secondary, L8onAl, is a more conventional 8-layer, reflection-enhancing coating specially optimized to complement the Q201 coating. This coating has the

opposite sign on both its linear polarization and retardance relative to Q201. Thus the small residual polarizations of these two coatings tend to cancel, resulting in a nearly polarization free Cassegrain design.

The coatings specified for the lens surfaces are a two-layer coating of the V coating family of designs. A region of solution was found with the remarkable property that the linear polarization and linear retardance both changed signs within 50 nm in wavelength of each other. Thus, by varying the thicknesses of the layers, low polarization coatings with several different useful properties were obtained. The two scalings used in the design were 1.0 for the coating v10c525 and 1.06 for vc105256. These coatings have by far the lowest polarization effects of any lens coatings investigated. Fabricating and testing samples of these coatings should be conducted in the next study phase.

Table 20. Coatings Specified for the Magnetograph.

Name	Type	Number of Layers	Polarization Magnitude	Reflectance or Transmission	Coating Design
V10C525	Antireflection	2	4.9e-7	99.7%	(.25H .25L)100 .254H H=1.52 L=1.45
Q201 .82L)	Reflective	201	2.8e-4	99.98%	(.062H H=2.15 L=1.38
L8onAl .25L)2	Reflective	9	1.4e-4	99.65%	.38H .29L .26H .25L (.25H H=2.38 L=1.38

All the polarization analyses of thin films performed here have assumed ideal, thin-film structures, materials which are uniform, isotropic, homogeneous and free from scattering. This is a sufficient assumption for the design and analysis of the thin films. Actual thin films possess extremely complex microstructure which contributes to scattering, inhomogeneity and anisotropy. The typical thin film microstructure is an array of columns growing up out of the substrate. This causes nonideal coating properties which will impair the performance of the system at some level.

The performance of the SAMEX magnetograph will be enhanced by using the finest coatings available, which will probably be deposited using ion-assisted thin film deposition. By bombarding the growing thin film with energetic ions, usually helium or argon, the growing thin film structure is pressed down and becomes denser (Martin, 1986). This disrupts the growth of the large columnar structures which are responsible for much of the scattering and anisotropy. The resulting films have lower scatter and greater uniformity. The ion-assisted thin film deposition technique is still new and not yet widespread in its use.

As part of the preliminary efforts leading to the actual fabrication of the SAMEX magnetograph, test coatings need to be prepared and coating vendors qualified. Several coating manufacturers should be contracted to produce small (2 x 2 inch) samples of the specified coatings. These coatings should be

tested for spectral transmission, polarization performance and scatter (bidirectional reflection measurements) as part of the final design and vendor qualification. The Marshall Space Flight Center and the University of Alabama in Huntsville Center for Applied Optics have the expertise for such coating characterization. These data would then be used to calculate the impact of the stray light coming from the coating scatter on the magnetic field accuracy of the magnetograph.

3.7 Further Sources of Instrumental Polarization

Two effects that could degrade the polarization performance of the SAMEX optics are coating anistropy and scattered light. Coating anisotropy is the variation of refractive index with direction in the coating. Coating anisotropy can be measured ellipsometrically. It frequently occurs where coatings have been deposited at non-normal incidence. Most coatings have a columnar microstructure which usually grows out of the substrate toward the source. For a nonnormal deposition angle, the resulting coatings have builtin birefringence. For the magnetograph optical design, this additional coating-induced retardance is a problem which must be held to acceptable levels in the final coatings. A level of anisotropy below a root sum squared birefringence of 0.0001 radians rms per coating is highly desirable.

Scattering depolarizes light: the scattered light is random and carries less information about its original polarization state. Coatings, because of their detailed microstructure, may

display substantial scattering. Considerable effort is being devoted on many approaches to producing optics with reduced scatter, including the ion-assisted deposition coatings already mentioned. Scattering in the coatings of the foreoptics will probably be the limiting factor in the accuracy of the magnetograph, now that the instrumental polarization of the Cassegrain telescope has been reduced by orders of magnitude.

3.8 Optical Tolerances

An optical tolerance study of the magnetograph is outside the scope of this study. However we would like to point out the areas of special study that are needed for a flight instrument.

The individual optical components need to be qualified for spaceflight. This would include operation under a vacuum for an extended period of time. The effects of particle radiation over the lifetime of the spacecraft must be resolved. The mechanical robustness of the optical system is to be defined. This would include the effect of thermal drift on the optical alignment. The general effects of mechanical fitting and sensitivity due to fabrication errors need to be addressed, including surface figure, tilts, decentrations, and optical coating variations. The overall alignment and calibration procedures are to be specified before the optical design is completed (Yoder, 1986).

4. CONCLUDING REMARKS

In this study we conclude theoretically, that the electromagnetic soliton in a current sheet could trigger the resistive instability for an uniform magnetic field configuration, which eventually turns in an eruptive instability at the onset of the magnetic field reconnection. Therefore, we may consider this physical scenario which could be a candidate for solar flare triggering mechanism. Experimentally, we presented an analysis of instrumental polarization of imaging optics. This optical system cold accurately measure the polarization state of sunlight in a narrow spectral bandwidth over the field view of an active region to make an accurate determination of the magnetic field in the region.

REFERENCES

Benz A. O.: 1986, Solar Physics 104, No. 1, 99.
Dobrott D., Prager, S. C. and Taylor, J. B.: 1977, Phys. Fluids 20, 1850.
Furth H. P., Killeen, J. and Rosenbluth, M. N.: 1963, Phys. Fluids 6, 459.
Hasegawa A.: 1975, Plasma Instabilities and Nonlinear Effects, New York.
Krall, N. A. and Trivelpiece A. W.: 1973, Principles of Plasma Physics, McGraw-Hill.
Landan, L. D. and Lifshitz, E. M.: 1960, Electrodynamics of Continous Media, p.61, Pergamon, Oxford.
Li Xiao-qing: 1985, Astrophys. Space Sci. 112, 13.
Pikel'ner, S. B. and Kaplan S. A.: 1978, Radiophys. Qu. Electron. 20, 904.
Priest E. R.: 1986, Solar Physics 104, No. 1, 1.
Shivamoggi, B. K.: 1985, Physics Reports 127, 99.

APPENDIX

POLARIZATION ABERRATION THEORY

Introduction

This appendix describe the method which have been developed to calculate the instrumental polarization of the SAMEX optics. A full development of the method is contained in "Polarization Aberrations" by Chipman (1987). The calculation requires performing thin film calculations during the optical design process to determine the two parts (eigenvectors) of an optical beam, as a function of the object and pupil coodinates.

The mathematical method of treating instrumental polarization will be first discussed in terms of the Jones and C-vectors and then the polarization aberration expansion will be derived.

The Jones Matrix and C Vector for the Characterization of Polarization

The most efficient mathematical method for treating the SAMEX instrumental polarization is the Jones calculus. The Mueller calculus is a more difficult representation which includes optical depolarization (scatters) properties. Such weak depolarization effects are more readily handled by experimential measurements. The Jones calculus (Jones 1941a-c,1942,1947, Azzam and Bashara 1977, Theocaris and Gdoutos) is a mathematical formalism for treating problems involving the description of polarized light and polarizers which uses the Jones vector for

the description of polarized light and the Jones matrix to characterize the polarizing properties of an optical element. The details of the following discussion are given by Chipman (1987). The elements of the Jones matrix and the C vector characterization are outlined first.

Definition of the Jones Vector in terms of the Electric Field Amplitudes

The Jones vector expression for the a quasi-monochromatic plane wave propagating parallel to the z axis with electric field amplitude

$$E(t) = E_x(t) + E_y(t) \quad ,$$

where,

$$\hat{E}_x(t) = \hat{n}_x \, E_{0,x}(t) \cos[(kz-wt) + e_x] \quad ,$$

and,

$$\hat{E}_y(t) = \hat{n}_y \, E_{0,y}(t) \cos[(kz-wt) + e_y] \quad ,$$

where $\hat{n}_x$ and $\hat{n}_y$ are direction unit vectors in the x and y direction with the light propagation in the z direction. There are 4 parameters $E_{0,x}$, $E_{0,y}$, e_x, and e_y defining the wave beside the wavelength.

The time dependent Jones vector is defined in terms of the electric field amplitudes as,

$$J(t) = \begin{bmatrix} E_x(t) \\ \\ E_y(t) \end{bmatrix} .$$

The components of J(t) are the instantaneous components of E(t).

The normalized Jones vector J is a time independent normalized vector where all the vector components of J(t) have been divided by the incident electric field amplitude,

$$J = J(t)/E_o(t) .$$

The normalized Jones vector is referred to as "the Jones vector" unless otherwise stated. Knowledge of J and E_o provides all the information necessary to reconstruct E(t) to within a constant phase factor.

Table C-1 lists the Jones vectors for the most common polarization states: horizontal linear, vertical linear, +45 degrees linear, -45 degrees linear, right circular and left circular polarized light. These vectors can be multiplied by an arbitrary phase factor without changing the polarization ellipse of the light; it only changes the absolute phase.

Having established the vector which defines the polarization state we now consider the matrices which represent the polarization effect of the optical elements and allow polarization calculations to be performed.

Table C-1. The Basic Jones Vector Representation for Linear and Circular Polarized Light

Linear Polarized Light			
Horizontal	Vertical	+45 Degrees	-45 Degrees
$\begin{vmatrix} 1 \\ 0 \end{vmatrix}$	$\begin{vmatrix} 0 \\ 1 \end{vmatrix}$	$s \begin{vmatrix} 1 \\ 1 \end{vmatrix}$	$s \begin{vmatrix} 1 \\ -1 \end{vmatrix}$
Circular Polarized Light			
Right Circular		Left Circular	
$s \begin{vmatrix} 1 \\ -i \end{vmatrix}$		$s \begin{vmatrix} 1 \\ i \end{vmatrix}$	
where $s = \frac{\sqrt{2}}{2}$			

In his original paper, Jones (1941a) shows that the relationship between the Jones vector incident on a polarizer, $\vec{J}$, and that transmitted or reflected by a polarization element, J', can always be related by a matrix, the Jones matrix, JJ. Only certain transformations of the field components are allowed, those describable by a matrix. Thus the fundamental relationship between the vector components of the electromagnetic fields before and after a polarizing element is,

$$J' = JJ\ J$$

The Jones matrix, JJ, is a two by two matrix with complex elements,

$$JJ = \begin{vmatrix} j(1,1) & j(1,2) \\ j(2,1) & j(2,2) \end{vmatrix}$$

where $j(k,l) = a(k,l) + i\ b(k,l)$.

Thus the Jones matrix has eight degrees of freedom. Thus there are eight different forms of polarization behavior. These eight forms are listed in Table 2E. Every Jones matrix corresponds to a physically realizable polarizer.

Sequences of Polarizers

The Jones matrix associated with an optical ray path through a sequence of polarization elements is just the matrix product of the Jones matrices for the individual polarizers. If an optical ray traverses a series of elements, 1, 2, ... Q, and the Jones matrices appropriate to that ray for each element are, JJ(1), JJ(2), ... JJ(Q), then the Jones matrix describing the polarization properties of the system along this ray path is given by the matrix product,

$$JJ = JJ(Q) \ldots JJ(2)\ JJ(1)$$

Since the Jones matrix of an optical element is dependent upon the wavelength, angle of incidence, orientation, and path through the element, each ray in each wavelength will usually have a different Jones matrix. Only if a collimated monochromatic beam through a series of planar optical interfaces can be assumed, then a single Jones matrix can be written for the entire cross section of the beam. This is the case in the polarimeter section of the magnetograph but not in the foreoptics.

Coordinate System

The Jones matrix is defined relative to an arbitrary x and y coordinate system. Since these coordinates have been defined for the Jones vector, the coordinate system of the Jones matrix is defined in terms of the Jones vector coordinates.

It is often desirable to align the Jones vectors coordinates with the s and p planes of an optical interface. Only for plane surfaces does the orientation of the s and p planes remain fixed across the surface. For nonplanar surfaces, it is necessary to maintain two sets of coordinates, the global x and y coordinates with respect to which the Jones matrix is defined, and a local s and p coordinate for each individual point on the interface. The local s and p coordinate system will have its x' and y' axes aligned with the local s and p planes of the surface for the evaluation of Jones matrices at given surface coordinates. Then, these local Jones matrices will be rotated to bring all the matrices into the global coordinate system.

Pauli Spin Matrix Basis and the C Vector

The Pauli spin matrices form a most useful basis for interpreting the Jones matrix "space" and define a basis set for the JJ matrix. The identity matrix, $\sigma(0)$ and the Pauli spin matrices, $\sigma(1)$, $\sigma(2)$, and $\sigma(3)$, are defined by:

$$\sigma(0) \quad \begin{bmatrix} 1 & 0 \\ 0 & 1 \end{bmatrix} \qquad \sigma(1) \quad \begin{bmatrix} 1 & 0 \\ 0 & -1 \end{bmatrix} \qquad \sigma(2) \quad \begin{bmatrix} 0 & 1 \\ 1 & 0 \end{bmatrix} \qquad \sigma(3) \quad \begin{bmatrix} 0 & -i \\ i & 0 \end{bmatrix}$$

An arbitrary Jones matrix will be expressed as,

$$JJ = \sum_{k=0}^{3} c(k)\, \sigma(k).$$

The c's are formed into a four element complex vector, the "C vector". The C vector expression

$$C = [\, c(0),\ c(1),\ c(2),\ c(3)\,] \ ,$$

an equivalent representation of the Jones matrix,

$$JJ = c(0)\ \sigma(0) + c(1)\ \sigma(2) + c(2)\ \sigma(2) + c(3)\ \sigma(3)$$

$$= \begin{bmatrix} c(0) + c(1) & c(2) - ic(3) \\ c(2) + ic(3) & c(0) - c(1) \end{bmatrix}$$

When necessary, ρ and ϕ refer to the amplitude and phase portions of the C vector elements,

$$C = [\rho(0)\ \exp(\tilde{\imath}\phi(0)),\ \rho(1)\exp(\tilde{\imath}\phi(1)),\ \rho(2)\exp(\tilde{\imath}\phi(2)),\ \rho(3))\exp(\tilde{\imath}\rho(3))]$$

The elements of C are related to the Jones matrix elements by the equations:

$$c(0) = (j(1,1) + j(2,2))/2 \quad , \quad c(1) = (j(1,1) - j(2,2))/2 \quad ,$$
$$c(1) = (j(1,2) + j(2,1))/2 \quad , \quad c(3) = (j(1,2) - j(2,1))/(-2\tilde{\imath}) .$$

The elements of the Jones matrix are related to the elements of C by the equations:

$$j(1,1) = c(0) + c(1) \quad , \quad j(1,2) = c(2) - \tilde{\imath}\, c(1) \quad ,$$
$$j(2,1) = c(2) + \tilde{\imath}\, c(3) \quad , \quad j(2,2) = c(0) - c(1) \quad .$$

The C vector, like the Jones matrix, has eight degrees of freedom. Table C-2 contains a description of the meaning of the real and imaginary parts of the c vector elements.

TABLE C-2. Interpretation of the C Vector Elements

Matrix	Coefficient	Meaning	
$\sigma(0)$	$\rho(0)$	Amplitude	Absorption
$\sigma(0)$	$\phi(0)$	Phase	Phase
$\sigma(1)$	$\rho(1)$	Amplitude	Linear Polarization along Axes
$\sigma(1)$	$\phi(1)$	Phase	Linear Retardance along Axes
$\sigma(2)$	$\rho(2)$	Amplitude	Linear Polarization, 45 deg
$\sigma(2)$	$\phi(2)$	Phase	Linear Retardance, 45 deg
$\sigma(3)$	$\rho(3)$	Amplitude	Circular Polarization
$\sigma(3)$	$\phi(3)$	Phase	Circular Retardance

The Jones Matrix and C Vectors for Specific Polarizers

Tables of Jones matrices for various polarizers are found in Azzam and Bashara (1977, Section 2.2.3), Hecht and Zajac (1974, Table 8.6), Shurcliff (1962, Appendix 2), and Theocaris and Gdoutos (1979, Table 4.1). A table listing of the Jones matrices and C vectors for the most common polarizers and retarders is given in Chipman (1987, Table 6).

The Meaning of the Coefficients of the C Vector

The primary reason for the introduction of the C vector is to simplify the representation of polarizers. Each of the elements of the C vector represents a specific type of polarizer behavior.

The real parts of the C vector all correspond to amplitude effects, absorption and dichroism. The phase portion of the C vector represent phase effects, propagation and birefringence. The first element, $c(0)=\rho(0)\exp(i\phi(0))$, is the coefficient of the identity matrix. Thus it must represent effects that are polarization state independent; these are amplitude and phase. The last element, $c(3)=\rho(3)\exp(i\phi(3))$, multiplies the spin matrix $\sigma(3)$ which is rotation invariant. Thus the $c(3)$ term represents the circular polarization effects; $\rho(3)$ describes circular polarization or circular dichroism and $\phi(3)$ describes circular retardance or circular birefringence. The remaining two elements, $c(1)$ and $c(2)$, represent linear polarization and linear retardance. Linear terms require two degrees of freedom: magnitude and orientation. Thus, $\rho(1)$ and $\rho(2)$ characterize

linear polarization or linear dichroism, $\rho(1)$ in the 0 degrees and 90 degrees directions, $\rho(2)$ in the + and -45 degrees directions. Likewise, $\phi(1)$ and $\phi(2)$ characterize linear retardance or linear birefringence.

Rotated Polarizers

If a polarizer with Jones matrix JJ is rotated through an angle θ (positive if counterclockwise), the Jones matrix becomes

$$JJ'(\theta) = R(\theta)\ JJ\ R(-\theta).$$

The $R(\theta)$'s are the Jones rotation matrices:

$$R(\theta) = \begin{bmatrix} \cos(\theta) & -\sin(\theta) \\ \sin(\theta) & \cos(\theta) \end{bmatrix}$$

The Jones rotation matrices obey the relations,

$$R(a)\ R(b) = R(b)\ R(a) = R(a+b)$$

and,

$$R(a)\ R(-a) = \sigma(0).$$

The identity matrix is invariant under rotation;

$$R(\theta)\ \sigma(0)\ R(-\theta) = \sigma(0).$$

Under rotation, $\sigma(1)$ and $\sigma(2)$ couple into each other;

$$R(\theta)\ \sigma(1)\ R(-\theta) = \sigma(1)\cos(2\theta) + \sigma(2)\sin(2\theta)$$

$$R(\theta)\ \sigma(2)\ R(-\theta) = -\sigma(2)\sin(2\theta) + \sigma(2)\cos(2\theta).$$

$\sigma(3)$ is invariant under rotation; $R(\theta)\ \sigma(3)\ R(-\theta) = \sigma(3)$. Having established the polarization calculus which describes the polarization optics, we now apply these matrices to the SAMEX optical system.

Instrumental Polarization

Two types of polarization calculations can be performed for the SAMEX magnetograph: instrumental polarization and transmitted light polarization. The first is the calculation of the polarization associated with ray paths through an optical system. This determines the instrumental polarization function as a function of pupil coordinates for a specified object point. The other type of calculation determines the state of polarization, such as a Jones vector, transmitted by the system along a given ray path for a specified input polarization state. By iterating this process, the Jones vector as a function of position in the exit pupil is calculated. This Appendix deals only with the instrumental polarization calculation. Once the instrumental polarization function for the system is known, the transmitted Jones vectors are readily determined for all input polarization states.

Polarizers are optical elements which divide an optical beam into two parts (Jones vector) and transmit those parts with a different transmission coefficient and a different phase. The two parts of the beam are referred to the eigenvectors or by the more descriptive term, "eigenpolarizations." The two eigenpolarizations are orthogonally polarized and are transmitted by the polarizer with no alteration of their polarization states; only the intensity and phase changes.

The word polarizer will be used to refer to both polarizers, such as dichroic or prism type, which have a different transmittance for the two eigenpolarizations, and retarders, which have equal transmittance but a different phase change for the polarizations. 'Polarized Light' by Shurcliff(1962) is the standard reference on the types of polarizers, their definitions, parameters and properties.

Transparent Systems

The SAMEX foreoptics are highly transparent and weakly polarizing and the following calculational method is optimized for this case. The ideal Jones matrix for a ray through a transparent nonpolarizing system is

$$JJ(\text{ideal}) = \exp(\tilde{\imath}d) \begin{bmatrix} 1 & 0 \\ 0 & 1 \end{bmatrix}$$

where d is the optical path length for the ray in radians. (The complex value $(-1)^{1/2}$ is denote by $\tilde{\imath}$). The Jones matrix operation on the Jones vector, which is composed of the two orthogonal

amplitude components, define the transmitted state of the ray. The above ideal Jones matrix is the identity matrix, which signifies that the system has no absorption or polarization. Since this is the desired form of the Jones matrix for the SAMEX foreoptics, the approach developed here obtains the instrumental polarization function as a Taylor series of the system Jones matrix in the ray coordinates about JJ(ideal). This approach is easily modified for systems which are not highly transparent or which contain strong polarizers by performing the Taylor series about the Jones matrix for the ray down the optical axis. This work deals primarily with this simpler version of the problem, transparent systems, to streamline the SAMEX calculations.

S-P Coordinates

To handle problems involving light at nonnormal incidence at curved optical surfaces, it is necessary to maintain two separate coordinate systems: x-y coordinates and s-p coordinates. The x-y coordinates are the global x, y and z coordinate system used to describe the optical system. The optical axis of radially symmetric optical systems coincides with the z axis.

The s-p coordinates are used to perform polarization calculations with the SAMEX coatings which are angle of incidence dependent. Most frequently, the functional form of the interface polarization is known in s-p coordinates. Thus, the rational for using s-p coordinates is that, typically, the Jones matrix for a ray at an optical interface will be calculated in the s-p coordinates. Then it will be rotated into the system x-y

coordinates. Once all the Jones matrices for the ray at all surfaces have been rotated into x-y coordinates, they can be cascaded to give the instrumental polarization along that ray path in the system x-y coordinates.

The s-p coordinates are based on the concept of the s and p planes. Consider light with unit wave vector k (normalized to one) incident at a surface with normal n. The plane of incidence, or "p-plane" is the plane which contains k and n. The plane perpendicular to the plane of incidence which contains k is the "s-plane". Two unit vectors perpendicular to k are defined to form an orthonormal basis for this coordinate system.

Instrumental Polarization

All optical elements display variation of their Jones matrices as the angle of incidence changes. Further, this always involves more than just a variation in the intensity and phase of the light; it also involves polarization and retardance. A fine optical element used in a transparent system will not display polarization effects at normal incidence; it may show some absorption, reflection loss or phase shift, but not polarization or retardance.

The Jones matrix can be decomposed and can be expressed as

$$JJ = \sum_{k=0}^{3} c(k)\,\sigma(k),$$

$$= c_0 \begin{pmatrix} 1 & 0 \\ 0 & 1 \end{pmatrix} + c_1 \begin{pmatrix} 1 & 0 \\ 0 & -1 \end{pmatrix} + c_2 \begin{pmatrix} 0 & 1 \\ 1 & 0 \end{pmatrix} + c_3 \begin{pmatrix} 0 & -\tilde{\imath} \\ \tilde{\imath} & 0 \end{pmatrix}$$

where $\sigma(k)$ are the identity matrix and the Pauli spin matrices which describe the specific polarization state. The c(k) defined a vector which then described the polarization properties of the element. At an angle of incidence i, the C vector will have the form

$$C_i = (c(0,i), c(1,i), c(2,i), c(3,i)) =$$

$$(\rho(0,i)e^{\tilde{i}\phi(0,i)}, \rho(1,i)e^{\tilde{i}\phi(1,i)}, \rho(2,i)e^{\tilde{i}\phi(2,i)}, \rho(3,i)e^{\tilde{i}\phi(3,i)})$$

where each component has an amplitude (ρ) and a phase (ϕ) part. The functional dependences of the C vector coefficients are calculated from the Fresnel equations and coating equations for the interface.

Weak Polarizers

A weak polarization element is defined as a polarizer having a C vector such that for some range of i:

$$|c(0,i)|^2 >> (|c(1,i)|^2 + |c(2,i)|^2 + |c(3,i)|^2)^{1/2}.$$

Such a polarization element transmits light in a polarization state similar to the incident state with only weak coupling into other polarization states. The polarization behavior is dominated by transmission with only traces of polarization or retardance. Any polarization present is at the few percent level or less, such that any linearly polarized incident beam has a transmission coefficient which varies a few percent or less with

orientation. Similarly, the retardation is degrees or less, far less than a quarter wave ($\pi/2$) retarder. Near normal incidence, metals in reflection (e.g. telescope mirrors) and dielectric refracting interfaces (e.g. relay lens) are weak polarizers. In addition, near normal incidence, anti-reflection coated lenses used in transmission and metals with reflection enhancing coatings are typically weak polarizers for wavelengths near the thin film design wavelength.

Amplitude Transmission Relations

The amplitude transmission equations for an interface are the equations which relate the amplitude and phase of the electric fields, E, at an interface. The most general amplitude transmission equations for a nonscattering linear interface are:

$$\begin{bmatrix} E'(s) \\ E'(p) \end{bmatrix} = \begin{bmatrix} a(ss)\ E(s) + a(ps)\ E(p) \\ a(sp)\ E(s) + a(pp)\ E(p) \end{bmatrix}$$

where for this section, the plane of incidence will be aligned with the y axis. This equation is equivalent to the Jones matrix equation,

$$\begin{bmatrix} E'(s) \\ E'(p) \end{bmatrix} = \begin{bmatrix} a(ss) & a(sp) \\ a(ps) & a(pp) \end{bmatrix} \begin{bmatrix} E(s) \\ E(p) \end{bmatrix}$$

For interfaces whose eigenpolarizations are linear polarized light oriented parallel and perpendicular to the plane of

incidence, the transfer of energy across the interface is separable into two uncoupled components which can be written in the form:

$$E'(s) = a(s)\ E(s) = \rho(s)\ \exp(i\phi(s))\ E(s)$$
$$E'(p) = a(p)\ E(p) = \rho(p)\ \exp(i\phi(p))\ E(p).$$

The amplitude transmission coefficients a(s) and a(p), or in polar coordinates, $\rho(s)$, $\phi(s)$, $\rho(p)$, and $\phi(p)$, are determined by the Fresnel equations for the interface. The type of energy transfer equation, where the s and p equations are separable, is a "separable amplitude transmission relation." Only polarization elements with linearly polarized light as the eigenpolarizations have the energy transfer equations in the separable form. This includes all the elements and coatings used in the SAMEX foreoptics.

The separable amplitude transmission relations correspond to a diagonal Jones matrix in s-p coordinates. The Jones matrix and C vector for an amplitude transmission interface in s-p coordinates are:

$$JJ(i) = \begin{bmatrix} a(s,i) & 0 \\ 0 & a(p,i) \end{bmatrix}$$

and,

$$C = 1/2\ [\ a(s,i)+a(p,i),\ a(s,i)-a(p,i),\ 0,\ 0\ ].$$

Taylor Series Representation of SAMEX Coatings

In optical aberration theory, expressions for the optical path length of ray segments through the the optical system are obtained by performing a Taylor series expansion on Snells law, the law of reflection and the grating equation, to obtain expressions for the optical path length as a power series expansion in the ray coordinates. Thus Snells law,

$$n \sin i = n' \sin i' ,$$

is rewritten for i' as,

$$i' = \arcsin[\ (n/n')\ \sin i\ ]$$

or

$$i' = (n/n')\ i + [(n/n')^3) - (n/n')]i^3/5 + O(i^5).$$

The polarization aberrations are generated in an analogous fashion. To obtain the variation of the Jones matrix in the exit pupil of a system, the appropriate coating equations are required in Taylor series form. For radially symmetric optical systems, expansions in the angle of incidence about normal incidence are used.

An isotropic interface appears unchanged as it is rotated about the surface normal. Ideally, and to a first approximation, the SAMEX coatings are isotropic. So, for any isotropic

interfaces the Fresnel equations are even functions since the surface, does not distinguish between angles of incidence of +i and -i.

An even function contains only even terms in its Taylor series expansion about the origin. Thus, the Taylor series representations of the coating equations has the form, where f(i) is a reflection or transmission coefficient, of

$$f(i) = f_0 + f_2\, i^2 + f_4\, i^4 + \ldots,$$

where

$$f_n = 1/n!\, \frac{d^n f(i)}{di^n}\Big|_{i=0}.$$

For weakly polarizing interfaces described by amplitude transmittance relations, the Taylor series forms of the Jones matrix and C vector are calculated as follows. First, the Taylor series expansion is determined for the amplitude transmission relations:

$$a(s,i) = a_0(s) + a_2(s)\, i^2 + a_4(s)\, i^4 + \ldots,$$
$$a(p,i) = a_0(p) + a_2(p)\, i^2 + a_4(p)\, i^4 + \ldots,$$

Then, the Taylor series expansion about i=0 in s-p coordinates for the Jones matrix is,

$$JJ(i) = \begin{matrix} a_0(s) & 0 \\ 0 & a_0(p) \end{matrix} + i^2 \begin{matrix} a_2(s) & 0 \\ 0 & a_2(p). \end{matrix}$$

The corresponding C vector expansion in s-p coordinates is

$$C = [\, c(0,0)+c(0,2)i^2 + \ldots\ ,\ c(1,0)+c(1,2)i^2 + \ldots\ ,\ 0,\ 0]$$

where the nth order c-vector component is given by

$$c(0,n) = 1/2\ (a_n(s) + a_n(s))$$
$$c(1,n) = 1/2\ (a_n(s) - a_n(s)).$$

A matrix equation to calculate c(0,n) and c(1,n) from thin film program results is given by Chipman (1987). For the SAMEX coatings characterized by separable amplitude transmission relations, the diagonal and circular polarization components, c(2,n) and c(3,n), are always zero. The normalized C vector for the separable amplitude transmission relations is

$$C = t\ [\, 1+d(0,2)i^2 + \ldots\ ,\ d(1,0)+d(1,2)i^2 + \ldots\ ,\ 0,\ 0\ ]$$

where

$$t = c(0,0) \quad \text{and} \quad d(k,n) = c(k,n)/c(0,0)\ .$$

The Jones matrix and C vector for coordinates other than the s-p coordinates are obtained from the polarization rotation operation. For example, the s-p coordinates are rotated with

respect to the x-y coordinates by θ, the orientation of the plane of incidence. The Jones matrix in x-y coordinates JJ(x,y) is related to the Jones matrix in s-p coordinates JJ(sp) by the equation

$$JJ(x,y) = R(-\theta)\ JJ(s,p)\ R(\theta).$$

The Taylor series coefficients for the Fresnel equations which govern an uncoated dielectric or metal surface have been determined for use in determining the instrumental polarization of a conventional Cassegrain telescope. The notation a(s) and a(p) will refer to either the reflected or transmitted amplitude transmission coefficient, while t(s), t(p), r(s) and r(p) are used to refer unambiguously to the transmitted or reflected components. The Fresnel amplitude transmission equations are:

$$t(s,i) = (\ 2 \cos i \sin i')/(\sin(i+i'))$$
$$= (2n \cos i)/(n \cos i + n' \cos i')$$

$$t(p,i) = (\ 2 \cos i \sin i')/(\sin(i+i') \cos(i-i'))$$
$$= (2n \cos i)/(\ n' \cos i + n \cos i')$$

$$r(s,i) = (-\sin(i-i'))/(\ \sin(i+i')\ )$$
$$= (\ n \cos i - n' \cos i')/(\ n \cos i + n' \cos i')$$

$$r(p,i) = (\ \tan(i-i'))/(\tan(i+i'))$$
$$= (\ n' \cos i - n \cos i')/(\ n' \cos i + n \cos i')$$

The Fresnel equations depend on the ratio of the indices, n and n', but not on the values of the refractive indices individually. This relative refractive index ratio is defined as

$$N = n/n' \quad .$$

The Fresnel equations are equally valid for real n, corresponding to transparent media, or complex n, corresponding to absorbing media or metals.

The second order Taylor series expansions for the Fresnel amplitude coefficients about i=0 are:

$$t(s,i) = (2\,N)/(N+1) + i^2\,(N(N-1))/(N+1) \quad ,$$
$$t(p,i) = (2\,N)/(N+1) + i^2\,(N^2(N-1))/(N+1) \quad ,$$
$$r(s,i) = (N-1)/(N+1) - i^2\,(N-1)/(N(N+1)) \quad ,$$
$$r(p,i) = (N-1)/(N+1) + i^2\,(N-1)/(N(N+1)) \quad .$$

The direct method for calculating the Taylor series coefficients of a coating series given in the last section are impractical for multilayer coatings due to the complexity of calculating the partial derivatives of the appropriate amplitude transmission equations. The Taylor series coefficients can be obtained numerically from the s and p amplitude transmissions evaluated at a series of angles of incidence. An algorithm to sixth order has been given by Chipman (1987). The algorithm was used with the thin film design programs Filmstar and Films to

obtain the Taylor series expansions of the transmitted and reflective amplitudes as a function of the angle of incidence for use in the polarization aberration calculations for SAMEX.

CASCADED WEAK POLARIZERS

In this section the Jones matrix describing the instrumental polarization for light propagating along a ray path through the SAMEX foreoptics is derived. Results are also given for the instrumental polarization associated with paraxial rays as functions of the Taylor series of the C vectors representing the optical interfaces. The notation used in this section is compiled in Table C-3.

Table C-3. Notation for Section

C	C vector
c(k)	d(k) coefficients rotated into arbitrary plane of incidence
d(k)	Normalized C vector components in s-p coordinates
i	Angle of incidence
JJ	Jones matrix
k	Pauli spin matrix index: 0,1,2,3
d	Length of a ray segment
q	Surface index
Q	Total number of surfaces
v	Orientation of the plane of incidence
r(k)	Absorption or polarization coefficient
σ	Pauli spin matrix
t	Normal transmittance
p(k)	Phase or retardance coefficient

Subscript Ordering: k, l, q.

For example, d(1,2,3), is the coefficient for: the $\sigma(1)$ polarization basis state, that is second order in the angle of incidence Taylor series, i^2, for q=3, the third interface.

Consider an optical system with Q optical interfaces numbered in the order encountered from q=1 to Q. No symmetry regarding the optical configuration is assumed. Light propagates along a specified ray path such as would be calculated by an optical ray trace calculation. At each interface some polarization is introduced due to differences in the optical constants across the interface. In addition, polarization is associated with the ray path between interfaces due to optically active crystals, dichroism, birefringence, gradient index materials or other polarizing mechanisms. But for the polarization analysis for SAMEX foreoptics, polarization associated with the optical path between interfaces was zero. Therefore only interface induced polarization is considered here.

Homogeneous Optical Systems

A homogeneous interface has optical properties independent of spatial coordinates on the interface. The Jones matrices are functions only of the angle of incidence, plane of incidence, and optical properties of the interface media, JJ = JJ(i,θ,n,n') and similarly C = C(i,θ,n,n'). The foreoptics and polarimeter sections of the SAMEX Magnetograph are homogeneous optical systems.

Likewise, a homogeneous medium has optical properties independent of spatial coordinates. An anisotropic crystalline medium is homogeneous if it consists of a single crystal. The refractive index varies with direction but not with position.

Radially Symmetric Systems of Lenses, Mirrors and Coatings

The polarization properties of optical systems comprised of lenses, mirrors and "fine" coatings will be developed. A radially symmetric optical system has an axis of symmetry, the optical axis. It is assumed that the optical elements and materials used in transmission are highly transparent and nonpolarizing, as is usual in lenses. The polarization contribution from the path lengths through highly transparent elements is small relative to the polarization arising at the interfaces and is neglected.

The polarization associated with ray paths near the optical axis, or in the paraxial regime, will be derived. For this paraxial development to be accurate, it is only necessary that the angles of incidence are small enough that the polarization associated with the interfaces is adequately approximated by a second order expansion of the C vector as a function of the angle of incidence. For an uncoated lens or mirror, this approximation is generally valid for $i < 30$ degrees. Calculation of the fourth and higher order coefficients allows estimation of the accuracy of these second order equations. The paraxial region for this polarization analysis is typically orders of magnitude larger than the paraxial region of geometrical optics (the region where the fourth and higher order wavefront aberrations are negligible.)

Homogeneous and isotropic interfaces do not display polarization at normal incidence. There is only an amplitude and

Homogeneous and isotropic interfaces do not display polarization at normal incidence. There is only an amplitude and phase change which is represented by the complex number, t, the normal amplitude transmittance. An isotropic interface such as a lens, mirror or coating has a C vector Taylor series in s-p coordinates ($\theta = 0$) of the form

$$C(i,\theta)\big|_{\theta = 0} = t\ [1,0,0,0] + i^2\ t\ [d(0,2),d(1,2),0,0] + \\ + i^4\ t\ [d(0,4),d(1,4),0,0] + \ldots$$

For an arbitrary orientation θ of the plane of incidence, the C vector is

$$C(i,\theta) = t\ [1,0,0,0] + i^2\ t\ [c(0,2)t,c(1,2)t,c(2,2)t,0] \\ + i^4\ t\ [c(0,4)t,c(1,4)t,c(2,4)t,0] + \ldots$$

where the c's are determined from the d's by a rotational change of basis. Since homogeneous and isotropic interfaces do not display circular retardance or circular polarization, $\sigma(3)$ is not included to simplify the mathematics.

The C Vector for a Paraxial Ray

The SAMEX instrumental polarization will be analyzed by a paraxial optics development. Consider a paraxial ray path through an optical system from surfaces q=1 to Q with angles of incidence, i(q), and orientations of the plane of incidence, $\theta(q)$. The Jones vector associated with the axial ray (down the

optical axis,) i(q)=0 for all q, is

$$JJ = t(q)\ \sigma(0)\ t(q-1)\ \sigma(0)\ldots t(2)\ \sigma(0)\ t(1)\ \sigma(0) = T\ \sigma(0)$$

where

$$T = \prod_{q=1}^{Q} t(q).$$

The complex amplitude transmittance down the axis, T, is the product of the normal incidence complex amplitude transmittances at each surface.

The Jones matrix associated with a ray at interface q can be expressed in terms of the expansion of the interface Jones matrix as

$$JJ(i,v,q) = t(q)\ [\sigma(0)+ i^2(q)(c(0,2,q)\sigma(0)+c(1,2,q)\sigma(1)+c(2,2,q)\sigma(2)) + i^4(q)(c(0,4,q)\sigma(0)+c(1,4,q)\sigma(1)+c(2,4,q)\sigma(2))+\ldots]$$

The Jones matrix associated with the entire paraxial ray path resulting from keeping terms to second order at each interface is (where X represents multiplication carried onto the next line)

$$JJ = t(q)(\sigma(0)+ i^2(q)c(0,2,q)\sigma(0)+c(1,2,q)\sigma(1)+c(2,2,q)\sigma(2))\ X$$
$$t(q-1)(\sigma(0)+i^2(q-1)(c(0,2,q-1)\sigma(0)+c(1,2,q-1)\sigma(1)+c(2,2,q-1)\sigma(2))X$$
$$t(2)(\sigma(0)+i^2(2)(c(0,2,2)\sigma(0)+c(1,2,2)\sigma(1)+c(2,2,2)\sigma(2))X$$
$$t(1)(\sigma(0)+i^2(1)(c(0,2,1)\sigma(0)+c(1,2,1)\sigma(1)+c(2,2,1)\sigma(2)).$$

Associated with each interface are four terms. Carrying out all the multiplications leads to 4^Q terms, all in even powers in i. Collecting terms of equal power in i, there is one term at zero'th order and 3Q terms at second order. If i is assumed small, the large number of higher order terms are of diminishing importance. Collecting zero and second order terms in JJ_o and JJ_2 the expression for JJ is

$$JJ_0 + JJ_2 = T\ \sigma(0) + T\ \sigma(0) \sum_{q=1}^{Q} i^2(q)c(0,2,q)$$

$$+ T\ \sigma(1) \sum_{q=1}^{Q} i^2(q)c(1,2,q)$$

$$+ T\ \sigma(2) \sum_{q=1}^{Q} i^2(q)c(2,2,q).$$

Since no polarization or retardance was assumed on axis, the contributions to the second order polarization for this ray are just sums of contributions from each surface. The multiplication taking place at second order for the $\sigma(1)$ term is of the form

$$i^2(q)\sigma(1)\sigma(0)\sigma(0)\sigma(0)\ldots\sigma(0) + \sigma(0)i^2(q-1)\sigma(1)\sigma(0)\sigma(0)\ldots\sigma(0) +$$
$$\ldots + \sigma(0)\sigma(0)\sigma(0)\sigma(0)\ldots i^2(q)\sigma(1)$$

where the c-dependence is not shown explicity.

This equation contains the useful result that, when no elements display polarization or retardance at normal incidence, as in the SAMEX foreoptics, there is no order dependence in the

second order terms. Only one non-identity matrix term occurs in each second order matrix product. The second order polarization associated with the paraxial ray path is obtained by a simple summation of second order polarization contributions at each intercept. Chipman (1987) gives a complete account of this derivation.

Paraxial Optics Geometry

The polarization aberrations for SAMEX are a description of the polarization behavior of an optical system expressed as an expansion about the center of the object and the center of the pupil. Thus it is appropriate and convenient to obtain the derivations from a paraxial ray trace; appropriate, because understanding the instrumental polarization near the center of the pupil and image is key to understanding instrumental polarization in general; convenient because the paraxial ray trace is linear, and thus easy to manipulate.

The paraxial coordinate system used is a normalized right handed coordinate system. The z axis is the optical axis of a rotationally symmetric optical system. Light initially travels in the direction of increasing z. Figure C-1 shows the notation.

For a rotationally symmetric system, the object can be located on the y axis without loss of generality. The object coordinate H is normalized such that H = 0 in the center of the field (on the optical axis) and H = 1 at the nominal edge of the field of view.

The location where a ray strikes the entrance pupil is

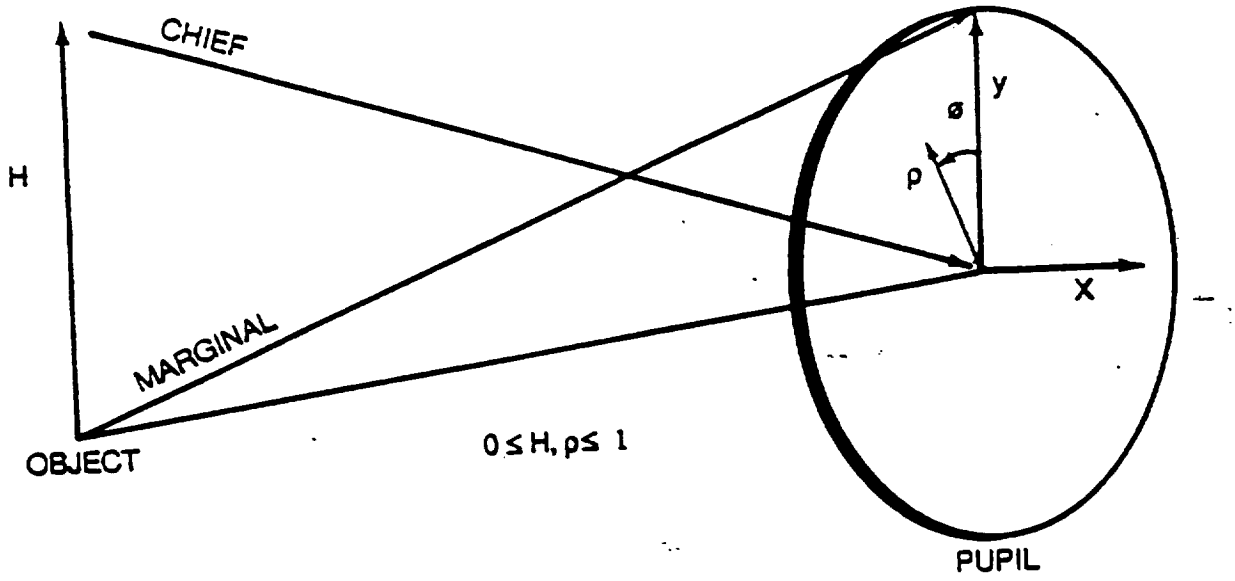

Figure C.1. Paraxial coordinate system. The paraxial system is a normalized right-handed coordinate system. The z axis is the optical axis of a rotationally symmetric optical system; light initially travels in the direction of increasing z. Rays through an optical system are characterized by ray coordinates at the object and entrance pupil. H is the normalized object coordinate, ρ is the normalized pupil radius, and ϕ is the polar angle in the pupil measured counterclockwise from the y axis. The normalized Cartesian coordinates in the pupil are x and y. The chief and marginal rays are also shown.

specified by the polar pupil coordinates ρ and ϕ. ρ is normalized such that at the edge of a circular pupil $\rho = 1$. The angle ϕ is defined here as it is in much of geometric optics, and in defiance to most analytical geometry, as being zero on the 'y axis' and increasing counterclockwise. Normalized Cartesian pupil coordinates x and y can be used. They are defined as: $x = \rho \sin(\phi)$ and $y = \rho \cos(\phi)$.

Expressions for the angle of incidence i and the orientation of the plane of incidence ϕ of a ray at a given surface q will be expressed in terms of the marginal i(m,q) and chief ray i(c,q) angles of incidence at that surface. Details of the derivation may be found in Chipman (1987, section D). Note, however, for a radially symmetric system the angle of incidence should be a function of H^2, ρ^2, and $H\rho\cos\phi$ since the function should be invariant to rotation of the system about the optical axis and must give the same result when -x is substituted for +x where $x = \rho\cos\phi$.

Assume that a paraxial ray trace has been performed for a specific system and that i(m,q) and i(c,q) have been calculated. A ray from normalized object coordinate H which passes through pupil coordinates ρ and ϕ will have an angle of incidence i(q) and orientation of the plane of incidence θ(q) at surface q equal to:

$$i(q) = [H^2 i^2(c,q) + 2H\rho \cos(\phi)\, i(c,q)\, i(m,q) + \rho^2\, i^2(m,q)]^{1/2}$$

$$\theta = \sin^{-1} [\rho \sin(\phi)\, i(m)/|i|] \quad .$$

Figure C-2 shows the paraxial angle and plane of incidence for three field angles. The magnitude of the angle of incidence is represented by the length of the lines. The orientation of the lines corresponds to the orientation of the plane of incidence. Note that off axis, the pattern is a shifted version of the on axis pattern. The incidence angle is given by the pupil coordinate (ρ,ϕ) and the image coordinate (H) since these coodinate define the optical path of a single ray.

POLARIZATION ABERRATIONS

Introduction

This section derives the polarization aberrations for SAMEX as a Taylor series description of the instrumental polarization associated with paraxial rays through the foreoptics. Polarization aberration is a description of the polarization behavior of an optical system expressed by a expansion about the center of the object and center of the pupil. Table C-4 gives an overview of polarization aberration theory. The results are obtained in a form very similar to the wavefront aberrations. In particular, terms closely related to defocus, tilt, piston error as well as the Seidel and higher order aberrations can be associated with all eight of the basis Jones matrices. Since polarization effects are typically orders of magnitude smaller than wavefront effects, fewer terms are needed for a sufficient description. A method of calculating aberration coefficients for specific systems is developed in the next section.

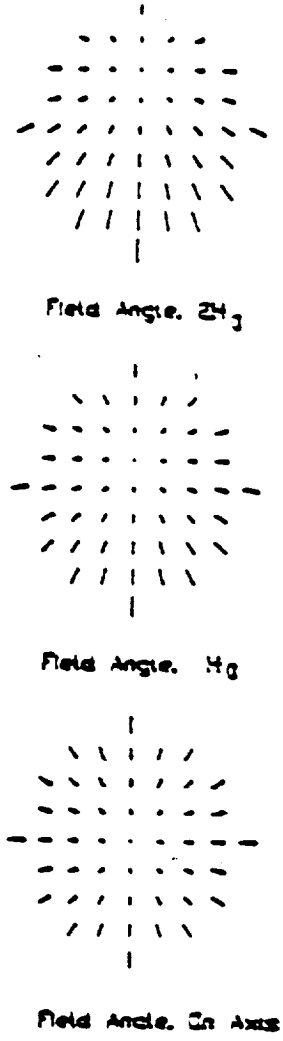

Figure C.2. Paraxial angles and plane of incidence for three field angles. The magnitude of the angle of incidence is represented by the length of the lines. The orientation of the lines corresponds to the orientation of the plane of incidence. Note that in the off-axis cases, the pattern is a shifted version of the on-axis pattern.

Table C-4. Polarization Aberration Theory Outline

(1) Jones Vector

The Jones vector is a complex 2-component vector describing the electromagnetic field.

$$J = \begin{pmatrix} Ex \\ Ey \end{pmatrix}$$

(2) Paraxial Ray Trace

The angle of incidence, i, of any ray can be written in terms of the angle of incidence of the chief and marginal rays, i(c) and i(m).

$$i(c),\ i(m)$$

(3) Coating Calculation

Thin film design programs calculate the amplitude transmission coefficients for s and p light, t(s,i) and t(p,i).

$$t(s,i),\ t(p,i)$$

(4) Taylor Series Representation

The amplitude transmission coefficients, t(s,i) and t(p,i), are transformed to with a Taylor series expansion about normal incidence.

$$t(s,i) = t_o(1 + t(s,2)i^2 + \cdots$$

$$t(p,i) = t_o(1 + t(p,2)i^2 + \cdots$$

(5) Jones Matrix for an Interface

The second order Jones matrix for an interface can be written in terms of three Polarization Aberration terms represented by coefficients.

$$P(1,0,2,2,q),\ P(1,1,1,1,q),\ P(1,2,0,0,q)$$

(6) Aberrations Sum for System

The second order polarization aberrations for the system is the sum of the aberration contributions of each interface.

$$P(1,0,2,2) = \sum_q P(1,0,2,2,q)$$

$$P(1,1,1,1) = \sum_q P(1,1,1,1,q)$$

$$P(1,2,0,0) = \sum_q P(1,2,0,0,q)$$

(7) Polarization Accuracy

Summarize the performance of the system with a single number, the polarization accuracy (Δp). This is the maximum fraction of light coupled into the orthogonal polarization state. This occurs at the edge of the field of view.

$$\Delta_p$$

The Polarization Aberration Expansion

The wavefront polynomial expansion describes the variation of the optical path difference through an optical system as a function of ray coordinates. A closely related expansion will be presented for all four basis polarization matrices $\sigma(0)$, $\sigma(1)$, $\sigma(2)$, $\sigma(3)$. The polarization aberration expansion for radially symmetric systems uses a very similar polynomial expansion to describe all eight basis polarization vectors. The principal difference is a modified form for the linear polarization and linear retardance terms since these involve both a magnitude and an orientation.

The eight forms of polarization behavior can be characterized by four complex numbers, for example, the four elements of either the Jones matrix or the C vector. We introduce a new set of complex parameters, the complex polarization aberration coefficients which gives a description of the polarization behavior of an optical interface. It should be emphasized that the amplitude and phase of the coefficients are generally unrelated. They refer to different aspects of the instrumental polarization. The amplitude part of the coefficient describes amplitude and polarization effects while the phase part describes phase and retardance. When necessary the amplitude and phase of the polarization aberration coefficient, P, will be denoted by A and Φ where,

$$P = A \exp(\tilde{\imath}\, \Phi) \cdot$$

The complex aberration coefficient is written to contain polarization, amplitude, effects, retardance, and phase effects in a single term. The following polarization aberration expansion for zeroth and second order is used. The subscripts are defined as follows:

$$P(k,u,v,w) = A(k,u,v,w)\ \exp(\tilde{i}\phi(k,u,v,w)) \quad ,$$

where: k is the type of polarization behavior,
u is the order of the H dependence, H^u,
v is the order of the ρ dependence, ρ^v, and,
w is the order of the ϕ dependence, $(\cos(\phi))^w$.

The indices u, v, and w are used exactly as they are for the wavefront aberrations, as shown in the next section.

The polarization aberration expansion of the Jones matrix for the SAMEX foreoptics is

$$JJ(H,\rho,\phi) = \sum_{k=0}^{3} c(k,H,,r,p)\ \sigma(k)$$

$$= \sum_{k=0}^{3} \sum_{u} \sum_{v} \sum_{w} P(k,u,v,w)\ H^u\ \rho^{\,v}\ \cos^w(\phi)\ \sigma(k).$$

Here we define the aberration coefficients as an expansion of the Jones matrix in terms of the ray coordinates ρ, ϕ, and H. The C vector coefficients in this polarization aberration expansion are:

Amplitude and Phase term:

$$
\begin{aligned}
c(0,H,\rho,\phi) = \; & A(0,0,0,0) + A(0,2,0,0)H^2 + \\
& + A(0,1,1,1)\, H\, \rho \cos(\phi) + A(0,0,2,0)\, \rho^2 \\
& + \tilde{\gamma}(\phi(0,0,0,0) + \phi(0,2,0,0)H^2 \\
& + \phi(0,1,1,1)H\, \rho \cos(\phi) + \phi(0,0,2,0)\, \rho^2),
\end{aligned}
$$

Linear Polarization and Retardance terms:

$$
\begin{aligned}
c(1,H,\rho,\phi) = \; & A(1,0,0,0) + A(1,2,0,0)\, H^2 + \\
& + H\, \rho\, (A(1,1,1,1) \cos(\phi) - A(2,1,1,1) \sin(\phi)) \\
& + \rho^2 (A(1,0,2,0) \cos(2\phi) - A(2,0,2,0) \sin(2\phi)) \\
& + \tilde{\gamma}\, (\phi(1,0,0,0) + \phi(1,2,0,0)\, H^2 + \\
& \quad H\, \rho\, (\phi(1,1,1,1) \cos(\phi) - \phi(2,1,1,1) \sin(\phi)) + \\
& \quad \rho^2 (\phi(1,0,2,0) \cos(2\phi) - \phi(2,0,2,0) \sin(2\phi))) .
\end{aligned}
$$

Diagonal Polarization and Retardance terms:

$$
\begin{aligned}
c(2,H,\rho,\phi) = \; & A(2,0,0,0) + A(2,2,0,0)\, H^2 + \\
& + H\, \rho\, (A(2,1,1,1) \cos(\phi) + A(1,1,1,1) \sin(\phi)) \\
& + \rho^2\, (A(2,0,2,0) \cos(2\phi) + A(1,0,2,0) \sin(2\phi)) \\
& + \tilde{\gamma}\, (\phi(2,0,0,0) + \phi(2,2,0,0)\, H^2 + \\
& \quad H\, \rho\, (\phi(2,1,1,1) \cos(\phi) + \phi(1,1,1,1) \sin(\phi)) + \\
& \quad \rho^2\, (\phi(2,0,2,0) \cos(2\phi) - \phi(1,0,2,0) \sin(2\phi)))
\end{aligned}
$$

Circular Polarization and Retardance terms:

$$
\begin{aligned}
c(3,H,\rho,\phi) \;=\; & A(3,0,0,0) + A(3,2,0,0)H^2 + \\
& + A(3,1,1,1)\, H\, \rho \cos(\phi) + A(3,0,2,0)\, \rho^2 \\
& + \tilde{\gamma}\,(\phi(3,0,0,0) + \phi(3,2,0,0)H^2 \\
& + \phi\,(3,1,1,1)H\, \rho \cos(\phi) + \phi(3,0,2,0)\rho^2),
\end{aligned}
$$

There are thirty two terms in this polarization aberration expansion to second order arising from four terms in each of the eight degrees of freedom of the Jones matrix. The terms may be grouped as follows:

A(0,u,v,w)	Amplitude terms
A(1,u,v,w)	Linear polarization terms
A(2,u,v,w)	Diagonal polarization terms
A(3,u,v,w)	Circular polarization terms
ϕ(0,u,v,w)	Wavefront or phase terms
ϕ(1,u,v,w)	Linear retardance terms
ϕ(2,u,v,w)	Diagonal retardance terms
ϕ(3,u,v,w)	Circular retardance terms
P(k,0,0,0)	"Constant Piston" terms
P(k,2,0,0)	"Quadratic Piston" terms
P(k,1,1,1)	"Tilt" terms
P(k,0,2,0)	"Scalar Defocus" terms
P(k,0,2,2)	"Vector Defocus" terms

The names of the wavefront aberrations: piston, quadratic piston, defocus and tilt, are used here in an extended sense, to

describe variations of components of the Jones vector which share the same functional dependences as the wavefront aberrations. Defocus is a ρ^2 variation of a parameter. Tilt is H ρ cos(ϕ) variation. Quadratic piston is H^2 variation. Thus, "amplitude defocus" means a ρ^2 amplitude variation. Likewise the "circular retardance tilt" is a the H ρ cos(ϕ) circular retardance variation, and so on.

This polarization aberration expansion is an equation which describes all possible second order variations of the Jones matrix, just as the second order wavefront aberration expansion spans the set of all second order wavefront variations. Thus the polarization aberration expansion characterizes quadratic variations of all forms of wavefront, amplitude, polarization and retardance.

This polarization aberration expansion is a summation of terms in the different Pauli spin matrix components, not a product. Thus the four C vector elements can be pictured as acting in parallel, almost side by side in the aperture, but not in series. Each term describes an amount of a particular form of polarization, independent of the other contributions.

An "aberration term" is to be considered as containing all the algebraic terms in the expansion with the same coefficient. Most of the coefficients occur only once and the aberration term contains only one algebraic term. The exceptions are the terms, A(1,1,1,1), Φ(1,1,1,1), A(1,0,2,2), Φ(1,0,2,2), A(2,1,1,1), Φ(2,1,1,1), A(2,0,2,2), and Φ(2,0,2,2). These aberration terms have components both along the axes and at 45 degrees.

With SAMEX, the principal concerns are with the linear piston, linear tilt and linear defocus terms, both in polarization and retardance. These are going to be the largest terms present which corrupt the incident polarization state. These values are given in the Table 19 for SAMEX.

For a detail discussion of the physical meaning of the polarization aberration coefficients see Chipman (1987), however a discussion of the orgin of tilt and piston, P(0,2,0), P(1,1,1), and P(2,0,0) terms is included below.

A distinction is made between scalar and vector aberrations. The wavefront aberrations are scalar aberrations, single valued functions of object and pupil coordinates. The linear polarization and linear retardance aberrations are vector aberrations since a magnitude and orientation is associated with these at each point. Amplitude, circular polarization and circular retardance aberrations are scalar since they are single valued and range positive and negative.

Figure C-3 (top) shows the chief and limiting rays at an interface for objects on axis and at the edge of the field of view. Figure C-3 (bottom) is a plot of the value of the angle of incidence along the y axis as a function of ρ. Tilt terms naturally occur because as the object point moves off axis, the angle of incidence increases at one edge of the beam and decreases at the other edge. Tilt contains the first order portion of this correction.

Figure C-4 shows the off-axis angle of incidence squared and the decomposition of this into defocus, tilt and piston terms.

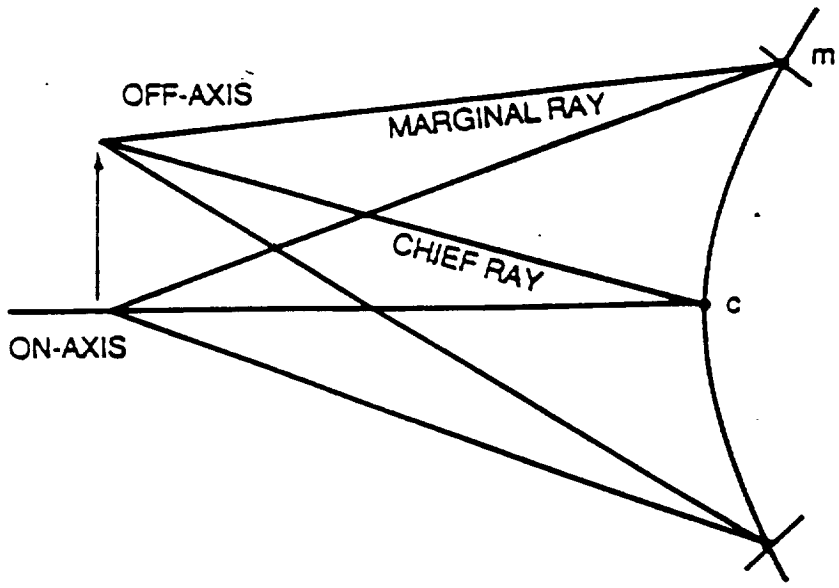

A.

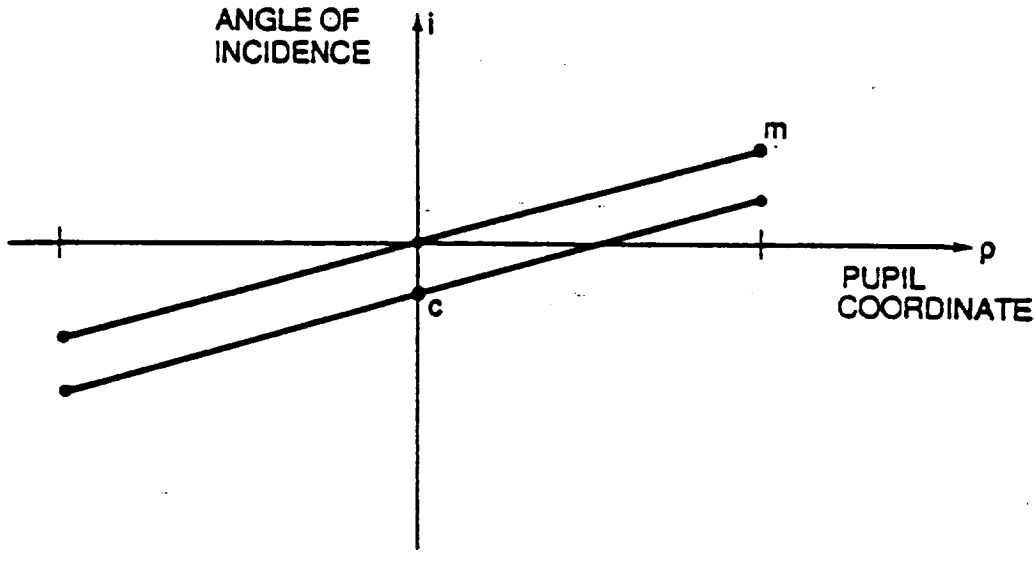

B.

Figure 2.3 Angles of incidence for objects on and off axis. In the top frame, the chief and limiting rays at an interface are shown for objects on the optical axis and at the edge of the field of view. In the lower part of the figure, the angle of incidence for rays incident along the y axis (in the paraxial system) is plotted as a function of the normalized radius ρ.

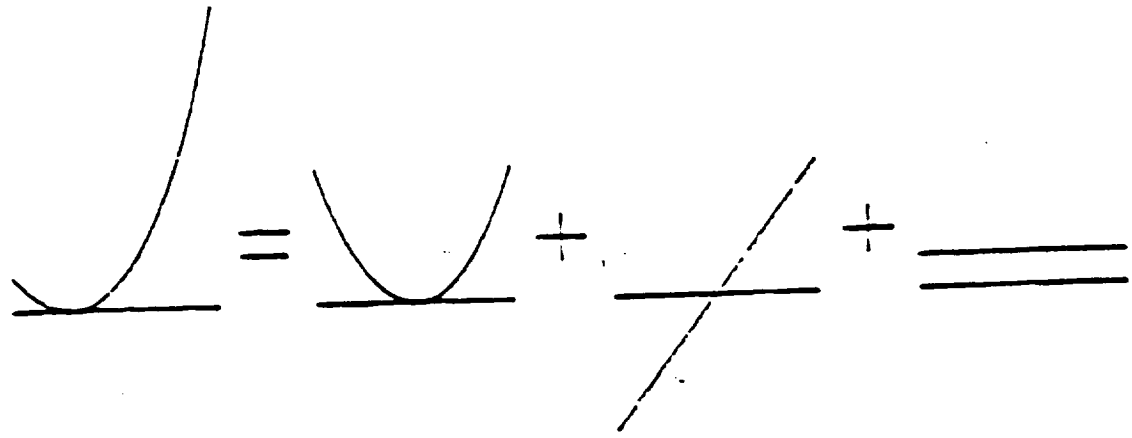

$$(x+a)^2 = x^2 + 2ax + a^2$$

Off-axis Angle of Incidence Squared — Defocus — Tilt — Piston

Figure 6.4 Quadratic effects of off-axis angles of incidence. The square of the off-axis angle of incidence is shown along with its decomposition into defocus, tilt and piston terms.

These terms are required to describe a quadratic variation whose vertex is located at an arbitrary position on the y axis because

$$x^2 + (y-a)^2 = x^2 + y^2 - 2y\,a + a^2 \,.$$

In this case since a is a linear function of H,

$$a = k\,H \,,$$

then the quadratic polarization variation becomes

$$\begin{aligned} c(x^2 + (y-kH)^2) &= c(x^2+y^2) - 2c\,y\,k\,H + c\,k^2H^2 \\ &= P(0,2,0)\rho^2 + P(1,1,1)2H\,\rho\cos(\phi) + P(2,0,0)H^2, \end{aligned}$$

where P(0,2,0), P(1,1,1), and P(2,0,0) are the defocus, tilt and quadratic piston aberration coefficients and the polarization index is not shown. Tilt and piston terms arise naturally from decentered defocus. Similarly, the fourth order wavefront aberrations coma, astigmatism, field curvature and distortion arise naturally from decentered spherical aberration, ρ^4.

CALCULATION OF ABERRATION COEFFICIENTS

The method used to calculate the second order polarization aberration coefficients for the SAMEX foreoptics given the C vector power series for each interface is detailed in this section.

Single Surface Aberrations for Amplitude Transmittance Relations

For homogeneous and isotropic interfaces characterized by amplitude transmittance relations, such as lenses, mirrors and thin film coatings, the polarization aberrations at a interface simplify considerably. At these interfaces the Fresnel equations and related thin film equations are separable into s and p components, so the Jones matrices representing the interface in s-p coordinates are diagonal. The off-diagonal terms, diagonal polarization $\sigma(2)$ and circular polarization $\sigma(3)$, are not present. Further, with isotropic media, the s and p amplitude transmission coefficients at normal incidence must be equal. Thus the amplitude transmission functions can be expanded as:

$$a(s,i) = a(0)(1 + a(s,2)i^2 + \ldots)\ \exp(\tilde{\imath}(d(0) + d(s,2)i^2 + \ldots)$$
$$= t\ (1+(a(s,2) + \tilde{\imath}\, d(S,2))i^2 + \ldots)\ ,$$

$$a(p,i) = a(0)(1 + a(p,2)i^2 + \ldots)\ \exp(\tilde{\imath}(d(0) + d(2,p)i^2 + \ldots)$$
$$= t\ (1 + a(p,2) + \tilde{\imath}\, d(p,2)i^2 + \ldots)$$

where:

$$t = a(0)\exp(\tilde{\imath}\, d(0)).$$

The s-p coordinate Jones matrix expansion to second order is

$$JJ(i) = \begin{bmatrix} a(s,i) & 0 \\ 0 & a(p,i) \end{bmatrix}$$

$$= t\,(\sigma(0)(1 + A(2) + \tilde{\imath}D(2))i^2) + \sigma(1)(a(2) + \tilde{\imath}d(2))i^2).$$

where

$$A(2) = (a(s,2)+a(p,2))/2,$$

$$a(2) = (a(s,2)-a(p,2))/2,$$

$$D(2) = (d(s,2)+d(p,2))/2,$$

$$d(2) = (d(s,2)-d(p,2))/2,$$

The s-p coordinate C vector Taylor series expansion to second order is

$$C(i) = t\,(1,0,0,0) + i^2\, t\,(A(2)+\tilde{\imath}D(2),\ a(2)+\tilde{\imath}d(2),\ 0,\ 0).$$

The x-y coordinate C vector Taylor series for orientation of the plane of incidence θ is

$$C(i,\theta) = t(1,0,0,0) + i^2\, t\,(A(2)+\tilde{i}D(2),$$
$$(a(2)+\tilde{i}d(2))\cos(2\theta),\ (a(2)+id(2))\sin(2\theta),\ 0).$$

The normal-incidence polarization aberration terms (the constant piston terms) are zero:

$$P(1,0,0,0) = P(2,0,0,0) = P(3,0,0,0) = 0\ .$$

There is no polarization or retardance on axis, only the amplitude and phase transmission factor t.

All terms for off-axis diagonal and circular polarization are zero:

$$P(2,u,v,w) = P(3,u,v,w) = 0\ .$$

Thus, the single surface C vector in paraxial coordinates is obtained by substituting the paraxial representation of $i(H,\rho,\phi)$ and $v(H,\rho,\phi)$ into $C(i,v)$ yielding

$$c(0,H,\rho,\phi) = t + t\,d(0,2)[\,H^2\,i^2(c) + 2H\,\rho\cos(\phi)\,i(c)i(m) + \rho^2\,i^2(m)]$$

$$c(1,H,\rho,\phi) = t\,d(1,2)\,[\,H^2\,i^2(c) + 2H\,\rho\cos(\phi)\,i(c)i(m) + \rho^2\cos(2\phi)\,i^2(m)]$$

$$c(2,H,\rho,\phi) = t\,d(1,2)\,[\,2H\,\rho\sin(\phi)\,i(c)i(m) + \rho^2\sin(2\phi)\,i^2(m)]$$

$$c(3,H,\rho,\phi) = 0.$$

Since there is no diagonal polarization, the only contributions to c(2) arises from the rotation of linear polarization from the s-p coordinates into the x-y coordinates.

Polarization Aberration Coefficients for Systems

Since the polarization aberrations are only being evaluated to second order in the angle of incidence, the difference between spheres, parabolas, conics or other radially symmetric aspherics does not occur at this order. The relevant shape parameter here is only the vertex radius of curvature. The angle and plane of incidence differences between these types of interfaces are the same at second order but will differ at fourth order and higher.

For surfaces q=1 to Q, each surface is characterized by three complex parameters from the normalized C vector expansion:

$$d(0,0) = t(q), \quad d(0,2,q), \quad \text{and } d(1,2,q) .$$

The single surface polarization aberration coefficients are:

$$P(0,0,0,0,q) = t(q)$$
$$P(0,2,0,0,q) = t(q)\, d(0,2,q)\, i^2(c)$$
$$P(0,1,1,1,q) = 2t(q)\, d(0,2,q)\, i(c)i(m)$$
$$P(0,0,2,0,q) = t(q)\, d(0,2,q)\, i^2(m)$$
$$P(1,2,0,0,q) = t(q)\, d(1,2,q)\, i^2(c)$$
$$P(1,1,1,1,q) = 2t(q)\, d(1,2,q)\, i(c)i(m)$$
$$P(1,0,2,2,q) = t(q)\, d(1,2,q)\, i^2(m).$$

The polarization aberration coefficients for the system are calculated by chain multiplying the single surface polarization aberration expressions and keeping terms to second order in H and ρ. The zero and second order Jones matrices for the q'th interface are:

$$JJ_0(q,H,\rho,\phi) = P(0,0,0,0,q)\ \sigma(0) = d(0,0,q)\ \sigma(0) = t(q)\ \sigma(0),$$

$$JJ_2(q,H,\rho,\phi) = \sigma(0)\ [H^2\, P(0,2,0,0,q) + 2H\ \rho\ \cos(\phi)P(0,1,1,1,q) + \rho^2\, P(0,0,2,0,q)\ ]$$

$$+\ \sigma(1)\ [\ H^2\, P(1,2,0,0,q) + 2H\ \rho\ \cos(\phi)P(1,1,1,1,q) + \rho^2\cos(2\phi)P(1,0,2,2,q)\ ]$$

$$+\ \sigma(2)\ [\ 2H\ \rho\ \sin(\phi)P(1,1,1,1,q) + \rho^2\sin(2\phi)P(1,0,2,2,q)\ ]$$

$$= \sigma(0)\, t(q)d(0,2)\, [\, H^2 i^2(c) + 2H\, \rho \cos(\phi) i(c) i(m)$$

$$+ \rho^2 i(m)^2\,]$$

$$+ \sigma(1)\, t(q)d(1,2)[H^2\, i(c)^2 + 2H\, \rho \cos(\phi) i(c) i(m) + \rho^2 \cos(2\phi)\, i^2($$

$$+ \sigma(2)\, t(q)d(1,2)[\, 2H\, \rho \sin(\phi) i(c) i(m) + \rho^2 \sin(2\phi) i^2(m)\,] \quad .$$

Multiplication of the single surface Jones matrices yields

$$JJ(H,r,p) = \prod_{q=Q,-1} JJ(q,H,\rho,\phi)$$

$$= \prod_{q=Q,-1} [\, JJ_0(q) + JJ_2(q,H,\rho,\phi)\,] .$$

Since $JJ_0(q)$ is a constant function, independent of H, ρ, and ϕ, the (H,ρ,ϕ) dependence can be dropped. This expression contains 2^Q terms. The order of a term is the sum of the powers of H and ρ, $H^u\, \rho^v \cos(\phi)^w$, i.e. order = u + v .

There is one first order term and Q second order terms.

The zero order Jones matrix is

$$JJ_0 = \prod_{q=Q,-1} JJ_0(q,H,\rho,\phi)) = \prod_{q=1} t(q) = T \quad ,$$

the system amplitude transmittance. The second order Jones matrix is greatly simplified since, for isotropic surfaces, all zeroth order Jones matrices are a constant times the identity matrix $\sigma(0)$. The second order only contains products which contain a single second order term. The second order Jones matrix is

$$JJ_2(H,\rho,\phi) = \sum_{q=1,Q} JJ_2(q,H,\rho,\phi) \quad .$$

At second order the weakly polarizing isotropic interfaces do not display order dependence. The product of any two second order terms is fourth order. The order dependence enters at fourth and higher order. Second order is a simple sum of polarization contributions. Collecting the piston, tilt and defocus terms from the second order Jones matrix provides the coefficients for the system polarization aberration expansion to second order:

$$\begin{aligned}
P(0,0,0,0) &= T \quad , \\
P(0,2,0,0) &= T \sum_{q=1,Q} d(0,2,q)\ i^2(c) \quad , \\
P(0,1,1,1) &= 2T \sum_{q=1,Q} d(0,2,q)\ i(c)i(m) \quad , \\
P(0,0,2,0) &= T \sum_{q=1,Q} d(0,2,q)\ i^2(m) \quad , \\
P(1,2,0,0) &= T \sum_{q=1,Q} d(1,2,q)\ i^2(c) \quad , \\
P(1,1,1,1) &= 2T \sum_{q=1,Q} d(1,2,q)\ i(c)i(m) \quad , \\
P(1,0,2,2) &= T \sum_{q=1,Q} d(1,2,q)\ i^2(m) \quad .
\end{aligned}$$

The other three zero order coefficients and the other six second order coefficients are all zero:

$$P(1,0,0,0) = P(2,0,0,0) = P(3,0,0,0) = 0 ,$$
$$P(2,2,0,0) = P(2,1,1,1) = P(2,0,2,0) = 0 ,$$
$$P(3,2,0,0) = P(3,1,1,1) = P(3,0,2,0) = 0 .$$

The amplitude and polarization coefficients are the real parts of the P coefficients

$$A(k,u,v,w) = Re(P(k,u,v,w)) .$$

The retardation coefficients are the imaginary parts

$$\phi(k,u,v,w) = Im(P(k,u,v,w)) .$$

The polarization aberration coefficients are calculated for the foreoptics from the paraxial geometry and the normalized C-vectors for the coatings and interfaces.

Polarization Accuracy

The Jones vector gives the amplitude of the electric field and the square of the amplitude gives the intensity of the components. With the Jones matrix one is able to calculate the polarization effects for the optical system. From above the second order the Jones matrix which gives the linear polarization and linear retardence is

$$JJ_2(H,\rho,\phi) = \sigma(1)[H^2\ P(1,2,0,0) + 2\ H\ \rho\ \cos(\phi)\ P(1,1,1,1)$$

$$+ \rho^2\ \cos(2\phi)\ P(1,0,2,2)\ ].$$

$$+ \sigma(2)[(2H\rho\ \sin(\phi)\ P(1,1,1,1) + \rho^2\ \sin(2\phi)P(1,0,2,2)]$$

The on axis linear polarization and linear retardance of the SAMEX foroptics are characterized by the term linear defocus. The instrumental polarization function $JJ(H,\rho,\phi)$ for linear defocus is

$$JJ(H,\rho,\phi) = \tau[\sigma_0 + P(1,0,2,2)\rho^2(\sigma_1\cos2\phi - \sigma_2\sin2\phi]$$

$$= \tau[\sigma_0 + (a_{1022} + j\delta_{1022})\rho^2(\sigma_1\cos2\phi - \sigma_2\sin2\phi)]\ .$$

Here, τ is the amplitude transmittance of the system down the optical axis. It (τ) describes the polarization independent reflection and absorption losses associated with the ray down the optical axis at normal incidence at all interfaces. $P(1,0,2,2)$ describes the linear polarization (a_{1022}) and linear retardance (δ_{1022}) associated with the marginal ray.

Maximum coupling occurs when the incident light is circularly polarized, since circularly polarized light can always be decomposed into equal components of $\hat{J}_r$ and $\hat{J}_t$ everywhere in the pupil. The coupling is zero in the center of the pupil (where the polarization and retardance vanishes) and increases to a maximum coupling fraction of

$$I_{c,max}(H,1,\phi) = |P(1,0,2,2)|^2 = a_{1022}^2 + \delta_{1022}^2$$

at the edge of the pupil. The net fraction of incident circular polarized light coupled into the orthogonal circular polarized state is given by the integral over the pupil of

$$I_c = \frac{|\tau|^2}{\pi} \int_0^{2\pi} d\phi \int_0^1 \rho d\rho \left|\rho^2 \tau P(1,0,2,2)\right|^2$$

$$= \frac{|\tau P(1,0,2,2)|^2}{3} .$$

For incident linear or illiptical polarized light, the fraction of coupled intensity is less because the light is not composed of equal fractions of eigenstates.

The coupling is minimum for incident linear polarized light, which will be in one of the eigenpolarizations along one axis in the pupil and in the orthogonal eigenpolarization along the orthogonal axis. The fraction of coupled energy will be calculated assuming an incdient polarization state of horizontal linear polarized light $\hat{H}$ for calculational simplicity, the same fraction is coupled for any linear polarized incident state. The polarization state transmitted by an optical system described by linear polarization defocus for $\hat{H}$ in is

$$J(H,p,\phi) = \tau(\hat{H} + P(1,0,2,2)\ \rho^2(\hat{H}\cos 2\phi - \hat{V}\sin 2\phi)).$$

The fraction of incident $\hat{H}$ light couplied into $\hat{V}$ light is equal to

$$I_c = \frac{|\tau|^2}{\pi} \int_0^{2\pi} d\phi \int_0^1 d\rho \left| \vec{J}(H,\rho,\phi) \cdot \hat{V} \right|^2$$

$$= \frac{|\tau|^2}{\pi} \int_0^{2\pi} d\phi \int_0^1 \rho d\rho \left| P(1,0,2,2)\rho^2 \sin 2\phi \right|^2$$

$$= \frac{|\tau P(1,0,2,2)|^2}{\pi} \int_0^{2\pi} \sin^2 2\phi d\phi \int_0^1 \rho^5 d\rho$$

$$= \frac{|\tau P(1,0,2,2)|^2}{6} .$$

This is the mininmum fraction of energy coupled by linear defocus aberrations. Since any elliptically polarized incident beam can be written as a sum of linear and circularly polarized light, the coupling fraction for arbitrarily polarized light lies in the range.

$$\left| \frac{\tau P(1,0,2,2)}{6} \right|^2 < I_c < \left| \frac{\tau P(1,0,2,2)}{3} \right|^2 .$$

When unpolarized of circularly polarized light is incident on the optical system, maximum polarization coupling occurs. This maximum is the polarization accurracy of a system and is calculated by the coupling integral, $I_{c,max}$,

$$I_{c,max} = \frac{1}{\pi} \int \int_{pupil} \left| c^2(1) + c^2(2) + c^2(3) \right| \rho d\rho d\phi .$$

This integral must be evaluated numerically except for some special cases (see section 3.5). However, an analytic upperbound on the polarization accurracy can be easily established by using the triangle inequality

$$I_{c,max} < \frac{1}{\pi} \int\int_{pupil} [((Re[c(1)])^2 + (Re[c(2)]^2 + (Re[c(3])^2)^2$$

$$+((Im[c(1)])^2 + (Im[c(2)])^2 + (Im[c(3)])^2)^2] \rho d\rho d\phi \ .$$

We can evaluate the upper bound on the polarization accurracy using the second order polarization aberration expansion coefficients. The following integration is for the real part of the aberration coefficients. a_{luvw}

$$I = \frac{|\tau|^2}{\pi} \int^{2\pi} d\phi \int_0^1 \rho d\rho [(a_{1200}H^2 + a_{1111}H\rho \cos\phi + a_{1022}\rho^2 \cos 2\phi)^2$$

$$+ (a_{1111}H\rho \sin\phi + a_{1022}\rho^2 \sin 2\phi)^2]$$

$$= |\tau|^2 [a_{1200}^2 H^4 + \frac{a_{1111}^2 H^2}{2} + \frac{a_{1022}^2}{3}] .$$

The corresponding integral, $I_{imaginary}$, is obtained by substituting the imaginary part of the polarization aberration coefficients, δ_{luvw}, for a_{luvw} in the above expression. The upperbound on the polarzation coupling is

$$I_{c,max} < I_{real} + I_{imaginary}$$

$$= |\tau|^2 \left[a_{1200}^2 H^4 + \frac{a_{1111}^2 H^2}{2} + \frac{a_{1022}^2}{3} + \delta_{1200}^2 H^4 + \frac{\delta_{1111}^2 H^2}{2} + \frac{\delta_{1022}^2}{3}\right]$$

$$= |\tau|^2 \left[|P(1,2,0,0)|^2 H^4 + \frac{|P(1,1,1,1)|^2 H^2}{2} + \frac{|P(1,0,2,2)|^2}{3}\right].$$

This is the second order upper bound to the polarization coupling for systems of weak polarizers.

Hence the average effect over the image and pupil can be obtain by integrating over ρ, and ϕ. The polarization accuracy, Δ_p, defined as the maximum fraction of light (intensity) which can be coupled into orthogonal polarization state. The incident polarized state is given by the Jones vector, $\vec{J}$. This vector is effectively rotated by the optical system and the rotation is given by the Jones matrix, JJ. The amount of polarization along the orthogonal state of polarization, $\vec{J}'$, of the incident polarization state is given by the projection of $JJ(\vec{J})$ into J',

$$JJ(\vec{J}) \cdot \vec{J}'.$$

This value is given by the square of the second order Jones matrix and is given in terms of the polarization aberration coefficients. (For the incident light in the polarization state $I_o\hat{p}$, then the result of instrumental polarization is to couple the polarization into the orthogonal state $\hat{q}$. The amount

of coupling is given by

$$I_o\hat{p} + I_o(1-\Delta_p)\hat{p} + \Delta_p I_o\hat{q}$$

where Δ_p = polarization accuracy.) From the above results, the polarization accuracy is given in terms of the second order polarization abberation coefficients P(1,0,2,2), P(,1,1,1,1), and P(1,2,0,0) :

$$\Delta_p = \frac{1}{\pi} \int \left| JJ_2(H=1,\rho,\phi) \right|^2 \rho d\rho d\phi$$

or

$$\Delta_p = 2P^2(1,2,0,0) + \frac{1}{2}P^2(1,1,1,1) + \frac{1}{3}P^2(1,0,2,2)$$

where the integrations have been carried out for the squared terms and estimated for the crossed terms. For the SAMEX magnetograph design given herein the polarization accuracy value of

$$\Delta_p < 1.4 \times 10^{-7}$$

is obtained for specially selected optical coatings was obtained. These second order aberration coefficients are given in Section II-4. The second order coefficients are sufficients since the next order that contributes is the forth order. The polarization effects would be on the order of $(\Delta_p)^2$.